

DEPARTMENT OF PHYSICS  
UNIVERSITY OF JYVÄSKYLÄ  
RESEARCH REPORT No. 8/2005

**STUDIES OF ELECTRON CYCLOTRON  
RESONANCE ION SOURCE  
PLASMA PHYSICS**

**BY  
OLLI TARVAINEN**

Academic Dissertation  
for the Degree of  
Doctor of Philosophy

*To be presented, by permission of the  
Faculty of Mathematics and Science  
of the University of Jyväskylä,  
for public examination in Auditorium FYS-1 of the  
University of Jyväskylä on December 16, 2005  
at 12 o'clock*



Jyväskylä, Finland  
December, 2005

## **PREFACE**

The work presented in this thesis has been carried out at the JYFL Accelerator Laboratory in the University of Jyväskylä and at Argonne National Laboratory during the years 2003-2005.

First, I would like to thank my supervisor Dr. Hannu Koivisto for giving me an opportunity to work in the ion source group of the JYFL Accelerator Laboratory and for his invaluable guidance and support in the course of this work. Another person who deserves my sincere gratitude is Mr. Pekka Suominen, without whom I could not have finished this thesis. I wish to thank him not only for professional help and fruitful comments but also for all the cheerful moments that we have spent together in work, free time and international conferences and summer schools.

I extend my thanks to all the people working at the JYFL Accelerator Laboratory, especially my closest colleagues in cyclotron- and RADEF-groups. I am also indebted to the technical personnel of our laboratory. I have been privileged to work and share thoughts with colleagues from accelerator laboratories all over the world. I would like to thank especially the ion source people from Argonne National Laboratory and Lawrence Berkeley National Laboratory. I would also like to express my gratitude to the referees of this work, Dr. Sandor Biri and Dr. Hans Beijers, for valuable comments.

I wish to thank Mr. Marcus Rinkiö for genuine friendship and unforgettable time that we have spent together studying physics and playing beach volley. I like to thank my family: mother, father and brother for their encouragement. Finally, I direct my most heartfelt thanks to my loving wife Paula for constant support and for providing a “physics-free environment” at home, which has helped me to separate work from leisure.

Jyväskylä, November 2005

Olli Tarvainen

## ABSTRACT

This thesis consists of an introduction to the plasma physics of electron cyclotron resonance ion sources (ECRIS) and a review of the results obtained by the author and co-workers including discussion of related work by others. The thesis begins with a theoretical discussion dealing with plasma physics relevant for the production of highly charged ions in ECR ion source plasmas. This is followed by an overview of different techniques, such as gas mixing and double frequency heating, that can be used to improve the performance of this type of ion source. The experimental part of the work consists of studies related to ECRIS plasma physics.

The effect of the gas mixing technique on the production efficiency of different ion beams was studied with both gaseous and solid materials. It was observed that gas mixing improves the confinement of the heavier element while the confinement of the lighter element is reduced. When the effect of gas mixing on MIVOC-plasmas was studied with several mixing gases it was observed that applying this technique can reduce the inevitable carbon contamination by a significant factor.

In order to understand the different plasma processes taking place in ECRIS plasmas, a series of plasma potential and emittance measurements was carried out. An instrument, which can be used to measure the plasma potential in a single measurement without disturbing the plasma, was developed for this work. Studying the plasma potential of ECR ion sources is important not only because it helps to understand different plasma processes, but also because the information can be used as an input parameter for beam transport simulations and ion source extraction design. The experiments performed have revealed clear dependencies of the plasma potential on certain source parameters such as the amount of carbon contamination accumulated on the walls of the plasma chamber during a MIVOC-run. It was also observed that gas mixing affects not only the production efficiency of the ion beams but also their energy distribution. This finding strongly supports the conclusion that ion cooling explains the beneficial effect of this technique. It was demonstrated with simulations that the momentum spread of the ion beam, which is partly due to the the plasma potential, affects the emittance of the ion beams through dispersive ion optical components. An important observation was that double frequency heating does not affect the emittance of the ion beams. The result confirms that this method can be used to improve the extracted beam currents of highly charged ions without adversely affecting the beam quality.

## TABLE OF CONTENTS

<b>PREFACE</b> .....	<b>1</b>
<b>ABSTRACT</b> .....	<b>2</b>
<b>TABLE OF CONTENTS</b> .....	<b>3</b>
<b>1. INTRODUCTION</b> .....	<b>5</b>
<b>2. PLASMA PHYSICS OF ELECTRON CYCLOTRON RESONANCE ION SOURCES</b> .....	<b>7</b>
2.1. Definition of plasma and plasma conditions.....	7
2.2. The operation principle of electron cyclotron resonance ion sources.....	9
2.3. Electron cyclotron resonance heating .....	10
2.3.1. <i>The propagation of electromagnetic waves in magnetoplasmas</i> .....	11
2.3.2. <i>Electron energy in ECRIS plasmas</i> .....	15
2.4. Collisions in ECRIS plasmas .....	18
2.4.1. <i>Ionizing collisions and charge exchange</i> .....	18
2.4.2. <i>Electron-electron and ion-ion collisions</i> .....	21
2.5. Confinement of charged particles in ECRIS plasmas .....	24
2.5.1. <i>Trapping of charged particles in the magnetic bottle</i> .....	25
2.5.2. <i>Plasma potential</i> .....	27
2.5.3. <i>Measurement of the plasma potential</i> .....	31
2.5.4. <i>Confinement of ions in ECRIS plasmas</i> .....	32
<b>3. PRODUCTION OF HIGHLY CHARGED ION BEAMS WITH ECR ION SOURCES</b> .....	<b>38</b>
3.1. Methods to improve the performance of ECR ion sources .....	38
3.1.1. <i>Wall coating and plasma chamber material</i> .....	39
3.1.2. <i>Biased electrode technique</i> .....	40
3.1.3. <i>Gas mixing</i> .....	41
3.1.4. <i>Multiple frequency heating</i> .....	42
3.1.5. <i>Afterglow and long pulse operation modes</i> .....	44
3.2. Methods for introduction of material into the ECRIS plasma .....	45
3.2.1. <i>Gaseous elements and compounds</i> .....	45
3.2.2. <i>Evaporation oven</i> .....	45
3.2.3. <i>The MIVOC method</i> .....	46
3.2.4. <i>Sputtering</i> .....	47
3.3. Ion beam extraction and the quality of ion beams produced with ECR ion sources.....	48
3.3.1. <i>The plasma meniscus and Child-Langmuir law</i> .....	48
3.3.2. <i>Emittance and brightness of an ion beam</i> .....	49
3.3.3. <i>The effect of ion optics on the emittance</i> .....	52
<b>4. EXPERIMENTAL APPARATUS</b> .....	<b>55</b>
4.1. ECR ion sources used in the experiments.....	55
4.2. Plasma potential measurement instrument.....	56
4.3. Emittance scanner.....	59
<b>5. PRODUCTION EFFICIENCY AND REDUCTION OF CARBON CONTAMINATION OF AN ECRIS</b> .....	<b>60</b>
5.1. The effect of gas mixing on the ion beam production efficiency from gaseous compounds .....	60
5.2. Reducing the carbon contamination by gas mixing .....	62
5.3. Removal of the carbon contamination .....	65
5.4. Distribution of the carbon contamination .....	68
<b>6. PLASMA POTENTIAL AND EMITTANCE MEASUREMENTS</b> .....	<b>70</b>
6.1. Beam current decay curves .....	70
6.1.1. <i>Determination of the plasma potential</i> .....	71
6.1.2. <i>Simulated beam current decay curves</i> .....	72
6.2. Effect of different ion source parameters on the plasma potential and emittance.....	74

---

6.2.1. Plasma potential and beam current decay curves vs. charge state of the ion beam .....	75
6.2.2. Plasma potential vs. microwave power and gas feed rate .....	84
6.2.3. Plasma potential vs. mass of the ionized gas .....	85
6.2.4. Plasma potential vs. negative voltage of the biased disk .....	87
6.2.5. Plasma potential vs. strength of the (axial) magnetic field .....	88
6.2.6. Plasma potential vs. axial / radial microwave power ratio .....	89
6.2.7. The effect of carbon contamination on the plasma potential .....	90
6.2.8. Momentum spread of the ion beam and its influence on the emittance .....	92
6.2.9. The effect of gas mixing on the emittance and plasma potential .....	96
6.2.10. The effect of microwave frequency on the plasma potential and emittance .....	104
6.2.11. The effect of multiple frequency heating on the plasma potential and emittance .....	106
6.2.12. The effect of microwave radiation bandwidth on the plasma potential .....	108
<b>7. SUMMARY .....</b>	<b>109</b>
<b>REFERENCES.....</b>	<b>111</b>

### 1. INTRODUCTION

High-energy ion beams are used for nuclear physics and particle interaction research in various accelerator laboratories around the world. Charged particles which are accelerated to high energies are produced with ion sources. Therefore, the performance of the ion source plays a crucial role in the experiments. In addition to basic research, ion sources are used in industrial and medical applications such as ion beam lithography, plasma propulsion and cancer treatment.

The design of the ion source depends on the ion beam requirements. For example, in order to obtain high energies with cyclotrons, the charge state of the ion beam injected into the accelerator has to be sufficient as the final particle energy depends quadratically on the ion charge. Most heavy ion accelerators, such as the JYFL K-130 cyclotron [1], use Electron Cyclotron Resonance Ion Sources (ECRIS [2]) for the production of multiply charged ions. This type of plasma ion source is suitable for long-term operation requiring intense ion beams of heavy elements since there are no wearing parts such as cathodes in an ECRIS. Because of their reliability and capability to produce multiply charged ion beams from the majority of stable elements, ECR ion sources have become the most common ion sources for heavy ion production in accelerator laboratories.

At the University of Jyväskylä, Department of Physics, two ECR ion sources [3, 4] are used for the production of highly charged ion beams for nuclear physics research and applications. For example, high penetration ( $\geq 100 \mu\text{m}$  in silicon) and high LET ion beam cocktails used for space electronics irradiation tests at the RADEF station [5] require constant development of the JYFL ECR ion sources.

In order to understand the plasma processes in the ECRIS-plasma and consequently to improve the performance of the ion sources, a number of experiments have been carried out. An instrument which can be used to provide information about the plasma properties was developed for this work. Information about the plasma potential and ion beam energy spread as a function of various parameters has been obtained with the aid of the instrument. The information can be used to enhance the production efficiency of ECR ion sources and to improve the quality (intensity and emittance) of the extracted ion beams.

The properties of ECR-heated plasmas and production of highly charged ion beams with an ECRIS are considered in Chapters 2 and 3. Different methods to improve the performance of ECR ion

---

sources are also discussed in Chapter 3. The ion sources and beam diagnostics used in the experiments are introduced in Chapter 4. Chapter 5 deals with the effect of the gas mixing technique [6] on the production efficiency of metal ion beams produced with the MIVOC-method [7]. Reduction of the inevitable carbon contamination due to the use of the MIVOC-method is also studied in this chapter. In Chapter 6 the results of plasma potential, ion beam energy spread and emittance measurements are presented. Finally, in Chapter 7 conclusions are drawn.

## 2. PLASMA PHYSICS OF ELECTRON CYCLOTRON RESONANCE ION SOURCES

Electron cyclotron resonance ion sources (ECRIS) are typical plasma ion sources. They were originally developed utilizing information obtained in fusion research in the 1960's when it was demonstrated that open-ended configurations for plasma confinement could not fulfill the Lawson criterion for fusion [8]. The Lawson criterion states that the product of the plasma density and the confinement time of ions has to exceed a certain limit in order to obtain net yield from a fusion reaction. However, while fusion research concentrated on toroidal machines it was realized by Geller that open-ended devices could be suitable for the production of multiply charged ion beams. The first report of an ion source based on electron cyclotron heating of the plasma by microwaves was published in 1972 [9]. A milestone in the development of ECR ion sources was reached in 1974 when Geller built a device called SUPERMAFIOS, which can be considered as a basis for the design of a modern ECRIS. A historical overview of ECRIS development can be found in references [2, 10, 11].

In order to design a well-performing ECR ion source one has to take into account several plasma processes related to the production of highly charged ions in an ECR-heated plasma. A review of the most important aspects of plasma physics with respect to ECR ion sources and their operation principle will be presented below. All equations are given in SI-units unless states otherwise.

### 2.1. Definition of plasma and plasma conditions

In an ECR ion source ions are produced in a magnetically confined plasma, which is heated by microwaves. A plasma can be practically defined as: a quasineutral gas that exhibits collective behavior when exposed to external electromagnetic fields. It is of note that plasma also exhibits collective behavior via long range Coulomb interaction. There is no well-defined phase transition point from the gaseous state to plasma that consists of electrons, ions and neutral atoms or molecules. The most significant difference between plasma and neutral gas is the number of freely moving charges that make plasma a good conductor. Plasma also has properties that are characteristic of liquids, for example it is nearly incompressible. Ionized gas can be considered as a plasma if the following so-called plasma conditions are fulfilled:

- (i) The typical length scale (dimension)  $L$  of plasma has to exceed the shielding length  $\lambda_D$  (Debye length) of the plasma. The Debye length determines how far the charge

imbalance due to thermal motion in the equilibrium state or the impact of an external electric potential can extend in plasma or in ionized medium. The condition can be written for electrons as

$$L \gg \lambda_{De} = \sqrt{\frac{\varepsilon_0 k T_e}{e^2 n_e}}, \quad (1)$$

where  $\varepsilon_0$  is the permittivity constant ( $\approx 8.854 \cdot 10^{-12}$  F/m),  $k$  the Boltzmann constant ( $\approx 1.38 \cdot 10^{-23}$  J/K),  $T_e$  the electron temperature (in Kelvins),  $e$  the elementary charge ( $\approx 1.602 \cdot 10^{-19}$  C) and  $n_e$  the electron density. If this condition is not valid, the plasma is not necessarily macroscopically neutral.

- (ii) In order to have collective behavior, the number of particles inside the Debye sphere must be sufficient i.e.

$$n_e \lambda_D^3 \gg 1. \quad (2)$$

- (iii) The frequency  $f_{pe}$  of collective plasma (electron) oscillations must be higher than the collision frequency  $\nu_{en}$  of electrons and neutrals

$$f_{pe} = \frac{\omega_{pe}}{2\pi} = \frac{1}{2\pi} \sqrt{\frac{n_e e^2}{\varepsilon_0 m_e}} > \nu_{en}, \quad (3)$$

where  $m_e$  is the electron mass ( $\approx 9.11 \cdot 10^{-31}$  kg). Equation (3) defines the plasma oscillation frequency  $\omega_{pe}$ . If this plasma condition is not valid, there are no collective phenomena and the dynamics of the system is dominated by the motion of neutrals. This condition is fulfilled as the degree of ionization of the plasma increases. Usually ionized gas can be considered to be plasma when its degree of ionization exceeds a few percent [12].

## 2.2. The operation principle of electron cyclotron resonance ion sources

The production of multiply charged ions with an ECR ion sources requires the following: (i) appropriate magnetic field strength and structure, (ii) adequate microwave frequency and power, (iii) good vacuum, (iv) constant flow of material into the plasma chamber and (v) suitable extraction system.

The so-called minimum-B magnetic field structure inside the plasma chamber is generated by solenoids (axial field) and hexapole magnets (radial field). It follows from the geometry that the minimum of the magnetic field is obtained at the center of the plasma chamber. The strength of the field increases towards the walls of the plasma chamber forming nearly ellipsoidal concentric surfaces on which the field strength is constant.

The ionization starts when neutral gas and microwaves are fed into the plasma chamber. There are always some free electrons present in the plasma chamber that are moving on helical orbits. When an external rapidly changing electric field  $\vec{E}_{ext}$  is generated by the microwaves, free electrons can gain energy if their gyration frequency  $\omega_{ce}$  equals the frequency of the applied electromagnetic waves  $\omega_{RF}$  i.e.

$$\omega_{ce} = \frac{eB}{m_e} = \omega_{RF}, \quad (4)$$

where  $B$  is the magnetic field. This is called electron cyclotron resonance. The location of the resonance layer in the ECRIS plasma chamber depends on the magnetic field strength and microwave frequency. For 14 GHz microwaves the corresponding magnetic field is 0.5 T on the ellipsoidal resonance surface. The electrons are heated stochastically and the plasma is ignited as electrons collide with the neutrals and ionize them. The plasma ignition proceeds like an avalanche since the number of free electrons increases due to stepwise ionization until an equilibrium of electrons, multiply charged ions and neutrals is obtained. The created plasma is further confined in the magnetic field in order to produce highly charged ions.

The vacuum in the plasma chamber has to be good enough in order to produce highly charged ions. This is due to charge exchange between ions and neutrals that becomes more likely when the

pressure increases. Ions are extracted from the plasma chamber with the aid of high voltage as they follow the electrons along the magnetic field lines to the extraction area. The extraction of ions can be considered as a loss process from the magnetic bottle. In the extraction region ions experience an accelerating electric field due to the potential difference of the ion source and the beam line. Figure 2.1 shows a schematic drawing of an ECR ion source. The magnetic field values given in the figure correspond to those of the JYFL 14 GHz ECRIS.

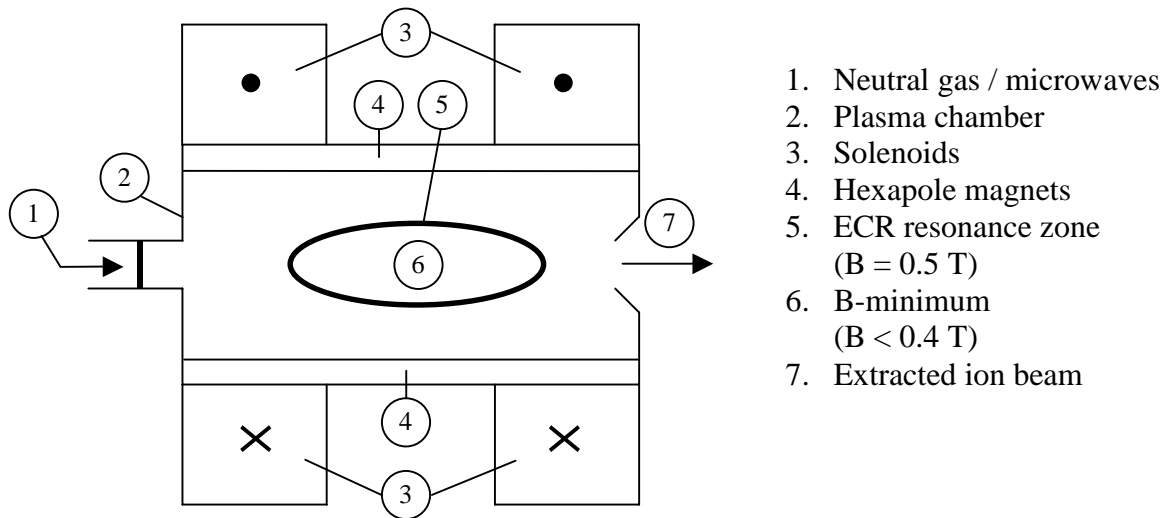


**Figure 2.1** A schematic drawing of an electron cyclotron resonance ion source. The given magnetic field strengths correspond to the JYFL 14 GHz ECRIS.

### 2.3. Electron cyclotron resonance heating

The propagation of electromagnetic waves and electron heating in the plasma of ECR ion sources is not completely understood. This is due to the unique magnetic field structure, varying plasma density, boundary conditions set by the plasma chamber walls, resonance(s) and cut-offs. In order to treat the problem analytically, simplifications such as linearization, single-particle theories, cold plasma approximations and diagonalized plasma pressure tensors are normally used. The propagation of magnetohydrodynamic waves in the plasmas has been omitted in the following since their importance in the case of electron heating in ECRIS plasmas is minor (the effect of MHD waves on ion temperature is discussed later).

### 2.3.1. The propagation of electromagnetic waves in magnetoplasmas

The propagation of electromagnetic waves can be treated using cold plasma theory, since the phase velocity of the wave is normally significantly higher than the thermal velocity of the particles in the plasma excluding the very close proximity of the resonance. Furthermore, ions can be treated as a steady background in the case of microwaves (in GHz-range). The wave propagation can be described with the aid of the Lorentz force (5) and the wave equation (6) derived from Maxwell's equations:

$$m_e \frac{d\vec{v}}{dt} = -e(\vec{E} + \vec{v} \times \vec{B}_0) \quad (5)$$

$$\vec{k} \times (\vec{k} \times \vec{E}) = \frac{\omega^2}{c^2} \left( \vec{E} + i \frac{\vec{j}}{\varepsilon_0 \omega} \right) \quad (6)$$

where  $\vec{v}$  is the electron velocity,  $\vec{E}$  the electric field of the wave,  $\vec{B}_0$  the external magnetic field,  $\vec{k}$  the wave vector,  $\omega$  the microwave frequency,  $c$  the velocity of light ( $\approx 2.998 \cdot 10^8$  m/s) and  $\vec{j} = -n_{e0} e \vec{v}$  the current density. In order to derive the resonance condition for electron cyclotron resonance it is sufficient to consider only the propagation of electromagnetic waves parallel to the external magnetic field  $\vec{k} \parallel \vec{B}_0$ . Waves propagating perpendicular to the external magnetic field  $\vec{k} \perp \vec{B}_0$  would result in upper hybrid resonance (UHR), which will not be considered here since there is no evidence on their importance in ECRIS plasmas. The phase velocity,  $v_p$ , of the wave propagating parallel to external magnetic field can be derived from equations (5) and (6).

$$v_p = \frac{\omega_{RF}}{k} = \frac{c \sqrt{1 \pm \frac{\omega_{ce}}{\omega_{RF}}}}{\sqrt{1 \pm \frac{\omega_{ce}}{\omega_{RF}} - \frac{\omega_{pe}^2}{\omega_{RF}^2}}}. \quad (7)$$

The plasma oscillation frequency  $\omega_{pe}$  can be determined from equation (3). Here the + sign corresponds to so-called L-wave (left-hand polarized) and – sign to so-called R-wave (right-hand polarized). In electron cyclotron resonance the electrons are heated by the R-wave. Under the

correct conditions the L-wave would heat ions in ion cyclotron resonance (MHz-range). However, there is no ion cyclotron resonance in ECR ion sources and therefore only the R-wave will be considered. Equation (7) shows that the R-wave can propagate (phase velocity is not imaginary) in magnetoplasma if

$$0 < \omega_{RF} < \omega_{ce} \text{ or } \omega_{RF} > \frac{\omega_{ce} + \sqrt{\omega_{ce}^2 + 4\omega_{pe}^2}}{2} = \omega_{co}. \quad (8)$$

When  $\omega = \omega_{ce}$  the gyration of electrons is in resonance with the electric field of the wave, which is the resonance condition for electron cyclotron resonance. Equation (7) shows that the phase velocity of the wave  $v_p \rightarrow 0$  in the resonance. Therefore, the cold plasma theory is not applicable when determining the behavior of the wave in the close proximity of the resonance. At the point where  $\omega = \omega_{co}$  so-called cut-off occurs preventing wave propagation through the cut-off. The cut-off frequency depends not only on the external magnetic field but also on the electron density of the plasma. The electron density of an ECRIS plasma is typically on the order of  $10^{11} \text{ cm}^{-3}$  though there is spatial variation (see for example ref. [8]). Figure 2.2 shows magnetic field values at the resonance and cut-off for 6.4 GHz and 14 GHz microwaves as a function of electron density of the plasma. Three possible propagations and the corresponding wave vectors of the wave are also presented (a) decreasing magnetic field and electron density, (b) decreasing magnetic field and constant electron density (c) decreasing magnetic field and increasing electron density.

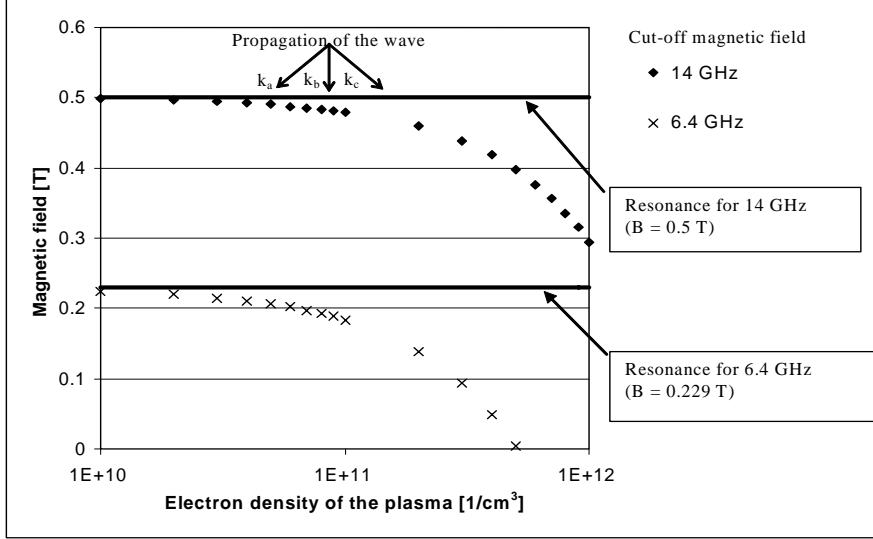


**Figure 2.2** The resonance and cut-off magnetic fields for different microwave frequencies as a function of the electron density. Three different propagations are presented: (a) decreasing magnetic field and electron density (b) decreasing magnetic field and constant electron density (c) decreasing magnetic field and increasing electron density.

In an ECRIS the microwaves travel into decreasing magnetic field (magnetic beach) due to the minimum-B structure as they enter the plasma chamber. As figure 2.2 shows, the wave encounters the resonance before reaching cut-off regardless of the spatially varying electron density. In this case, the energy of the waves can be coupled to electrons in the neighborhood of the resonance, which causes their velocity  $v_{\perp}(\text{energy})$  in a direction perpendicular to the magnetic field to increase. As the wave passes the resonance either transmission or absorption occurs in the case of propagation towards the magnetic beach [13]. If the propagation is towards an increasing magnetic field, reflection can also occur at the resonance according to ref. [14]. Between resonance and cut-off (see figure 2.2) the phase velocity of the wave is imaginary and the wave can tunnel through this region without being damped [14]. According to warm plasma theory the relative absorption factor of the microwave power  $P_{\text{absorbed}}/P_{\text{incident}}$  at the resonance for waves propagating towards the magnetic beach can be written

$$\frac{P_{\text{absorbed}}}{P_{\text{incident}}} = 1 - e^{-\pi\eta}, \quad (9)$$

with  $\eta = \frac{\omega_{pe}^2}{\omega c |B_{res}^{-1} (dB/dz)_{res}|}$ , where  $B_{res}$  is magnetic field at resonance [15]. Since there is no

reflection in this simplified case, the remaining power is transmitted through the resonance. Figure

2.3 shows the absorption and transmission coefficients in the case of 14 GHz microwaves as a function of plasma density. A value of 5.5 T/m, which is typical for the JYFL 14 GHz ECRIS, was used for the magnetic field gradient on the resonance.

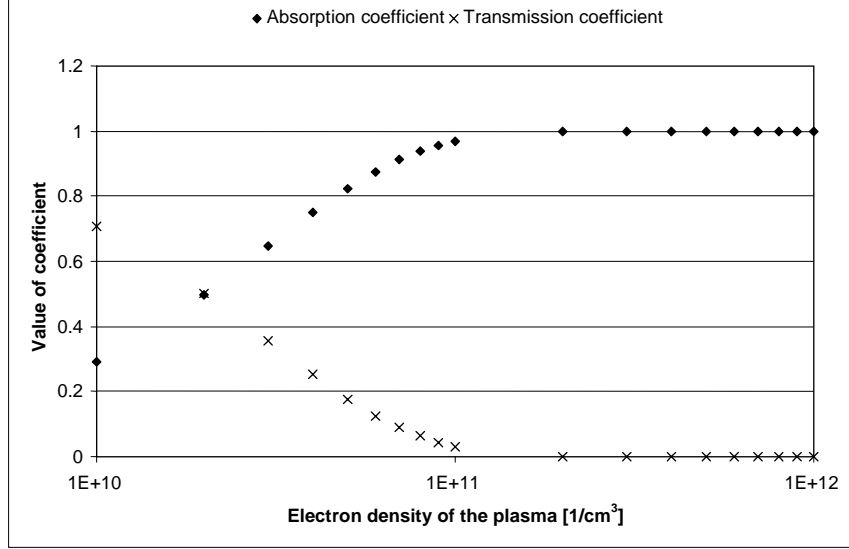


**Figure 2.3** Microwave power absorption and transmission coefficients at resonance as a function of the electron density. A Microwave frequency of 14 GHz was used in the calculation.

Figure 2.3 shows that for electron densities exceeding  $10^{11} \text{ cm}^{-3}$  the power of the wave is absorbed almost completely as the wave encounters the resonance. The results presented in reference [13] show that at high density or high collisionality the transmitted power falls significantly below its initial value well before reaching the precise resonance. The effective width of the resonance  $\Delta z$  can be written [13]

$$\Delta z \approx \sqrt{\frac{2\pi v}{\omega \alpha}}, \quad (10)$$

where  $v$  is the velocity of electrons entering the resonance and  $\alpha = B_{res}^{-1} (dB/dz)_{res}$ . For 14 GHz microwaves the width of the resonance zone is approximately 3 mm with electron energies from 5 to 10 eV (cold electrons). However, reflections in the plasma chamber generate interference of waves that can significantly affect the energy absorption. Due to the reflections there are electromagnetic waves propagating in different directions, which can result in zero electric field at the resonance (as a superposition of individual fields), the so-called field null condition. Under this

condition the absorption is significantly reduced since the average energy gain  $E_g$  of a single electron traversing the resonance zone is [13]

$$E_g = \frac{\pi e^2 |\vec{E}|^2}{m_e v \omega \alpha}. \quad (11)$$

The decrease of the absorbed power can be minimized by designing the magnetic field structure such that the resonance zone is larger than the typical width of the field null. This can be realized by setting the gradient of the magnetic field low enough near the location of the resonance (resonance width increases when field gradient decreases; see equation (10)). Another issue that has to be taken into account is the coupling of microwaves into the plasma chamber. Although absorption increases with increasing plasma density, significant power can be reflected before entering the actual ECRIS plasma if the plasma density gradient is too high in the waveguide [13].

### 2.3.2. *Electron energy in ECRIS plasmas*

The energy of an individual electron either increases or decreases as it traverses the resonance, depending on the phase difference between its gyromotion and the electric field of the microwaves. Consider two electrons entering the resonance with the same initial energy but opposite phases. The energy gain of the electron in the accelerating phase is higher than the energy loss of the electron in the decelerating phase assuming that the number of turns they make at the resonance is the same. This is a result of increasing (decreasing) radius of curvature due to the energy gain (loss) on the resonance, which affects the work  $W = \int \vec{F} \cdot d\vec{l} = -\int e\vec{E} \cdot d\vec{l}$  done on the electron (by the electron) as the length of the integral path increases (decreases). This effect is illustrated in figure 2.4.

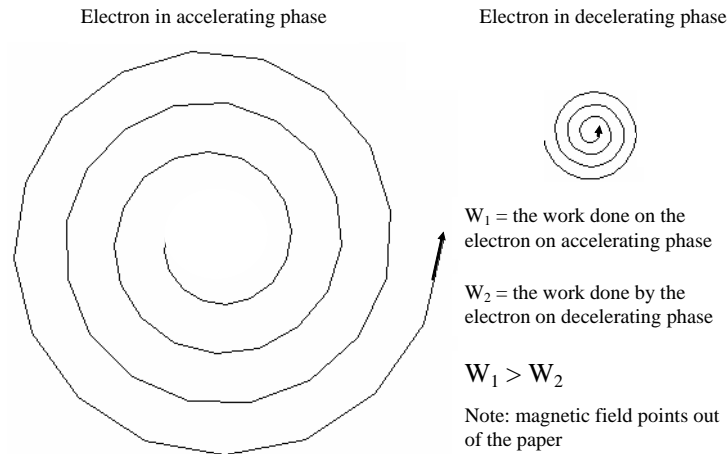


**Figure 2.4** The effect of acceleration and deceleration on the electrons gyration radius in a magnetic field.

It has been shown [16] that the electrons in an ECRIS plasma are far from thermodynamical equilibrium. The electron distribution function is strongly non-Maxwellian and can be represented by three populations [17]: a cold one ( $T_e \leq 50$  eV, approximately 50 % of all the electrons) whose energy distribution is Maxwellian, a warm one (energies up to  $\approx 10$  keV) and a hot one (energies up to a few hundred keV), the latter being well confined in the magnetic field. In reference [16] the energy distribution of the electrons was studied experimentally with the aid of three diagnostic means; bremsstrahlung, electron cyclotron emission and diamagnetism. Figure 2.5 presents the temperature of the warm/hot electrons  $T_e$  [keV] as a function of microwave power measured with the 18 GHz Minimafios ECRIS. The figure is based on the results presented in reference [16].

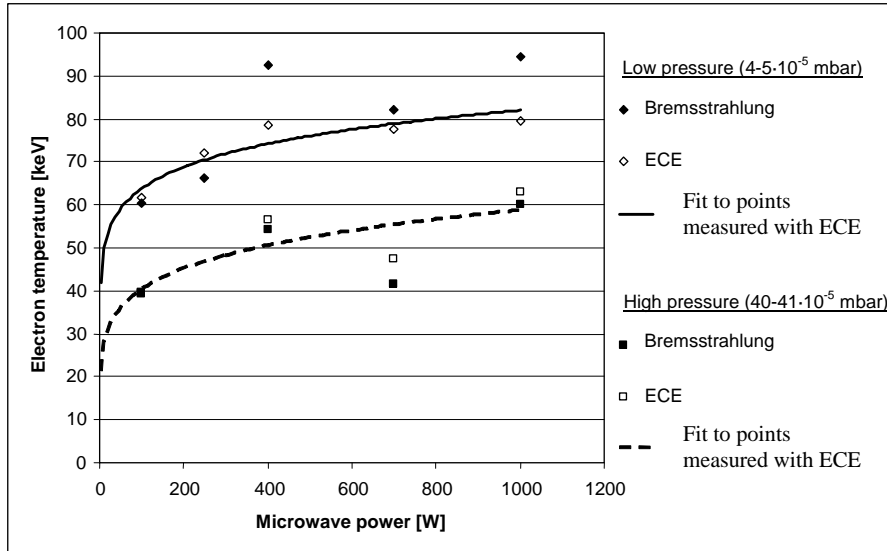


**Figure 2.5** Electron temperature  $T_e$  [keV] in an ECRIS plasma (Minimafios; 18 GHz) as a function of neutral gas pressure and microwave power [16]. The results are determined from bremsstrahlung and electron cyclotron emission (ECE) spectra.

The figure shows that  $T_e$  is higher for low plasma density (pressure). In that case, the same power is absorbed by fewer electrons and the electron temperature averaged over the whole warm/hot population is higher. Another conclusion is that  $T_e$  increases with increasing microwave power until the slope of the temperature curve becomes smaller at about 200 W. This can be explained qualitatively in the following way: when the electron traverses the resonance zone it receives an energy kick perpendicular to the magnetic field and becomes trapped inside the ellipsoidal surface defined by the resonance layer. The electron no longer traverses the resonance due to improved confinement and the rf-heating becomes inefficient [16]. However, the highest electron energies in an ECRIS plasma are several hundreds of keV (the factors limiting the maximum energy are discussed in reference [16]). For example, in the case of the JYFL 14 GHz ECRIS the maximum energy of the bremsstrahlung (X-ray) spectrum produced by an oxygen plasma has been measured to be approximately 330 keV while the distribution was peaked at 70 – 80 keV [4], increasing only slightly with increasing microwave power. The optimum microwave power depends on the beam requirement. For example, if the intention is to produce highly-charged ions, it is beneficial to use rather high microwave power in order to assure that the average energy of the electrons is sufficient to obtain high ionization cross sections (to be discussed later in section 2.4.1.).

It has been recently found (with the superconducting ECR ion source VENUS, Versatile ECR ion source for NUclear Science; see for example ref. [18]) that the electron temperature deduced from the bremsstrahlung spectrum is strongly dependent on the ion source magnetic field configuration.

It was observed that the electron temperature increases linearly with increasing  $B_{\min}/B_{\text{ECR}}$  ratio [19] ( $B_{\text{inj}}$  and  $B_{\text{ext}}$  were kept unchanged). The increase of the spectral temperature with  $B_{\min}$  can be related to reduced magnetic field gradient at the resonance. According to equation (11) the energy gain of a single electron traversing the resonance depends inversely on the magnetic field gradient, which can explain the observation. The effect of the magnetic field gradient on the electron heating has been studied theoretically (with simulations) in references [20] and [21]. It was found that electron heating becomes more efficient with higher microwave frequency and/or with lower magnetic field gradient at the resonance.

#### 2.4. Collisions in ECRIS plasmas

The plasma of an ECR ion source is a mixture of ions, electrons and neutrals that undergo collisions with each other. The collision frequency,  $\nu$ , is usually defined in terms of an average over all velocities  $v$  in the Maxwellian distribution, namely

$$\nu = n \langle \sigma v \rangle, \quad (12)$$

where  $n$  is the particle density and  $\sigma$  the cross section for the collision. The collisions in ECRIS plasmas can be divided in two categories: (i) collisions directly related to ion production i.e. ionizing electron-ion collisions and charge exchange reactions mainly with neutrals and (ii) collisions affecting the plasma confinement and temperature of different constituents i.e. electron-electron, ion-ion and non-ionizing electron-ion collisions.

##### 2.4.1. Ionizing collisions and charge exchange

The stepwise ionization in ECRIS plasmas occurs in collisions of neutrals or ions with electrons whose kinetic energy exceeds the ionization potential of the atom. Changes of the ion density (of a certain charge state) can be described by three dominant processes; step-by-step ionization by electron impact, charge exchange and diffusion [22]. The evolution in time for each ion density  $n_i^q$  of species  $i$  and charge state  $q$  is given by

$$\frac{dn_i^q}{dt} = n_e \langle \sigma v \rangle_{q-1 \rightarrow q}^{\text{ion}} n_i^{q-1} + n_{0i} \langle \sigma v \rangle_{q+1 \rightarrow q}^{\text{cex}} n_i^{q+1} - n_e \langle \sigma v \rangle_{q \rightarrow q+1}^{\text{ion}} n_i^q - n_{0i} \langle \sigma v \rangle_{q \rightarrow q-1}^{\text{cex}} n_i^q - \frac{n_i^q}{\tau_{\text{conf}}^q}, \quad (13)$$

where  $n_{0i}$  is the neutral density of atomic species  $i$  and  $\tau_{conf}^q$  the confinement time of charge state  $q$  (time that ion can be trapped in the magnetic field and maintain its charge state). The first term is the production rate of charge state  $q$  from charge state  $q-1$  by electron impact and the second term from charge state  $q+1$  by charge exchange reactions with neutrals. The third term corresponds to ionization from charge state  $q$  to  $q+1$  and the fourth term to charge exchange from  $q$  to  $q-1$ . The last term, which is characterized by the confinement time, refers to diffusive ion losses of charge state  $q$  to the walls of the plasma chamber or to extraction.

According to equation (13), the ionic densities of multiply charged ions that reflect the performance of the ion source depend on the particle densities, confinement time and cross sections of different reactions. The ionization cross section can be estimated with the aid of the Lotz formula [23]

$$\sigma_{q-1 \rightarrow q} = 4.5 \cdot 10^{-14} \sum_k \xi_{q-1,k} \frac{\ln(E_e / I_{qk})}{E_e I_{qk}} \text{cm}^2. \quad (14)$$

Here  $E_e$  is the energy of bombarding electrons,  $I_{qk}$  the binding energy of electrons in the  $k^{\text{th}}$  subshell of the ion (may be the ground state or an excited state) and  $\xi_{q-1,k}$  the number of equivalent electrons in the subshell which has to lose an electron for the transition  $q-1 \rightarrow q$ . According to equation (14) the ionization cross section  $\sigma_{q-1 \rightarrow q}$  of the reaction  $A_{q-1} + e^- \rightarrow A_q + 2e^-$  depends strongly on the energy of bombarding electrons and binding energy of the electrons. Table 2.1 shows some ground state binding energies of the least bound electrons for different noble gases [24].

Element	Atomic No.	Binding energy [eV]							
		I e <sup>-</sup>	II e <sup>-</sup>	III e <sup>-</sup>	IV e <sup>-</sup>	V e <sup>-</sup>	VI e <sup>-</sup>	VII e <sup>-</sup>	VII e <sup>-</sup>
He	2	24.5	54.4	-	-	-	-	-	-
Ne	10	21.6	41.1	63.5	97	126.3	157.9	-	-
Ar	18	15.8	27.6	40.9	59.8	75.0	91.3	124.0	143.4
Kr	36	14.0	24.6	36.9	43.5	63	94	-	-
Xe	54	12.1	21.2	31.3	42	53	58	135	-

**Table 2.1** Binding energies for noble gases [24].

The binding energies of the least bound electrons decrease as the atomic number of the element increases. The binding energy increases with increasing charge state of the ion and therefore the

energy of the bombarding electrons in an ECRIS plasma has to be sufficient. In the case of highly charged ions the ionization process usually requires several consecutive collisions. The ion is initially excited in a collision with an electron. If the ion encounters another energetic electron before the excited state is discharged, ionization can occur. As an example figure 2.6 shows the cross sections for the reactions  $O + e^- \rightarrow O^+ + 2e^-$  and  $O^{6+} + e^- \rightarrow O^{7+} + 2e^-$  as a function of electron energy.

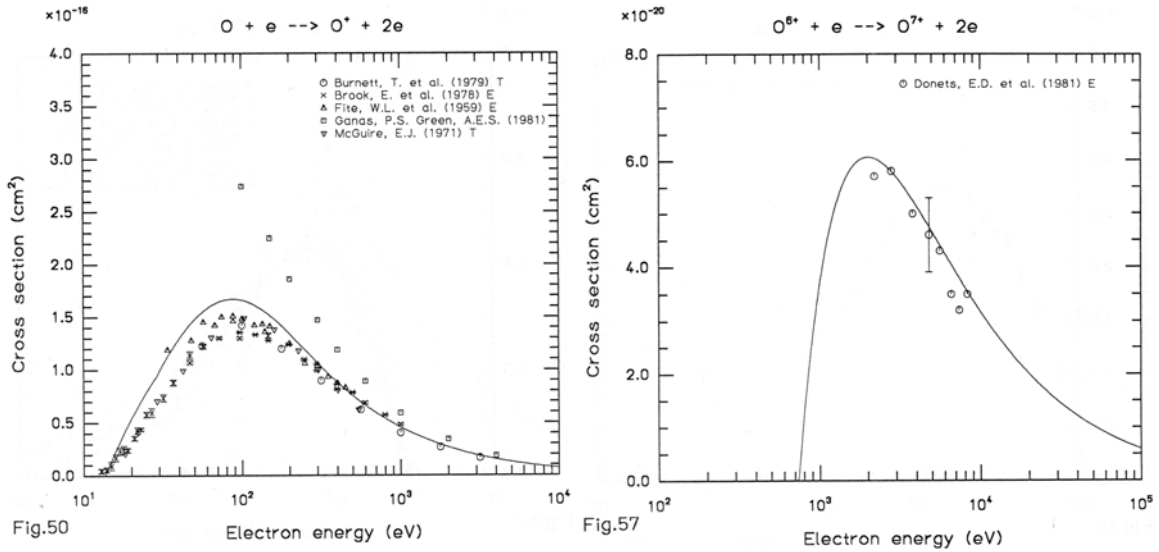


**Figure 2.6** Ionization cross sections for two different charge states of oxygen as a function of the energy of bombarding electrons [25].

The ionization cross section decreases by four orders of magnitude as the charge state of oxygen increases from neutral atoms to  $O^{6+}$  ion while the optimum energy of bombarding electrons increases from 90 eV to 2 keV. Increasing the electron energy over the optimal value causes the ionization cross section to decrease, which means that in an ECRIS the warm electron population is responsible for ionization rather than the hot electron population with energies of tens or hundreds of keV. In section 2.3.2. it was shown that the temperature (energy) increase of the electrons with increasing microwave power saturates at some point. Since the evolution of a certain charge density in time is strongly dependent on both the cross section for ionization and the electron density of the plasma (see equation 13), it can be concluded that better performance of ECR ion sources with high microwave power is due to increasing electron density [16]. The energy of bombarding electrons may even become too high for production of certain charge states as the microwave power is increased (up to saturation of the electron temperature).

Another important type of collision that affects the charge state distribution in ECRIS plasmas is charge exchange reactions between ions and neutrals. The following equation [26] can be used to calculate charge exchange cross sections for highly-charged ions colliding with neutrals:

$$\sigma_{q \rightarrow q-1} = \pi a_0^2 q Z^{1/3} \left( \frac{I_0}{I} \right)^{3/2}, \quad (15)$$

where  $a_0$  is the Bohr radius ( $\approx 0.53 \cdot 10^{-10}$  m),  $I_0$  the Bohr energy ( $\approx 13.6$  eV),  $I$  the ionization potential of the neutral atom (corresponding to the binding energy of the most loosely bound electron) and  $Z$  the atomic number. With the aid of this equation the charge exchange cross sections for  $O^{2+}$  and  $O^{6+}$  ions, for example, can be estimated to be  $3.5 \cdot 10^{-16}$  cm<sup>2</sup> and  $1.2 \cdot 10^{-15}$  cm<sup>2</sup>, respectively. The ionization and charge exchange cross sections are of the same order of magnitude for low charge-state ions while the charge exchange cross section is considerably larger than the ionization cross section for highly charged ions (compare to figure 2.6.). This emphasizes the importance of low neutral density along with high electron density for the production of highly charged ions in ECRIS plasmas.

#### 2.4.2. Electron-electron and ion-ion collisions

In section 2.3.2. it was presented that three electron populations co-exist in ECRIS plasmas. Since the collision frequency  $\nu$  is defined in terms of an average over all velocities  $v$  in the Maxwellian distribution, one cannot define any “universal” collision frequency applicable for all electron populations in ECRIS plasmas. However, to some extent these populations can be considered separately. The collision frequency  $\nu_{ee}$  of electron-electron collisions can be estimated to be [12]

$$\langle \nu_{ee} \rangle \approx \frac{n_e e^4 \ln \Lambda_e}{\varepsilon_0^2 m_e^{1/2} (kT_e)^{3/2}}, \quad (16)$$

where  $\ln \Lambda_e = \ln(n_e \lambda_{De}^3)$  is the so-called electron Coulomb logarithm. The electron-electron collision frequency depends strongly on the electron energy ( $kT_e$ ). In ECRIS plasmas the cold electron population (with energies of a few tens of eV) is highly collisional while the hot electron population (with energies of a few tens of keV) experiences less collisions. For example, the collision frequency of 10 eV electrons is approximately 26 MHz while the collision frequency of

100 keV electrons is approximately 26 Hz. In the calculation the following values were used:  $n_e = 5 \cdot 10^{11} \text{ 1/cm}^3$  and  $\ln \Lambda_e = 12$  (which is typical value for gas discharge plasmas [12]). The relativistic effect ( $\gamma$ -factor) was not taken into account in this example. The strong dependence of the collision frequency on the electron energy means that electron heating by collisionless absorption of the microwave power on the resonance dominates the collisional absorption of energy in electron-electron collisions, as long as the electron density of the plasma is sufficient (see figure 2.3) [13].

The behavior of ions in ECRIS plasmas differs significantly from the behavior of (warm) electrons. They are much heavier, move slower and experience many collisions with each other. The collision frequency,  $\nu_{ij}$ , and average time,  $\tau_{ij}$ , between collisions of ion species  $i$  and  $j$  is given by [22]

$$\nu_{ij} = \frac{1}{\tau_{ij}} \cong \frac{6.8 \cdot 10^{-8} \ln \Lambda_{ij}}{T_i^{3/2}} \frac{q^2}{A_i} \sum_j \sqrt{A_j} \sum_q n_j^q q^2, \quad (17)$$

where  $A_i$  is the mass number of ion species  $i$  and  $\sum_q n_j^q q^2 \approx n_e q_{eff}$  can be expressed with the aid of the electron density  $n_e$  and the mean ion charge state of the plasma  $q_{eff}$  (assuming the plasma to be quasineutral). In equation (17) the ion temperature is in units of eV and electron density in units of  $\text{cm}^{-3}$ . The ion temperatures in ECRIS plasmas have been estimated to be only a few electron volts [22]. For example, figure 2.7 shows the collision frequencies and average times between consecutive collisions for  $\text{O}^{7+}$  and  $\text{Ar}^{12+}$  ions (high charge states) in pure oxygen and argon plasmas as a function of the ion temperature. The following parameters were used in the calculation:  $n_e = 5 \cdot 10^{11} \text{ 1/cm}^3$ ,  $q_{eff\text{-oxygen}} = 5$ ,  $q_{eff\text{-argon}} = 8$  and  $\ln \Lambda_e = 12$ .

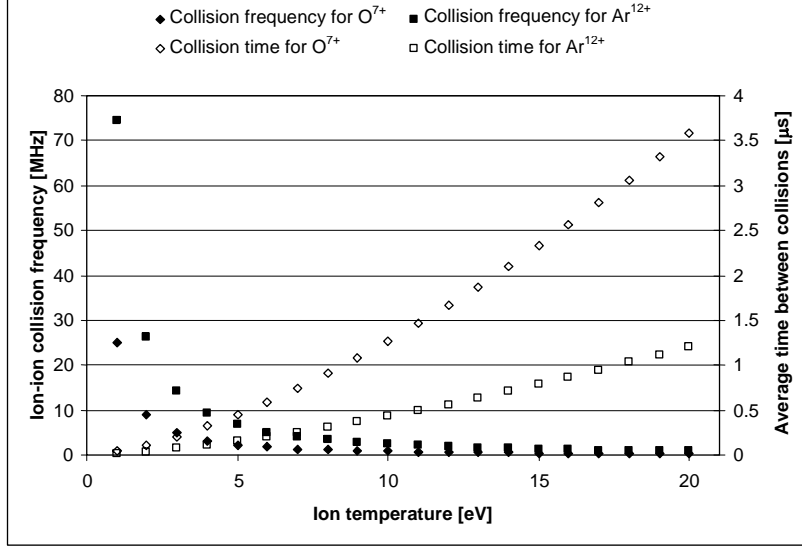


**Figure 2.7** Ion-ion collision frequency and average time between collisions for  $O^{7+}$  and  $Ar^{12+}$  ions in a pure oxygen or argon plasma. Plasma parameters typical for a 14 GHz ECRIS were used in the calculation.

As figure 2.7 shows, the ion-ion collision frequency depends strongly on the ion temperature. As the temperature increases, ions become less collisional. The figure also shows that the collision frequency of heavier ions (and therefore higher charges) is higher than the collision frequency of lighter ions. If the ions are highly collisional, all charge states should have the same ion temperature because their energy equipartition time  $\tau_{eq,i \rightarrow i}$  is much shorter than their confinement time [22]. The collisional energy transfer from electrons to ions can be estimated using an expression for the energy equipartition frequency  $\nu_{eq,e \rightarrow i}$  (18), which has been derived assuming steady-state conditions in the ECRIS plasma [22]

$$\nu_{eq,e \rightarrow i} = \frac{1}{\tau_{eq,e \rightarrow i}} \cong \frac{3.2 \cdot 10^{-9} \ln \Lambda_{ei}}{T_e^{3/2}} \sum_i \frac{\sum_q n_i^q q^2}{A_i}. \quad (18)$$

The units in equation (18) are the same as in equation (17). It can be seen that the equipartition frequency and time depend strongly on the electron energy. Therefore different electron populations have to be considered separately. For oxygen plasmas the equipartition times of the warm electron population ( $T_{e,warm} \approx 1$  keV) and of the hot electron population ( $T_{e,hot} \approx 100$  keV) are 5.3 s and 167 s, respectively (with the same plasma parameters as in figure 2.7). Ions cannot reach these energies since their confinement time in the plasma is much shorter, as we will see in section 2.5.4. However, the equipartition time between ions and cold electrons whose temperature,  $T_{e,cold} \approx 10$ -50

eV (around the plasma potential [17]), is significantly shorter. Figure 2.8 shows the energy equipartition times for oxygen and argon ions in pure plasmas with the cold electron population as a function of electron energy. The cold electron density  $n_{e,cold}$  was estimated to be half of the total electron density  $n_e$  (which was assumed to be  $5 \cdot 10^{11} \text{ cm}^{-3}$ ). This is due to the fact that approximately half of the electrons pass the resonance in accelerating (or decelerating) phase with respect to the electric field of the microwaves. All the other plasma parameters are the same as in the calculation for figure 2.7.

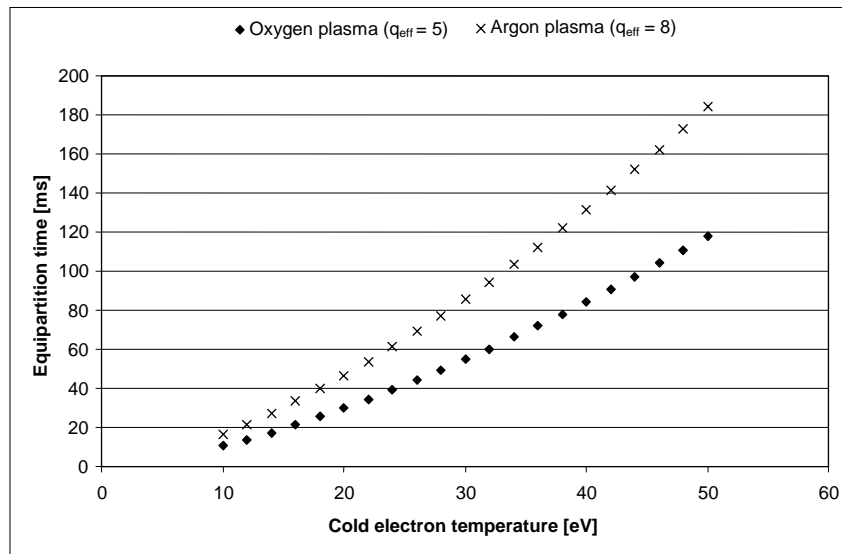


**Figure 2.8** Energy equipartition times with cold electron population for pure oxygen and argon plasmas. Plasma parameters typical of a 14 GHz ECRIS were used in the calculation.

The figure shows that the equipartition time between ions and the cold electron population is on the order of tens of milliseconds, and it is longer for the argon plasma due to the higher mass. In order to estimate the ion temperature in ECRIS plasmas the energy equipartition time has to be compared with the production and confinement times of different ions (charge states), which will be done in section 2.5.4.

## 2.5. Confinement of charged particles in ECRIS plasmas

The magnetic field in ECR ion sources is generated by solenoids and hexapole magnets. As a consequence, a so-called magnetic bottle that can be used to trap charged particles is formed. Figure 2.9 presents a plasma trapped in a magnetic field generated by solenoids (on the left) and permanent hexapole magnets (on the right). The superposition of these magnetic fields makes it possible to confine the ECRIS plasma both axially and radially.

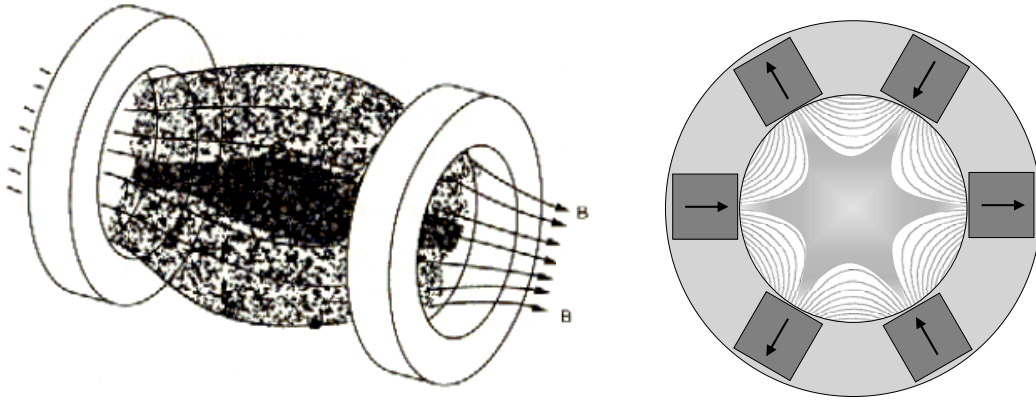


**Figure 2.9** Plasma trapped in a magnetic bottle generated by solenoids (on the left) [2] and permanent hexapole magnets (on the right).

### 2.5.1. Trapping of charged particles in the magnetic bottle

The condition for successful trapping of charged particles in a magnetic bottle can be derived from the conservation of energy and the magnetic moment  $|\vec{\mu}|$  of an individual particle [27]. It can be shown that the confinement of a charged particle depends only on the initial velocity components  $v_{\parallel}$  (parallel to the magnetic field) and  $v_{\perp}$  (perpendicular to magnetic field) as long as collisions do not cause the particle to scatter in a different direction. This can be explained as follows: in a uniform magnetic field there is no force that restricts the motion of the charged particle along the magnetic field (as it spirals around the field line) but in a magnetic bottle the force  $\vec{F} = -\mu\nabla\vec{B}$  restricts the motion in the direction of increasing magnetic field. As a consequence, the so-called loss cone in velocity space can be defined, with the aid of the magnetic field value at the location where the particle is created and the maximum magnetic field  $B_{max}$  (last possible turning point). In ECR ion sources it is reasonable to define the loss cone only for electrons since ions are highly collisional and their velocity components constantly changing. Furthermore, it can be assumed that free electrons are mainly created near the resonance zone. Consequently the pitch angle  $\theta$ , which defines the loss cone (see figure 2.10.) in the velocity space, can be written as

$$\theta = \arcsin\left(\frac{v_{\perp}}{v_{total}}\right) \cong \arcsin\left(\sqrt{\frac{B_{ECR}}{B_{max}}}\right) = \arcsin(R^{-1/2}), \quad (19)$$

where the subscript ECR refers to the magnetic field on the resonance and  $R = \frac{B_{\max}}{B_{ECR}}$  is the mirror ratio. Only particles whose pitch angle is greater than  $\theta$  (outside the loss cone) are confined in the magnetic bottle. If the pitch angle is less than  $\theta$ , the particle will be lost unless it scatters from the loss cone due to collisions. The perpendicular velocity of the electrons increases at the resonance as they gain energy from the microwaves and therefore become better confined. Their velocity vector moves outside the loss cone in velocity space because the parallel velocity component is not affected by the ECR-heating. However, overdense plasmas cannot be magnetically confined because the plasma oscillations perturb the motion of electrons in the magnetic field. Therefore mirroring of electrons is possible only if  $\omega_{ce} > \omega_{pe}$  [2].

The confinement time of electrons in an ECRIS plasma increases as the mirror ratio of the magnetic field increases, which leads to enhanced production of highly charged ions. For ECR ion sources it is reasonable to define axial and radial mirror ratios separately. According to the so-called magnetic field scaling laws the values of axial and radial mirror ratios  $R_{axial} = \frac{B_{injection}}{B_{ECR}}$  and  $R_{radial} = \frac{B_{radial}}{B_{ECR}}$  should be approximately 4 and 2, respectively. The magnetic field scaling laws were formulated on the basis of results presented by Gammino [28, 29]. Figure 2.10 presents the effect of increasing mirror ratio on the three dimensional loss cone in velocity space. Arbitrary units are used in the figure.

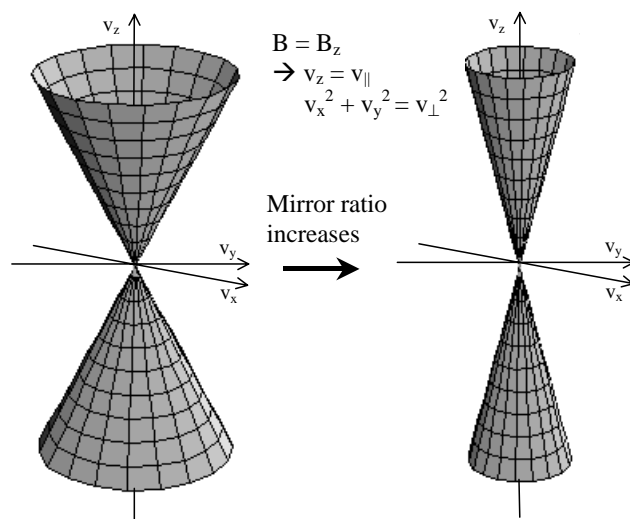


**Figure 2.10** The effect of increasing mirror ratio on the electron loss cone of the magnetic bottle in velocity space.

In an ECRIS the loss rate of charged particles in axial direction is dominated by the electron flux while the ion flux determines the radial diffusion (hexapole field was not included in the study) [30]. The extraction of highly charged ions from an ECRIS plasma can be considered as a favorable loss process, which takes place when the ions follow the electrons into the extraction. Theoretically, using a radial quadrupole field would be better for a plasma confinement device, as fewer magnetic field lines hit the walls resulting in less ion losses than in the case of hexapole field. However, the axial losses of a quadrupole do not concentrate like those of a hexapole, they spread radially, which is not convenient for ion beam extraction [31].

### 2.5.2. Plasma potential

One feature of an ECR-heated plasma is the positive plasma potential with respect to the walls of the plasma chamber. The potential builds up because electrons tend to diffuse out of the plasma faster than ions due to the higher mobility of electrons (see, for example, reference [32]). The electron diffusion is mainly due to low-energy electrons that are easily scattered into the loss-cone of the magnetic bottle, as their collision frequency with other electrons and ions depends on their energy as  $\nu_{ee,ei} \propto (kT_e)^{-3/2}$ . The positive plasma potential builds up to compensate the loss rates of positive and negative charge by retarding the losses of electrons and repelling ions [33]. The mobility of the ions  $\mu_i$  is defined by the formula

$$\mu_i = \frac{qe}{m_i \nu_{ij}}, \quad (20)$$

which implies that the plasma potential is higher for heavier ions (in a single-component plasma  $\nu_{ij} = \nu_{ji}$  depends on the ion mass as  $m_i^{-1/2}$ ). The value of the potential is on the order of tens of volts, being lower for well-performing ECR ion sources [32]. It is determined by the imbalance of charge densities (positive and negative) and therefore all the parameters such as microwave power and neutral gas pressure affecting the electron density or ion charge state distribution of the ECRIS plasma, for example, affect the value of the potential. It has been observed that a lower plasma potential coincides with the enhanced production of highly charged ions, probably because of the better ion confinement [34]. It has also been suggested that the stability of the plasma improves when the plasma potential is lower due to the reduced ion sputtering of the plasma chamber walls [35]. The positive plasma potential prevents low-energy electrons from escaping the plasma, which

causes the electron loss cone of the magnetic bottle to turn into a “loss hyperboloid”. This happens because the kinetic energy (velocity  $v = \sqrt{v_{\parallel}^2 + v_{\perp}^2}$ ) of the electrons has to be sufficient for them to overcome the potential barrier generated by the plasma potential. Figure 2.11 shows the effect of the plasma potential on the loss cone.

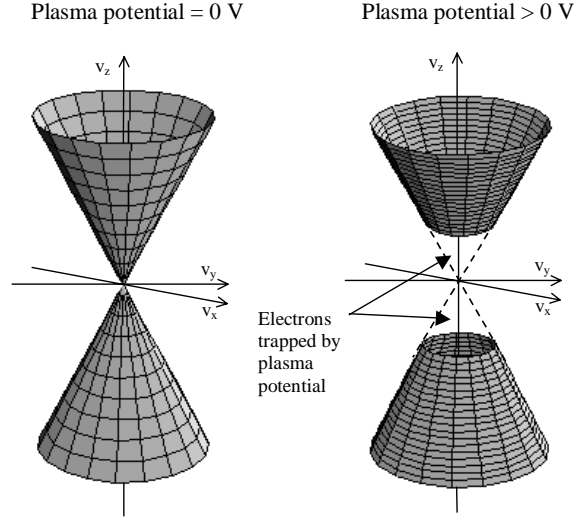


**Figure 2.11** The effect of non-zero plasma potential on the electron loss cone of the magnetic bottle in velocity space.

In principle, the plasma potential profile inside the plasma chamber of an ECRIS could be calculated from the electron and ion densities and their spatial distributions. The ion densities of different charge states have been estimated to be about or less than  $10^{11} \text{ cm}^{-3}$  [17]. The estimation was performed by measuring the density of  $\text{Ar}^{15+}$  ions by spectroscopic means and deducing the densities of other charge states from extracted ion currents. Although the measurements presented in reference [36] imply that highly charged ions are produced in the center of the plasma and low charge-state ions in the whole plasma volume, experimental data concerning the spatial distributions of ion densities for different charge states was not found. Therefore, the plasma potential profiles for ECRIS plasmas can be only estimated. According to Bibinov *et al.* [37] the plasma potential  $V_p$  of an ECRIS can be estimated to be

$$V_p = \frac{kT_{e,cold}}{2e} \left( 5.67 - \ln \left( \frac{q_{eff}}{A} \right) \right), \quad (21)$$

where  $T_{e,cold}$  is the temperature of the cold electron population,  $q_{eff}$  the mean charge of the ions escaping the plasma and  $A$  the mass number of these ions. Equation (21) gives the right order of magnitude for the plasma potential as long as ion-ion-collisions is the dominating collision process.

In order to model the ion confinement, it has been suggested that highly charged ions are trapped in a potential dip in the centre of the plasma [38]. The central dip would be caused by the strongly confined hot electron population, which has gained energy in the resonance. The existence of the potential dip requires the electron density to exceed the ion density in the centre of the plasma. Charge densities responsible for the plasma potential profile (minor excess of positive charge) also generate an electric field in the plasma. Figure 2.12 shows a possible charge density distribution and corresponding electric field and plasma potential profile in the plane perpendicular to the plasma chamber axis (in the middle of the plasma chamber). The charge density was assumed to be non-zero in the volume enclosed by the resonance zone. The maximum electron density was set to  $5 \cdot 10^{11}$   $1/\text{cm}^3$  and the ion density was chosen based on the results presented in reference [17], such that the resulting plasma potential was approximately 25 volts. The plasma was assumed to be elliptically symmetric and plasma dimensions typical for the JYFL 14 GHz ECRIS were used in the calculation; the plasma chamber radius  $r = 38$  mm ( $r = \sqrt{x^2 + y^2}$ ) and the radial distance from the chamber axis to the resonance  $r_{ECR} = 17$  mm. The boundary conditions for electric field and potential set by the conducting plasma chamber were taken into account in the calculations. The electric field was calculated by integrating over the charge density  $\rho$  (volume) (following from Maxwell's equation  $\vec{E} = \frac{1}{\epsilon_0} \int_V \rho(\vec{r})$ ) and the resulting potential profile by integrating the electric field in radial direction (following from the equation  $\vec{E} = -\nabla \phi$ ).

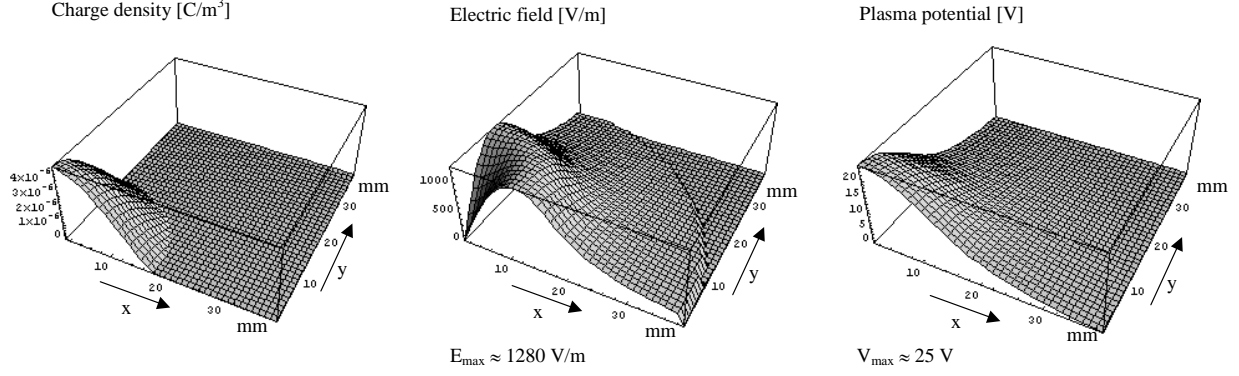


**Figure 2.12** Possible charge density distribution of an ECRIS plasma and corresponding electric field and plasma potential profile in the plane perpendicular to the plasma chamber axis. In the calculation the plasma was assumed to be elliptically symmetric and typical plasma dimensions for the JYFL 14 GHz ECRIS were used.

Figure 2.12 shows that in the plane perpendicular to the source axis the electric field corresponding to the plasma potential of 25 V (which is a typical value for the JYFL 14 GHz ECRIS) is on the order of 5-10 V/cm. The field strength in the plane parallel to the source axis is lower (3-7 V/cm) because the plasma dimension can be assumed to be larger in this direction, reflecting the shape of the resonance layer. This favors the conclusion that the electron flux dominates the axial particle losses while ions are diffused out of the plasma radially [30]. In the equilibrium state this ambipolar electric field balances the loss rates of negative and positive charge and therefore the ion losses from the ECRIS plasma can be modeled by ambipolar diffusion (see section 2.5.4.). The electric field affects the trajectories of charged particles spiraling around the magnetic field lines ( $\vec{F} = q\vec{E}$ ). The magnitude and direction of the electron (and ion) drift velocity  $v_{drift}$  due to the ambipolar electric field can be calculated from the equation

$$\vec{v}_{drift} = \frac{\vec{F} \times \vec{B}}{qB^2} = \frac{\vec{E} \times \vec{B}}{B^2}. \quad (22)$$

The first form of the drift velocity equation is applicable for all forces acting on the particles. For example, the drift velocity caused by the magnetic field gradient ( $\vec{F} = -\mu\nabla\vec{B}$ ) can be calculated from the equation.

### 2.5.3. Measurement of the plasma potential

Measuring the plasma potential of an ECRIS is an important matter, as according to reference [32], by lowering the potential one can improve the performance of the source. Measurement of the potential (and ion beam energy spread) gives valuable information for low energy beam transport simulations. The value of the plasma potential of an ECRIS plasma can be measured with at least three different methods:

- (i) The plasma potential can be deduced by inserting a Langmuir-probe (cold or emissive) directly into the plasma and measuring the particle fluxes as a function of the probe voltage [39, 40, 41]. In contrast to other methods described below, the probe can provide spatial information on the plasma potential. However, the probe disturbs the original plasma, for example by affecting the local electron density and electron energy distribution. In addition, the extracted ion beam currents of highly charged ions are reduced due to the probe.
- (ii) As the ions are extracted from an ECRIS they gain energy corresponding to the acceleration voltage (source potential) and plasma potential. If the source potential is known the plasma potential can be determined by measuring the magnetic rigidity of the ion beams with a dipole magnet [34, 42]. The plasma potential can be calculated from the equation

$$V_p = \frac{Qer^2}{2m_i} B^2 - V_{source}. \quad (23)$$

where  $Q$  is the ion charge state,  $e$  the elementary charge,  $r$  the bending radius of the magnet,  $B$  the measured magnetic field of the analyzing magnet,  $m_i$  the ion mass and  $V_{source}$  the source potential. Equation (23) does not take into account certain ion optical uncertainties such as the edge effects of the bending magnet. In order to achieve accurate results several measurements with different source voltages have to be performed. Special attention also has to be paid to collimation of the ion beams.

- (iii) Another possibility to determine the plasma potential is to measure the energy of the extracted ion beam by applying a decelerating voltage. The plasma potential can be

further deduced by measuring the beam current as a function of this voltage. This method has been used for an ECRIS plasma by Nadzeyka *et al.* who used a retarding field analyzer designed for atomic physics experiments to determine the plasma potential and energy spread of a 5 GHz ECRIS [43]. The operation of the plasma potential measurement instrument [44] developed for this work is based on this so-called retarding field method.

#### 2.5.4. Confinement of ions in ECRIS plasmas

In order to emphasize the difference between the confinement of electrons and ions in ECRIS plasmas it is essential to study their collision and gyration frequencies with the equations presented in the preceding chapters. If the electron density and Coulomb logarithm are again assumed to be  $5 \cdot 10^{11} \text{ cm}^{-3}$  and 12, respectively, the collision frequency for 1 keV electrons is approximately 26 kHz while the gyration frequency of the electrons in a 0.5 T magnetic field is 14 GHz. The collision frequency of  $^{40}\text{Ar}^{12+}$  ions ranges from 1 MHz up to tens of MHz depending on their thermal energy (see figure 2.7) while their gyration frequency in a 0.5 T magnetic field is approximately 2.3 MHz. The following conclusions can be drawn:

- (i) Ions are highly collisional compared to electrons and therefore ions with the same charge and mass are in thermal equilibrium (have the same temperature).
- (ii) Electrons are magnetically confined since their collision frequency is significantly lower than their gyration frequency (for all electron populations).
- (iii) Ions are not magnetically confined since their gyromotion in the magnetic field is strongly impeded by the collisions. Therefore, the confinement of ions has to be treated with diffusion models.

Before establishing a time hierarchy for ions in ECRIS plasmas, the concept of ion production time has to be considered. The production of multiply charged ions is dependent upon their ionization time,  $\tau_{ion}$  (the time required to ionize neutral atom to charge state  $q$ ), and the confinement time,  $\tau_{conf}$  (see equation 13), of each charge state [2]. The ionization and confinement times of different charge states can be extracted by studying the production times  $\tau_p$  ( $\tau_p = \tau_{ion} + \tau_{conf}$ ) and the beam intensities  $I_{q+}$ , together with ion densities  $n_q$  [17]. Table 2.2 shows production times for different charge states of  $^{40}\text{Ar}$  ions measured with a 14 GHz ECRIS at Argonne National Laboratory (ANL) and a fast-pulsed gas valve [45]. The production time was defined as being the time between the

introduction of the material of interest and the peak ion current produced through this material introduction. As table 2.2 shows, the production times increase with increasing charge state, being on the order of tens of milliseconds for highly charged ions. The production time was observed to be strongly dependent on the source settings (the values given here are the lowest that were reported for argon ions). The production times measured with lead (solid element) have been observed to be in the same range i.e. some tens of milliseconds [46]. The measurement was performed by pulsing the voltage applied to a sputter sample.

Charge state of $^{40}\text{Ar}$	1+	2+	3+	4+	5+	6+	7+	8+	9+	10+	11+	12+	13+
Production time [ms]	2	2	3	4	5	7	8	14	19	25	33	38	41

**Table 2.2** The production times of different charge states of  $^{40}\text{Ar}$ -ions measured with the 14 GHz ECRIS at ANL [45].

Some confinement times of different charge states for  $^{40}\text{Ar}$  ions deduced from measurements performed with the Caprice 10 GHz ECRIS are reported in reference [17]. The confinement times were estimated by measuring the ion densities and extracted beam currents. Figure 2.13 shows the calculated confinement times when the source was tuned for maximum output of  $\text{Ar}^{16+}$  (a) and  $\text{Ar}^{12+}$  ions (b), respectively.

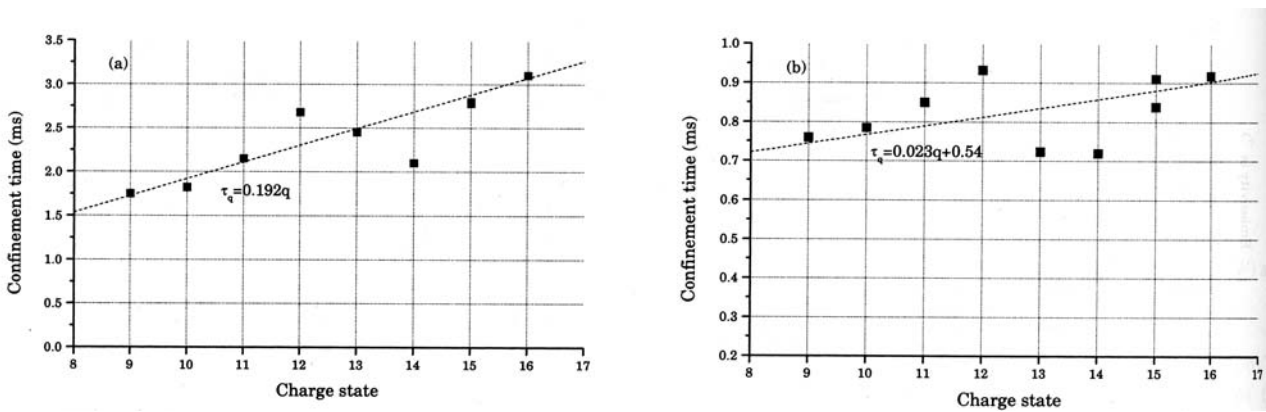


**Figure 2.13** Confinement times of  $^{40}\text{Ar}$  ions measured with the Caprice 10 GHz ECRIS. The source was tuned for maximum output of  $\text{Ar}^{16+}$  (a) or  $\text{Ar}^{12+}$  (b) [17].

Since the confinement times of different charge states of highly charged argon ions are in the range of 0.7-3.1 ms, it can be concluded that the main part of their rise time (tens of ms, see table 2.2.) is due to the ionization time. Moreover, the confinement times seem to be linearly dependent on the charge state of the ions.

The ion confinement in ECRIS plasmas can be treated theoretically with several models. In the following three ion confinement models will be discussed. As mentioned in section 2.5.2. it has been suggested that ions are trapped in a potential dip,  $\Delta\phi$ , in the central plasma, which leads into following formula [47] for ion confinement time

$$\tau_{conf} = R \frac{\pi^{1/2} L}{v_T} e^{\frac{|qe\Delta\phi|}{kT_i}}. \quad (24)$$

Here  $R$  is the mirror ratio,  $L$  the half-length of the plasma and  $v_T = \sqrt{\frac{2kT_i}{m_i}}$  the thermal velocity of the ions. However, this formula becomes questionable at high plasma densities, when the ions become very collisional [17]. In section 2.5.2. it was shown that the charge imbalance of the plasma that leads to a positive plasma potential also gives rise to an ambipolar electric field  $E$  inside the plasma chamber. Due to this electric field ambipolar diffusion affects the confinement of the ions in ECRIS plasmas. The ambipolar diffusion results in the following expression for the axial ion confinement time [17] (units:  $\tau$ , s;  $L$ , cm;  $n_e$ ,  $\text{cm}^{-3}$ ;  $T_i$ , eV;  $E$ , V/cm)

$$\tau_{conf} = 7.1 \cdot 10^{-20} L q \ln \Lambda \sqrt{A_i} \frac{n_e q_{eff}}{T_i^{3/2} E}. \quad (25)$$

The equation does not take into account radial ion losses. In addition to ambipolar diffusion, the ions experience a random thermal motion, which makes them diffuse out of the plasma. The axial confinement time related to this mechanism can be modeled as [17] (units:  $\tau$ , s;  $L$ , cm;  $n_e$ ,  $\text{cm}^{-3}$ ;  $T_i$ , eV)

$$\tau_{conf} = 7.1 \cdot 10^{-20} L^2 q^2 \ln \Lambda \sqrt{A_i} \frac{n_e q_{eff}}{T_i^{5/2}}. \quad (26)$$

Figure 2.14 shows the confinement times for  $^{40}\text{Ar}^{12+}$  ion calculated from these confinement models as a function of ion temperature. The following values typical of the JYFL 14 GHz ECRIS were used in the calculations:  $R = 4.2$ ,  $L = 4.5$  cm,  $n_e = 5 \cdot 10^{11} \text{ cm}^{-3}$ ,  $\ln \Lambda = 12$  and  $E = 4$  V/cm. The depth of the potential dip was assumed to be 1 V based on the discussion in reference [17].

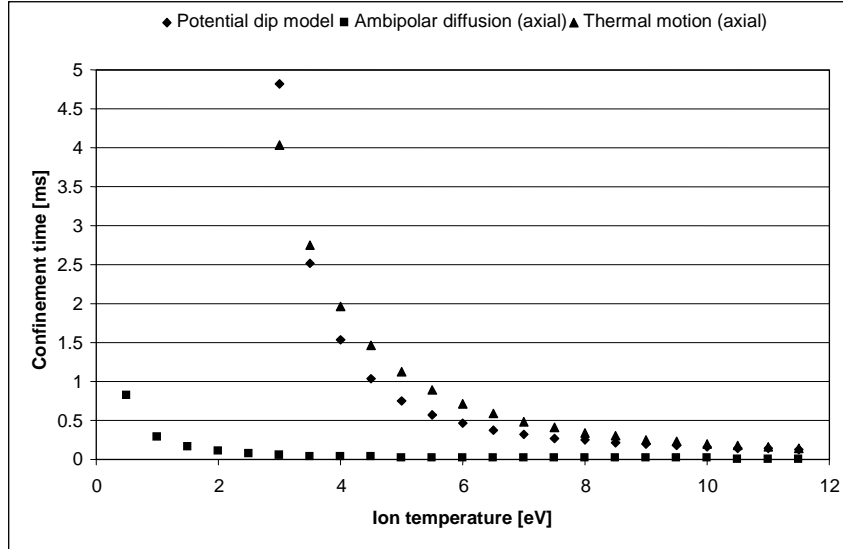


**Figure 2.14** The confinement time of  $^{40}\text{Ar}^{12+}$  ions as a function of the ion temperature calculated with different models: potential dip model (equation (24)), ambipolar diffusion model (equation (25)) and thermal motion model (equation (26)). Plasma parameters typical of the 14 GHz ECRIS were used in the calculations.

The figure shows that confinement times calculated from the (axial) ambipolar diffusion model are significantly lower than confinement times calculated from the other models with ion temperatures less than 10 eV. According to the measurement results presented in reference [17] (see figure 2.13.) the confinement time of  $^{40}\text{Ar}^{12+}$  ions is in the range of 0.9-2.7 ms. Therefore it seems that the ambipolar diffusion model results into too short confinement times even with very low ion temperatures ( $\approx 1$  eV). However, if the ion temperature is assumed to be independent of the charge state, it is the only model that gives the correct (linear) dependence on the ion charge. The other models (equations (24) and (26)) lead to the correct order of magnitude for the confinement time when the ion temperature is between 4 and 8 eV. The confinement times calculated from these models depend strongly on the ion charge, which is contradictory to the measurements showing a linear dependence on the charge state. However, if the ion temperature increases with increasing charge state, confinement times calculated from the thermal diffusion model would not depend strongly on the charge state since according to equation (26)  $\tau_{conf} \propto \frac{q^2}{T_i^{5/2}}$ . Another remark that can

be made based on the calculations shown in figure 2.14. is that if there was a potential dip in the core of ECRIS plasmas, it would be very shallow (around 1 V). The confinement times of ions depend exponentially on  $\Delta\phi$  and therefore, even a small increase of  $\Delta\phi$  would cause the confinement times to significantly exceed the confinement times deduced from the experimental data. The potential dip model is most probably well-suited to low-collisional hydrogen plasmas

typical for fusion devices, but not adapted to the rather cold collisional heavy ions of ECRIS plasmas [17].

In order to summarize the physics of ions in ECRIS plasmas the hierarchy of times for  $\text{Ar}^{12+}$  ions is presented in table 2.3 including ion-ion collision time  $\tau_{ii}$ , cyclotron period (gyration time)  $\tau_{ic}$ , confinement time  $\tau_{conf}$ , production time  $\tau_p$  ( $\tau_p = \tau_{ion} + \tau_{conf}$ ) and electron-ion energy equipartition times  $\tau_{eq,e \rightarrow i}$  with different electron populations. The given confinement and production times are based on experimental results presented in references [17] and [45], respectively. The temperatures of the electron populations were assumed to be 20 eV (around the plasma potential), 1 keV and 100 keV while the ion temperature was assumed to be 3 eV. The same plasma parameters as in the previous calculations were used. Changing the plasma parameters in the range, which is typical to ECR ion sources does not affect the order of magnitude of the values given in table 2.3. The times presented in the table are given in seconds.

$\tau_{ii} (T_i = 3 \text{ eV})$	$\tau_{ic}$	$\tau_{conf}$	$\tau_p$	$\tau_{eq,e \rightarrow i} (T_e = 20 \text{ eV})$	$\tau_{eq,e \rightarrow i} (T_e = 1 \text{ keV})$	$\tau_{eq,e \rightarrow i} (T_e = 100 \text{ keV})$
$7.0 \cdot 10^{-8}$	$4.4 \cdot 10^{-7}$	$\approx 2 \cdot 10^{-3}$	$\approx 40 \cdot 10^{-3}$	$47 \cdot 10^{-3}$	8.2	$8.2 \cdot 10^3$

Table 2.3 The hierarchy of times (in seconds) for  $\text{Ar}^{12+}$  ions in ECRIS plasmas.

The table shows that ions in ECRIS plasmas are not magnetically confined since their collision time is of the same order of magnitude as their cyclotron period. The confinement time of the ions is long enough (on the order of milliseconds) to obtain high charge states. The energy equipartition time of ions with the warm and hot electron populations is significantly higher than their production time and therefore it can be concluded that the electrons, which have gained energy at the resonance, do not heat the ions efficiently. In reference [22] it was reported that the ion temperature in ECRIS plasmas is only a few eV and that all ions have the same temperature. However, as table 2.3 shows the rise time of  $\text{Ar}^{12+}$  ions ( $\approx 40$  ms) is on the same order of magnitude as the energy equipartition time of the ions and the low-energy electron population. Therefore, it can be expected that ions have enough time to gain energy from the cold electron population. Another process that could heat the ions in an ECRIS plasma even more effectively than electron-ion collisions is the absorption of the ion sound wave [48, 49]. The ion sound wave is generated as the incoming electromagnetic wave decays into a high frequency upper hybrid wave and a low frequency ion sound wave due to non-linear processes. The ion sound wave induced ion heating depends quadratically on the ion charge [48, 49]. Therefore, it would be reasonable to expect the ion

temperature to increase with increasing charge state as their production time (the time that ions spend in the plasma) increases and ion sound wave heating becomes more efficient. The low charge-state ions do not have enough time to gain energy from the cold electron population while the temperature of highly charged ions can be close to the temperature of the low-energy electrons [48, 49]. Moreover, if the production time of highly charged ions exceeds the energy equipartition time with the cold electron population it can be assumed that all high charge states have the same ion temperature. In this case the best model to describe the ion confinement would be equation (26) that gives the right order of magnitude for the confinement times.

### 3. PRODUCTION OF HIGHLY CHARGED ION BEAMS WITH ECR ION SOURCES

Electron cyclotron resonance ion sources are highly versatile and ion beams from various elements, including radioactive isotopes, can be produced with them. Consequently, a number of new nuclear physics experiments have been carried out using ECR ion sources. However, some projectile-target combinations have extremely small reaction cross sections. Therefore it is necessary to pay attention to the performance of the ion source and the quality of the ion beams in order to achieve adequate beam currents and charge states. In this chapter, commonly used techniques to improve the performance of ECR ion sources and methods to ionize different elements will be discussed. Also the extraction of ion beams and factors affecting their quality will be considered.

#### 3.1. Methods to improve the performance of ECR ion sources

The requirements for production of multiply charged ions with ECR ion sources can be summarized as follows [8, 2]:

- (i) The electron energy in ECRIS plasmas has to be sufficient for ionization of the atoms to the required charge state.
- (ii) The confinement time  $\tau_{conf}$  of the ions has to be long enough to obtain high charge states.
- (iii) In order to reach high charge states it is necessary that the electron density,  $n_e$ , of the plasma is adequate.
- (iv) The neutral pressure has to be low enough in order to minimize recombination processes, in particular charge exchange.

The probability to produce highly charged ions is assumed to be proportional to the product  $n_e \cdot \tau_{conf}$ . The following commonly used methods to improve the performance of ECR ion sources are therefore somehow related to either increasing the electron density or the confinement time of the ions (or both). However, it has to be kept in mind that operation of an ECRIS involves making compromises. For example, it is not desirable to increase the confinement time of ions at the expense of decreasing the extracted beam currents, or to increase the gas feed rate in order to achieve higher densities at the expense of multiplying the rate of charge exchange.

### 3.1.1. Wall coating and plasma chamber material

The beneficial effect of wall coating was discovered by Lyneis *et. al.* [50]. The currents of highly charged oxygen ion beams increased by a factor of 2 after the source had been operated with SiH<sub>4</sub> gas. During the silicon-run the surface of the plasma chamber was covered by a silicon oxide layer. Two explanations were given for the improved performance [50]: (i) The secondary electron emission coefficient for the silicon oxide layer is substantially higher than for the clean copper chamber. Therefore the electron density of the plasma is increased due to cold electrons emitted from the walls of the plasma chamber. (ii) The plasma potential is modified by the insulating properties of the silicon oxide layer.

Similar improvements have been obtained by coating the plasma chamber with aluminum oxide [51] or by manufacturing the whole chamber out of aluminum [52]. A variation of the wall coating method is to use an aluminum liner that is inserted into the plasma chamber. For example, in reference [53] the aluminum liner was covered with a metal-dielectric layer of aluminum oxide with high secondary electron emission coefficient. The plasma chambers of modern ECR ion sources are usually made of aluminum or stainless steel (instead of copper, which was commonly used earlier). Table 3.1 shows the secondary electron emission coefficients  $\delta$  and optimal electron impact energies  $E_{\delta_{max}}$  for some materials [24].

Material	Al	C (soot)	Cu	SiO <sub>2</sub>	Al <sub>2</sub> O <sub>3</sub>	MgO
$\delta$	1.0 – 1.2	0.45	1.3	2.1 - 4	2 - 9	3 – 15
$E_{\delta_{max}}$ [eV]	300	500	600	400	-	400 - 1500

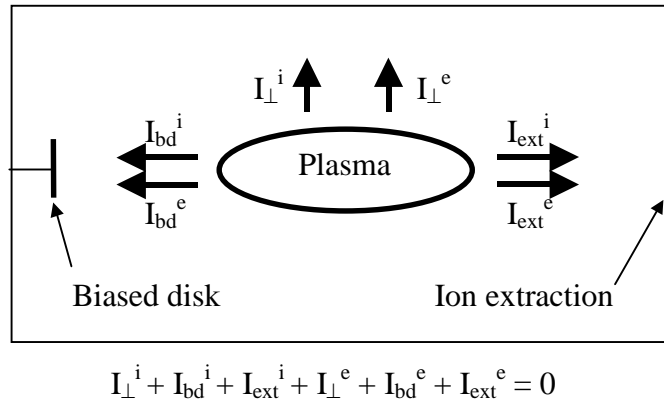
**Table 3.1** Secondary electron emission coefficients and optimal impact energies for some materials related to ECR ion sources [24].

Table 3.1 implies that the improved performance of the ion source due to oxide layers (silicon or aluminum) can be explained by higher secondary electron emission that affects the electron density of the plasma. Another method, in addition to wall coating, to directly increase the electron density of ECRIS plasma is to use an electron gun [54]. However, this method has not become widely applied due to the problems of stabilizing the output of highly charged ions.

**3.1.2. Biased electrode technique**

The first experiments on the application of a probe, insulated from the plasma chamber are reported in reference [55]. It was observed that by using a negatively biased disk (with a voltage of a few hundred volts with respect to source voltage) at the injection end of the plasma chamber, the intensities of highly charged ion beams could be increased significantly. Practically all new ECR ion sources are equipped with such a biased electrode [32].

Several experiments have been performed to explain the beneficial effect of the biased electrode. These include for example tests with a movable disk [56], tests with different sizes and shapes of disk [57] and tests with a pulsed disk [58]. The effect of the biased disk can be explained by studying the changes in the current system of the ECRIS plasma chamber i.e. so-called Simon short-circuit currents (see for example reference [59]). A schematic drawing of the Simon short-circuit current system in an ECRIS is presented in figure 3.1 showing also the balance equation of currents due to electron and ion losses. Note that the arrows in the figure indicate the direction of particle fluxes and that the (electric) current due to electron losses points to the opposite direction. The drain current of the ion source indicating the total extracted beam current is included in extraction end currents  $I_{ext}$ .



**Figure 3.1** Simon short-circuit currents in the ECRIS plasma chamber. The direction of the arrow shows the particle flux.

By applying a negative voltage to the biased disk the electron flux at the injection end of the source can be decreased as the disk repels electrons, which causes the electron density of the plasma to increase. However, to satisfy the current balance condition shown in figure 3.1 the ion fluxes (mainly in radial direction;  $I_{\perp}^i$ ) out of the plasma have to decrease. As a consequence, the source

performance improves not only because of the increased electron density but also because of longer ion confinement time. It has been observed recently that by placing a positively biased cylinder on the inner wall of the plasma chamber the extracted currents of high charge states can be increased [30]. This effect can also be explained by studying the Simon short-circuit currents of the ECRIS plasma chamber.

#### 3.1.3. *Gas mixing*

The gas mixing effect was discovered in the early 1980's by Drentje [6]. By adding a lighter element (excluding hydrogen) to the plasma, the intensities of highly charged ion beams produced from the heavier element can be increased. The fact that hydrogen is not a suitable mixing gas has been connected to the formation of negative hydrogen ions [60]. Since the discovery of the technique, various explanations for its beneficial effects have been suggested. According to reference [61] these explanations include

- (i) A dilution effect [62]; lowering the average charge state, which reduces the electron loss rate and thereby increases the electron density of the plasma.
- (ii) An ion cooling process due to the mass effect [63] in ion-ion collisions in conjunction with effective transport of ion (thermal) energy out of the plasma by the low mass and charge ions [64].
- (iii) Increase of the electron density due to improved ionization efficiency [65, 66].
- (iv) Decrease of the plasma potential resulting in better ion confinement and stability of the plasma [34, 67].

The present understanding of ECRIS plasmas favors the explanation based on the mass effect i.e. ion cooling in ion-ion collisions. Ion cooling has been experimentally studied by feeding a gas mixture consisting of  $^{18}\text{O}$ ,  $^{17}\text{O}$  and  $^{16}\text{O}$  having the same electronic properties into an ECRIS (see for example [68]). The output of high charge states was observed to be the best for the heaviest isotope (so-called isotope anomaly) supporting the existence of the mass effect. The simplest example to demonstrate the ion cooling process is to assume that ions experience head-on-collisions with each other [69]. With this model it can be seen that the thermal energy of the heavier ion decreases in the collision with the lighter ion (having the same initial thermal energies). A sophisticated model of the effects of ion cooling on ion temperature can be found from reference [22]. In that study oxygen was found to be a good mixing gas not only because of its rather low mass but also because of the

low ionization potential. However, the model assumes that the temperature of different ion species is the same, which is contrary to very recent measurement results [70] and calculations [49] implying that lighter ions are heated more effectively than heavier ions. The measurements indicated that ion cooling cannot solely explain the isotope anomaly if the ion temperature is assumed to be equal for all ion species and therefore a mass selective heating process i.e. ion Landau damping (of ion acoustic wave) was introduced in reference [70].

The ion cooling mechanism can be effective only if the average ion temperature of the plasma decreases. Therefore lighter ions with lower average charge have to transfer the energy out of the plasma effectively. This would mean that their ionization efficiency decreases compared to a pure plasma of lighter ions, which has been confirmed experimentally [66]. From equations (24) - (26) it can be seen that the confinement time of ions should increase when the ion temperature decreases regardless of the model used to calculate the confinement time.

#### ***3.1.4. Multiple frequency heating***

It has been demonstrated that the production of highly charged ion beams with ECR ion sources can be improved through the use of multiple frequency heating, which provides additional resonance surfaces for electron heating [71, 72]. At Argonne National Laboratory (ANL) it has been found with a traveling wave tube amplifier (TWTA) that it is beneficial to tune the secondary (and tertiary) frequency [73, 74] to maximize the output of highly charged ions. Double frequency heating with a tunable TWTA has also been utilized at JYFL and preliminary tests with three frequencies have been performed. In this case both secondary frequencies were launched through the same TWTA and the results are presented in ref. [75]. Figure 3.2 shows the extracted currents of different xenon ( $^{136}\text{Xe}$ ) ion beams for single (14 GHz / klystron) and double frequency heating modes (14 + 11.39 GHz / klystron + TWTA) measured with the JYFL 14 GHz ECRIS. Also, the improvement factor of the beam current due to two frequency heating is presented.

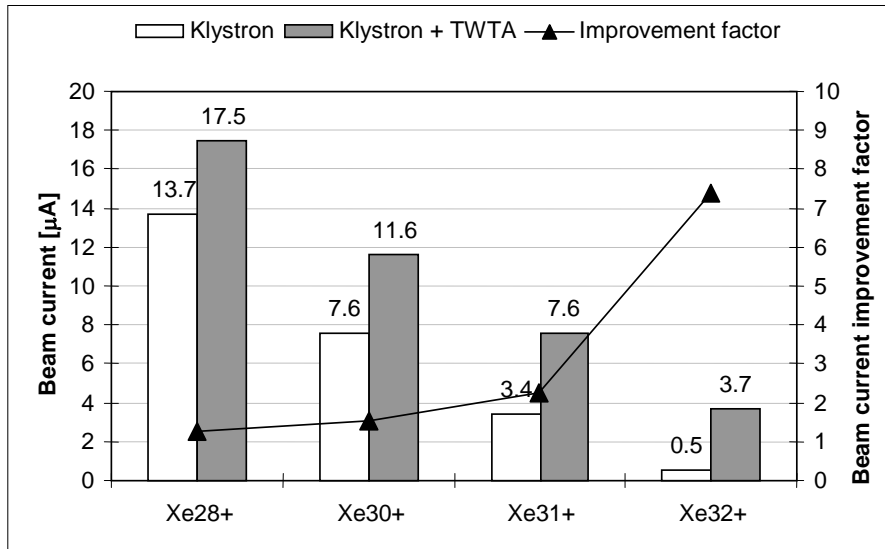


**Figure 3.2** The improvement of  $^{136}\text{Xe}$  ion beam currents when double frequency heating is used.

The physical processes affecting the performance of ECR ion sources due to the secondary frequency are mainly unknown. It has been observed experimentally that

- (i) The secondary resonance improves the production of highly charged ions and shifts the charge state distribution (CSD) towards higher charge states [73].
- (ii) The frequency gap between separate resonances should be adequate [73].
- (iii) The production times of highly charged ions decrease due to the secondary frequency [46].
- (iv) The plasma potential is slightly lower in double frequency heating mode compared to single frequency heating mode [76, 77, 46]. It has been proposed that the plasma potential profile could be modified by the secondary resonance [46].
- (v) The use of the secondary frequency makes it possible to reduce the consumption rate of the ionized material (observed at ANL [78] and at JYFL)

The improved intensities of highly charged ions together with decreased production times imply that the electron density is affected by the secondary resonance. A possible explanation for this is the randomization of the phase difference between electrons and microwaves at discrete resonance zones, which improves the confinement of electrons due to more effective ECR heating. Based on the results (i) - (v) it is impossible to deduce whether the confinement time of ions is simultaneously affected or not.

Multiple frequency heating experiments have shown that the performance of ECR ion sources can be enhanced by increasing the physical sizes or numbers of discrete resonant zones embedded within their plasma volumes. The resonance volume can be increased also by using a broadband rf-generator equipped with a traveling wave tube amplifier. The beneficial effects of broadband microwave radiation have been observed with the JYFL 6.4 GHz ECRIS [79]. The results of these studies have shown that high-charge-state beams (e.g., Ar<sup>11+</sup> and higher) can be enhanced by factors > 2 with broadband microwave radiation (200 MHz bandwidth) compared to those powered with narrow bandwidth (~1 MHz) radiation. Results speaking for the beneficial effect of broadband radiation have also been reported by Celona *et al.* [80] who compared the ion output of the SERSE ECR ion source [81] with klystron-based and TWT-based microwave generators with different bandwidths.

### ***3.1.5. Afterglow and long pulse operation modes***

ECR ion sources can be operated in two modes; in continuous mode and in afterglow mode. When the microwave power heating the electrons on the resonance is switched off, the intensities of highly charged ion beams increase and the charge state distribution shifts towards higher charge states. This rather peculiar phenomenon can be exploited by pulsing the microwaves so that the pulse length is on the order of 100  $\mu$ s with a pulse spacing of around 500  $\mu$ s [2]. However, the ion beams produced in this mode, called afterglow, are pulsed and therefore not applicable to cyclotrons.

The explanation for the increased beam currents after switching off the microwave power is based on the fact that at the resonance electrons gain energy (velocity) in the perpendicular direction with respect to the magnetic field. Therefore, due to ECR-heating a certain electron population is actively removed from the loss cone, which is defined in the velocity space (see figures 2.10 and 2.11). As the microwave power is turned off, the population that has been confined by the additional  $v_{\perp}$  provided by the resonance heating is no longer confined. These electrons can leak through the magnetic trap dragging ions with them. Additional ion losses contribute to extracted beam currents, which therefore increase. During the afterglow pulse the plasma state is maintained by the well-confined hot electrons that can be trapped for several milliseconds [2].

A “combination” of continuous and afterglow modes is so-called long pulse operation mode, which can be exploited for injection into accelerators. In this mode the accelerator utilizes the full length

of the beam pulse rather than the afterglow part only. The advantage of long pulse operation is that fewer neutrals accumulated on the walls of the plasma chamber circulate back to the plasma, which causes the charge state distribution of extracted ion beams to shift towards higher charge states compared to operation with continuous beam.

#### **3.2. Methods for introduction of material into the ECRIS plasma**

Electron cyclotron resonance ion sources can be used to produce multiply charged ion beams from a great variety of different elements. In order to carry out new experiments in the field of nuclear and applied physics several methods for introduction of material into ECRIS plasmas have been developed. Selection of the method depends mostly on the properties of the element. In the following the most common methods will be presented. In addition to the methods described here there are a few rarely used techniques including wall recycling [82], the insertion technique [83] and the laser ablation method [84], for example.

##### ***3.2.1. Gaseous elements and compounds***

The easiest means to introduce material into the plasma is to use elements or compounds that are gaseous at room temperature. These materials include for example noble gases (He, Ne, Ar, Kr, Xe) and compounds such as CO<sub>2</sub>, SiH<sub>4</sub>, BF<sub>3</sub>, CCl<sub>4</sub> and UF<sub>6</sub>. The material is normally fed into the plasma with a rate of 0.1-1 cm<sup>3</sup>/h (NTP). The molecules are dissociated and ionized in the plasma as a consequence of collisions with energetic electrons. With this method the ion source can be operated for a very long period of time without having to readjust the plasma conditions. However, the selection of appropriate materials is limited.

##### ***3.2.2. Evaporation oven***

Evaporation ovens can be used to produce ion beams from materials that are solids at room temperature. The maximum operating temperature of a modern miniature oven is about 2000 °C, which requires the heating process to be very localized and the radiative losses to be diminutive. At this temperature the vapour pressure of most materials is high enough for sufficient material evaporation. Resistively heated ovens can be used to produce ion beams from numerous materials such as Al, Cu, Ca, Bi and U, for example. The first resistively heated external ovens for the production of ion beams from solids were developed at Lawrence Berkeley National Laboratory

(LBNL) [85]. Since then ovens have been improved by several groups by choice of. For example, figure 3.3 shows a recently developed high temperature oven with a maximum operation temperature of about 2000 °C [86].

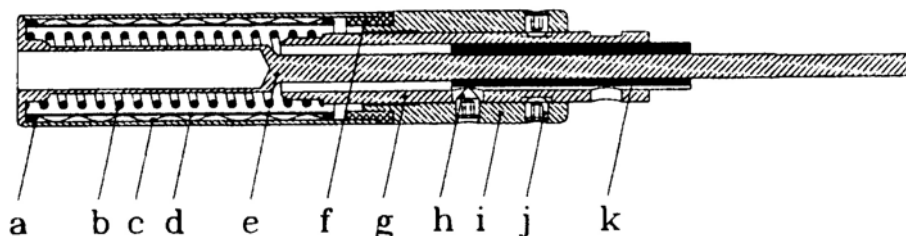


**Figure 3.3** The GSI high temperature oven [86]. (a) Ta cylinder, (b) heating wire, (c) reflection foil, (d) heat shield, (e) crucible holder, (f) ceramic ring, (g) filament holder, (h) grub screw, (i) oven guidance (j) grub screw (k) ceramic tube.

The gas mixing technique (normally nitrogen or oxygen) is often used together with evaporation ovens. The main problem of resistively heated evaporation ovens is the low ionization efficiency, approximately 10 % [87]. As a consequence the material consumption rate is rather high, which is a considerable problem in the case of expensive isotopes such as  $^{48}\text{Ca}$ .

### 3.2.3. The MIVOC method

The MIVOC method [7] is based on the fact that the consumption rate of a gaseous feed material in an ECR ion source can be quite low, of the order of  $0.1 \text{ cm}^3/\text{h}$  (NTP) in appropriate gas mixing conditions. It is thus possible to feed the ECRIS plasma with a low-pressure vapor of a volatile chemical compound kept at room temperature if the conductance of the feed line between the ECRIS plasma and the MIVOC chamber is sufficient. The molecules are allowed to flow from the MIVOC chamber into the plasma where energetic electrons break the compound molecules into individual atoms. These atoms are ionized and then extracted from the ion source. Utilization of the MIVOC method sets two demands for the compound: the evaporation rate of the compound has to correspond to the consumption rate of the ion gas and the element of interest has to be the heaviest atom in the compound to keep the ionization efficiency high. The MIVOC method can be used to produce ion beams from, for example, Mg, Ti, Fe, Ni, Ga and Zr.

Most of the MIVOC-compounds (such as ferrocene  $\text{Fe}(\text{C}_5\text{H}_5)_2$ ), contain carbon atoms. As a consequence, the drawback of the MIVOC method is carbon contamination of the plasma chamber.

A carbon layer on the plasma chamber surface affects the performance of the ion source by reducing the number of secondary electrons emitted from the walls of the chamber. Because the carbon layer is a better absorber of the energy of microwaves compared to the metal surface of the plasma chamber, it can also have an effect on the Q-value of the plasma chamber due to diminished multi-pass coupling of the electromagnetic waves and plasma [2]. This eventually affects the performance of the ion source. Carbon contamination of the plasma chamber can be prevented by using a liner. However, the liner becomes contaminated which also decreases the performance of the ion source.

#### ***3.2.4. Sputtering***

The sputtering method can be used to produce ion beams from refractory elements. In this method a material sample is placed into the plasma chamber. A negative voltage is applied to the sample in order to accelerate the ions of the plasma towards it. With the aid of the energy provided by the bombarding ions, atoms can be removed from the bulk material. The proportion of disengaged atoms with respect to bombarding ions is called the sputtering yield. The yield depends on the properties of the target, such as sublimation energy of the sputtered material, the mass and energy of the bombarding ions and the angle of incidence. The special features of ECR ion sources set two major restrictions for the sputtering method. The mixing gas that is used to maintain appropriate plasma conditions and to provide the sputtering ions has to be lighter than the element to be sputtered. Otherwise the intensities of desired ion beams would decrease dramatically due to the mass effect considered in section 3.1.3. Another restriction is the voltage applied to the sample. In order to obtain high sputtering yields, voltages from -2 to -10 kV have to be used. However, the negative voltage of the sample affects the plasma conditions because the sample acts as a source of neutrals and because an electric field causing the charged particles to drift is generated. Therefore it is not beneficial to use too high voltages in order to maximize the sputtering yield.

The sputtering method was used for the production of multiply charged ion beams with ECR ion sources for the first time at Argonne National Laboratory [88]. This method can be used to produce ion beams from Ti, V, Cr, Fe, Ni, Cu, Zn, Zr and Au, for example. The consumption rate of the material is usually in the range of 0.2...1 mg/h corresponding to the material consumption rate of miniature ovens for similar beam intensities.

### 3.3. Ion beam extraction and the quality of ion beams produced with ECR ion sources

The multiply charged ions produced in the ECRIS plasma are extracted with the aid of high voltage. In the extraction area the ions experience an electric field, which accelerates them into the beam line. The quality of the ion beams is mainly determined at the extraction. In this section the beam intensity restrictions set by the ion extraction and the plasma properties affecting the beam quality are treated.

#### 3.3.1. The plasma meniscus and Child-Langmuir law

The trajectories of the accelerated ions which determine the beam quality at the extraction, are influenced by several factors such as electric and magnetic field strengths, the shape of the emitting plasma surface and space-charge density of the beam itself [89]. The boundary layer between the plasma and the extracted ion beam is called the plasma meniscus. The depth, position and curvature of this layer depend on the plasma density and temperature of electrons and ions. Figure 3.4 presents the plasma meniscus in three cases: (a) overdense, (b) intermediate density and (c) underdense plasmas [89]

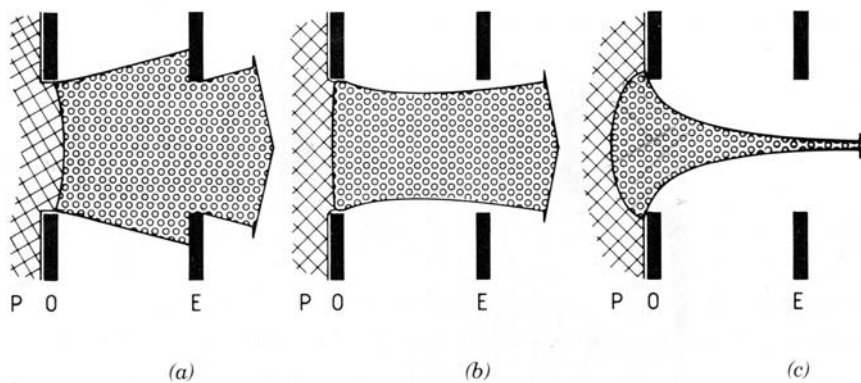


**Figure 3.4** The plasma meniscus for (a) overdense plasma, (b) intermediate density plasma and (c) underdense plasma. The notation P refers to plasma, O to outlet electrode (plasma electrode) and E to extraction electrode.

For overdense plasma (a) the meniscus is convex and a significant number of ions are lost as they hit the extraction electrodes. In the case of intermediate plasma density (b) the beam is better matched to the extraction, which makes this shape of plasma meniscus the most attractive regarding the extraction design. Finally, for underdense plasma (c) the meniscus is concave and although the beam is not lost at the extraction area, the space charge of the beam will create significant problems (beam blow up) further down the beam line. However, the magnitude of this effect depends on the

beam current. In order to achieve adequate beam extraction conditions (optimal shape of the plasma meniscus), the plasma properties of the ion source including plasma density, plasma potential and ion temperature, have to be taken into account when designing the extraction. The shape of the plasma meniscus is directly related to the plasma density while plasma potential and ion temperature affect the longitudinal and transversal momentum spread of the extracted ion beam.

The maximum current density  $j$  in units of mA/cm<sup>2</sup> that can possibly be expected for ion beams accelerated by an electric field is obtained under space-charge limited conditions and follows the Child-Langmuir law (a planar plasma meniscus is assumed) [89]

$$j \cong 1.73 \sqrt{\frac{Q}{M}} \frac{V^{3/2}}{d^2}. \quad (27)$$

Here  $Q$  is the charge state of the ion beam,  $M$  the ion mass [amu],  $V$  the acceleration voltage in kV and  $d$  the (first) extraction gap in cm. This equation holds under space-charge limited conditions i.e. when the ion source is capable of producing more ions than can be removed (per unit time). It is of note that if the ion beam is partly space-charge neutralized (accel-decel extraction system), the current density can slightly exceed the value given by the Child-Langmuir law.

### 3.3.2. Emittance and brightness of an ion beam

The quality of the ion beam extracted from an ion source is characterized by the beam emittance and brightness. For high quality ion beams the emittance should be as small as possible and the brightness as high as possible. The emittance of an ion beam describes the relative position and divergence of the beam particles i.e. the tranverse momentum of the ion beam. The root mean square emittance  $\varepsilon^{xx'-rms}$  of an ion beam can be defined as

$$\varepsilon^{xx'-rms} = \sqrt{(\overline{x^2} \cdot \overline{x'^2}) - (\overline{xx'})^2}, \quad (28)$$

in which the averages of the phase space coordinates  $x$  (position) and  $x'$  (divergence) are weighted by the beam intensity [89]. The area of the  $(x, x')$  phase space occupied by the beam i.e. the emittance  $\varepsilon^{xx'}$  and the normalized rms-emittance  $\varepsilon^{xx'-rms-norm}$ , which is independent of the beam

energy, can be further expressed as  $\varepsilon^{xx'} = 4\varepsilon^{xx'-rms}$  and  $\varepsilon^{xx'-rms-norm} = \beta\gamma\varepsilon^{xx'-rms}$ , respectively [89].

Here  $\beta = v/c$  and  $\gamma = 1/\sqrt{1-\beta^2}$  are the relativistic variables. The most comprehensive quantity that describes the beam quality is the beam brightness  $B_{beam}$ , which relates the beam current  $I$  and two transverse emittance values as (in the case of cylindrical symmetry the emittance in different planes,  $x$  and  $y$ , is the same)

$$B_{beam} = \frac{I}{\varepsilon^{xx'}\varepsilon^{yy'}}. \quad (29)$$

Two dominant factors contribute to the emittance of ion beams extracted from an ECRIS; ion temperature [89] and induced beam rotation caused by the magnetic field at extraction [90]. The normalized root mean square emittance of the ion beam in units of  $\pi$ -mm-mrad can be calculated theoretically from the following equation;

$$\varepsilon^{xx'-rms-norm} = \frac{0.0164r}{\pi} \sqrt{\frac{kT_i}{M}} + \frac{0.0402Br^2}{\pi} \frac{Q}{M}, \quad (30)$$

in which  $r$  is the radius of the extraction aperture [mm],  $kT_i$  the ion temperature [eV],  $M$  the ion mass [amu],  $B$  the magnetic field at extraction [T] and  $Q$  the charge state of the ion beam. Based on equation (30) the following conclusions can be made

- (i) The emittance of the ion beams should be dominated by the contribution of the magnetic field since according to theoretical estimations the ion temperature in an ECRIS plasma is only a few eV [22].
- (ii) The dominance of the emittance due to the magnetic field over the emittance due to ion temperature is smaller for low-charge state ions.
- (iii) The effective extraction radius of different charge states affects their emittance significantly. It has been deduced that highly charged ions originate near the source axis [36] while the low charge-state ions are produced in the whole plasma volume, which means that the effective extraction radius is smaller for highly charged ions. This reduces the dominance of the magnetic field emittance ( $\propto r^2$ ) over the ion temperature emittance ( $\propto r$ ) for highly charged ions.

- (iv) The emittance should increase with increasing charge state, which is contradictory to measurement results (see for example reference [91]). However, charge-state dependent effective extraction radii can explain this discrepancy.

These aspects are demonstrated in figure 3.5. Figure 3.5.a shows theoretically calculated contributions of the ion temperature and magnetic field to the emittance values (normalized rms-emittance) of different oxygen ion beams with an ion temperature of 5 eV. The total emittance is also presented in the figure. The influence of the effective extraction radius is demonstrated in figure 3.5.b, assuming the extraction radius to be 4 mm for  $O^+$  ions and to decrease linearly with increasing charge state to 1.6 mm for  $O^{7+}$  ions. This corresponds roughly to the estimation based on measurements presented in reference [91]. The same ion temperature (5 eV) was used in the calculation. In both cases the magnetic field at the extraction was chosen to be 0.9 T, which approximately corresponds to the field of the JYFL 14 GHz ECRIS.

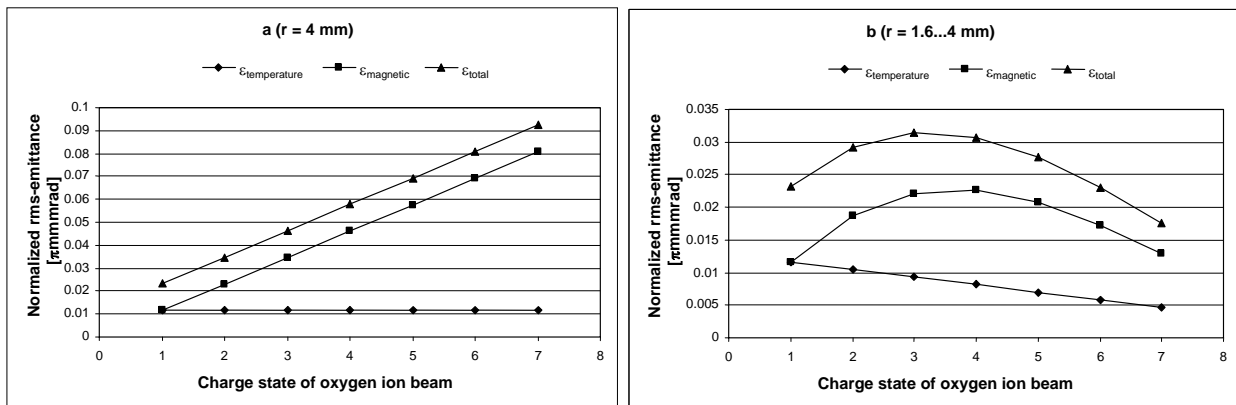


**Figure 3.5.** (a) Theoretical contributions of the ion temperature (5 eV) and magnetic field (0.9 T) to the emittance values of oxygen ion beams calculated from equation (30). (b) The effect of different effective extraction hole radii ( $r$ ) decreasing linearly from 4 mm for  $O^+$  to 1.6 mm for  $O^{7+}$  on the emittance.

Equation (30) does not take into account the effect of the hexapolar magnetic field on the emittance of ion beams extracted from an ECRIS. The hexapole field causes a strong plasma density variation in azimuthal direction resulting in azimuthal electrostatic field component which changes sign at the angle where the plasma density is at maximum. Due to non-linear effects the force created by this field component causes emittance growth at the extraction [92].

### 3.3.3. The effect of ion optics on the emittance

Theoretically the emittance of ion beams is determined in the plasma and at the extraction of the ion source. However, the longitudinal momentum spread of the ion beam affects the emittance through the dispersion in different ion optical components. In the case of ECR ion sources the momentum spread is mainly due to the plasma potential profile. The evolution of the ion beam in phase space (different planes) can be described in first order with the aid of the beam line transfer matrix, which can be calculated from the transfer matrices of different ion optical components (drift spaces, dipole magnets, solenoids etc.) that are used to bend and focus the ion beam. In the case of continuous beam the phase space coordinate values  $(x_1, x'_1, y_1, y'_1, (\Delta p/p)_1)$  in a certain location of the beam line can be calculated with the aid of a 5x5 transfer matrix as

$$\begin{pmatrix} x \\ x' \\ y \\ y' \\ (\Delta p/p)_1 \end{pmatrix} = \begin{pmatrix} R_{11} & R_{12} & R_{13} & R_{14} & R_{15} \\ R_{21} & R_{22} & R_{23} & R_{24} & R_{25} \\ R_{31} & R_{32} & R_{33} & R_{34} & R_{35} \\ R_{41} & R_{42} & R_{43} & R_{44} & R_{45} \\ R_{51} & R_{52} & R_{53} & R_{54} & R_{55} \end{pmatrix} \begin{pmatrix} x \\ x' \\ y \\ y' \\ (\Delta p/p)_0 \end{pmatrix} \quad (31)$$

where the subscript 0 denotes the original phase space coordinates. The individual matrix elements  $R_{ij}$  depend on the bending and focusing properties of the different ion optical components (magnetic fields, dimensions etc.). The matrix representation of the phase space coordinate values does not take into account space charge of the ion beam or non-linear effects. The orientation of the emittance ellipse in  $x$ - and  $y$ -planes perpendicular to each others and to beam propagation indicates if the ion beam is divergent, convergent, focused or almost parallel in these planes. The ellipse rotates in phase space and therefore its orientation and shape depend on the location in the beam line. Figure 3.6 shows some possible orientations of the emittance ellipse in  $(x, x')$  phase space.

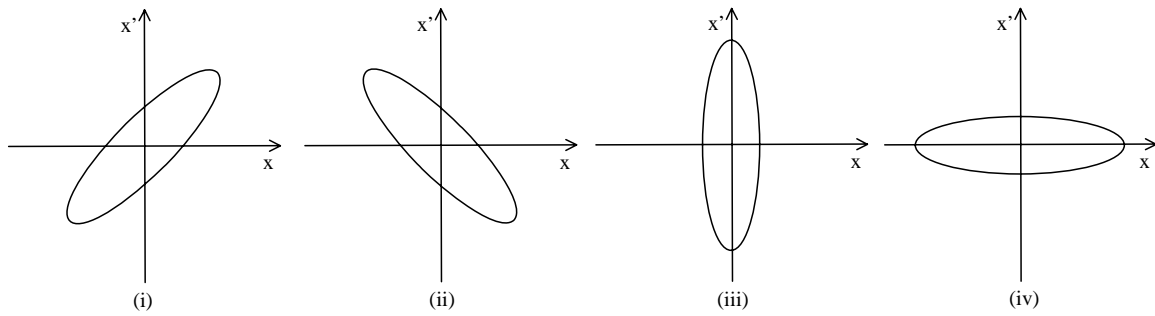


**Figure 3.6** The orientation for the emittance ellipse in the case of (i) diverging, (ii) converging, (iii) focused and (iv) almost parallel ion beam.

In the case of zero longitudinal momentum spread the phase space area enclosed by the emittance ellipse is conserved according to Liouville’s theorem and the emittance of the ion beam remains unchanged as the beam is transmitted through different ion optical components (under the assumption that correlation effects between particles can be neglected). However, if the momentum spread of the ion beam is non-zero, the so-called dispersive matrix elements ( $R_{15}$ ,  $R_{25}$ ,  $R_{35}$  and  $R_{45}$ ) affect the phase space coordinate values calculated from the transfer matrix. This causes the beam emittance to grow (not single particle emittance). The magnitude of the emittance growth depends on the location in the beam line and on the magnitude of the ion beam momentum spread. Figure 3.7 demonstrates the effect of non-zero momentum spread on the emittance in  $(x, x')$  phase space in the case of positive matrix elements  $R_{15}$  and  $R_{25}$  ( $R_{15} > R_{25}$ ). The figure shows the effect of dispersion on the area enclosed by the ellipses for three different initial momentum values (energies). In the figure the effect of dispersive matrix elements is exaggerated.

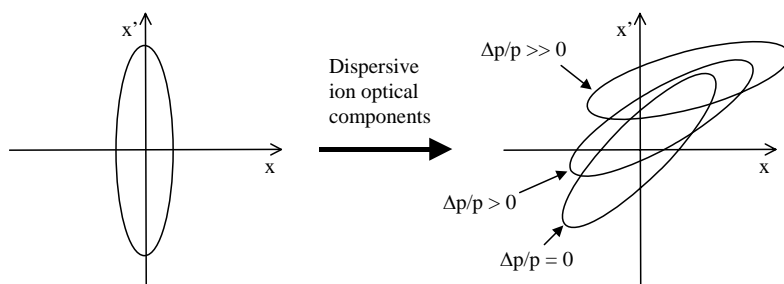


**Figure 3.7** The effect of dispersive ion optical components (dispersive matrix elements) on the area enclosed by the emittance ellipses. The initial emittance is shown on left and the resulting emittance ellipses for different initial momenta on right.

As the figure shows, dispersive ion optical components cause the emittance of ion beams to grow. Note that the beam emittance is the total area enclosed by the individual ellipses (with different

momentum spreads), which means that for non-zero momentum spread the emittance is no longer described by the area of an ellipse as the beam is transmitted through dispersive ion optical components.

In the case of ECR ion sources dipole magnets are normally used for mass-charge analysis of the ion beam. A dipole magnet is a typical example of a dispersive ion optical component, meaning that the first-order dispersive matrix elements are non-zero in the bending plane of the magnet. Ions with different initial energies are bent into separate trajectories, which causes the emittance to grow in the magnet's bending plane (corresponding to phase space coordinates  $x, x'$ ). The effect of the emittance growth can be transmitted also to the perpendicular plane (coordinates  $y, y'$ ) since the beam is usually focused with the aid of solenoid magnets. The solenoid field causes the beam to rotate and couples the  $x$ - and  $y$ -planes with each other, which causes the emittance to also grow in  $y$ -plane although solenoids are non-dispersive components in the first-order approximation [93].

The emittance of ion beams should be kept as low as possible before injection into the accelerator. The parameter that characterizes the quality of the ion beam that can be handled by the accelerator is called acceptance (same units as for emittance). If the emittance of the ion beam is higher than the acceptance of the accelerator, part of the beam will be lost at injection. For example, the area acceptance of the JYFL K-130 cyclotron is about  $100 \pi \cdot \text{mm} \cdot \text{mrad}$  meaning that the emittance values of ion beams should be lower than this at the cyclotron injection. Therefore, it is very important to design the beam line (together with the ion source) properly in order to minimize the emittance at the location of the accelerator injection. In practice this means that the dispersive matrix elements of the beam line transfer matrix have to be minimized in both planes in order to avoid problems caused by the momentum spread induced emittance growth.

## 4. EXPERIMENTAL APPARATUS

The experimental part of this work includes measurements of different plasma properties and their effects on beam quality with three different ECR ion sources. The experiments were carried out mainly at the Department of Physics, University of Jyväskylä (JYFL). Some measurements were also performed at Argonne National Laboratory (ANL). The ECR ion sources and most important beam diagnostic devices used in the experiments will be described in the following sections.

### 4.1. ECR ion sources used in the experiments

Three ECR ion sources were used in the experiments for this work; the JYFL 6.4 GHz ECRIS [3, 94], the JYFL 14 GHz ECRIS [4] and ECR2 [95] at Argonne National Laboratory. Drawings of the JYFL ECR ion sources are presented in figure 4.1. The design of the JYFL 14 GHz ECRIS and ECR2 at ANL is very similar. Table 4.1 summarizes some of the most important properties of these ECR ion sources. The values given for the JYFL 6.4 GHz ECRIS refer to those during the measurements (the source has been recently upgraded).

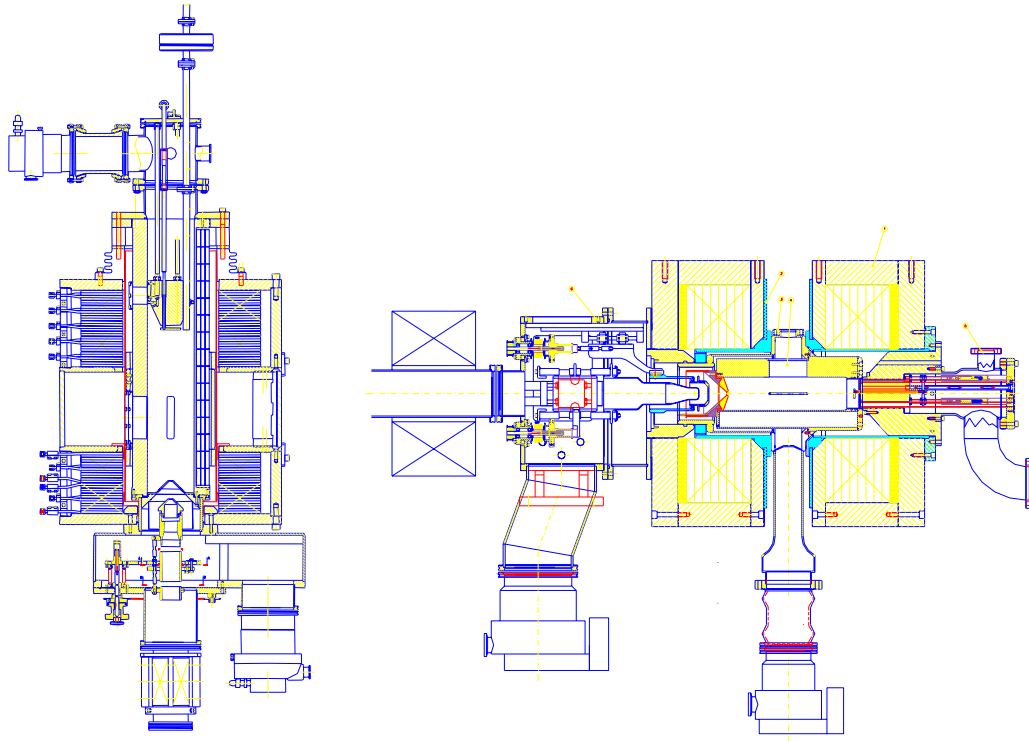


*Figure 4.1* Drawings of the JYFL 6.4 GHz ECRIS (on the left) and the JYFL 14 GHz ECRIS (on the right).

#### 4. EXPERIMENTAL APPARATUS

Ion source	JYFL 6.4 GHz ECRIS	JYFL 14 GHz ECRIS	ANL ECR2
<b>Plasma chamber:</b>			
Inner radius	70 mm	38 mm	38 mm
Volume	≈ 7.7 liters	≈ 1.1 liters	≈ 1.1 liters
Material	Copper	Aluminum	Aluminum
<b>Magnetic field:</b>			
$B_{\text{injection}}$	1.2 T	2.2 T	2.2 T
$B_{\text{extraction}}$	0.6 T	0.9 T	0.93 T
$B_{\text{minimum}}$	0.16 T	0.4 T	0.38 T
$B_{\text{radial}}$	0.44 T	0.85 T	0.95 T
<b>Microwaves:</b>			
Frequency	6.4 GHz	14 GHz + 10.75 – 12.4 GHz	14 GHz + 10.75 – 12.4 GHz
Power (operational max)	400 W	900 W + 350 W	1.3 kW + 350 W
Extraction voltage (max)	30 kV	30 kV	-

**Table 4.1** Properties of the ion sources used in the experiments.

The JYFL 6.4 GHz ECRIS was completed in 1991 for the nuclear physics program. The original design of the ion source was a modified copy of the RT-ECRIS [96] at NSCL-MSU. Since the construction of the JYFL 6.4 GHz ECRIS, which was originally a two-stage ion source, it has been upgraded to a single-stage source. The magnetic field structure of the source has also been modified resulting in a remarkable improvement in performance [94]. The designs of both the JYFL 14 GHz ECRIS and ANL ECR2 are based on the design of the AECR-U [97] ion source at LBNL. Both of the ion sources are normally operated with a microwave frequency of 14 GHz.

#### 4.2. Plasma potential measurement instrument

In order to study the effects of different ECR ion source parameters on the plasma properties an instrument was designed which makes it possible to measure the plasma potential accurately and relatively quickly without adjusting the ion source parameters during the measurement. The design of this instrument is based on the retarding field method discussed in section 2.5.3. The instrument is a simplified version of the three-grid device (designed for atomic physics studies) used by Nadzeyka *et al.* The plasma potential measurement instrument [44] is presented in figure 4.2 showing a schematic drawing (a) and a picture (b) of the device.

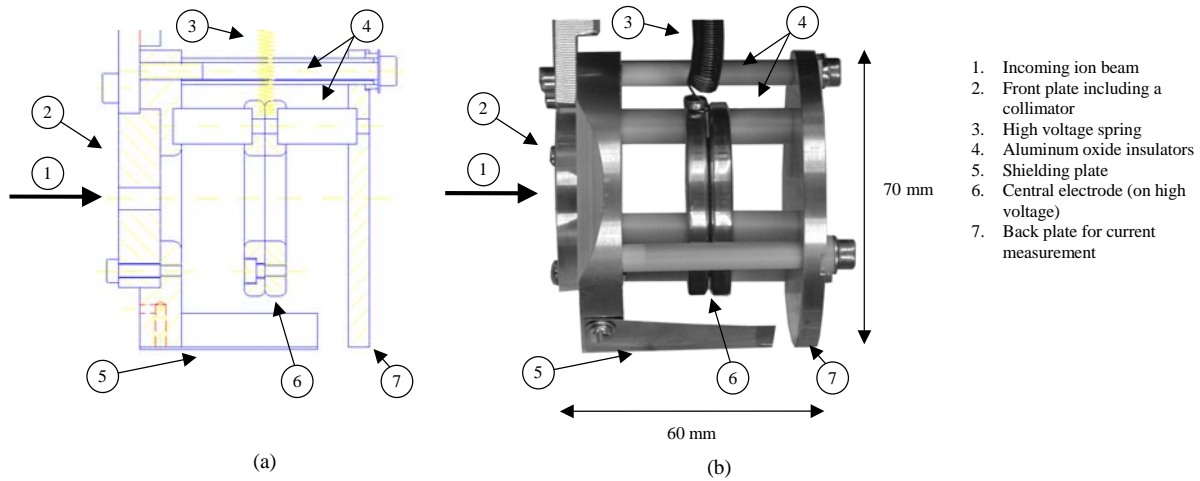


**Figure 4.2** The plasma potential measurement instrument.

The front plate of the instrument including the collimator is at ground potential (a collimator, with a diameter of 4 mm, was used in the experiments described later). The central electrode used for the beam deceleration is a mesh at high voltage (connected to high voltage duct with a spring), insulated from the front and back plates by aluminum oxide bars. The voltage can be adjusted and only particles whose kinetic energy exceeds the value  $E_k \geq QeV_{stopping}$  can pass the mesh. The secondary electrons emitted from the mesh cannot proceed to the current measurement electrode because the high voltage of the mesh drags them back. The effect of secondary electrons on grid analyzers is discussed in reference [98] (for electron energy measurements). The grounded back plate of the instrument, insulated from the front plate for the current measurement, is connected to a picoammeter. The aluminum oxide insulators between the mesh and the other electrodes have been designed to handle voltages up to 15 kV. The instrument can be moved in and out of the beam line with the aid of a bellows and consequently the plasma potential can be determined in a single measurement without adjusting the source itself. The shielding plate at the bottom of the device prevents the presence of an electric field in the middle of the beam line when the instrument is withdrawn. The plasma potential can be determined by increasing the voltage of the mesh,  $V_{mesh} = V_{source} + V_{adj}$  (sum of the source voltage and the adjustable voltage provided by voltage regulated power supply floating on the source potential; see figure 4.4). The method of determining the plasma potential from the measured beam current decay curve and the effect of ion beam optics on the measured value of the potential will be described in section 6.1.1. The behavior of the ion beam inside the plasma potential measurement instrument was studied with SIMION 7.0 simulations. Figure 4.3 shows the result of simulations for  $O^{6+}$  ion beam with two different stopping voltages

(beam behavior and equipotential lines of the retarding electric field). The effect of the shielding plate on the electric field was found to be negligible at the location of the ion beam.

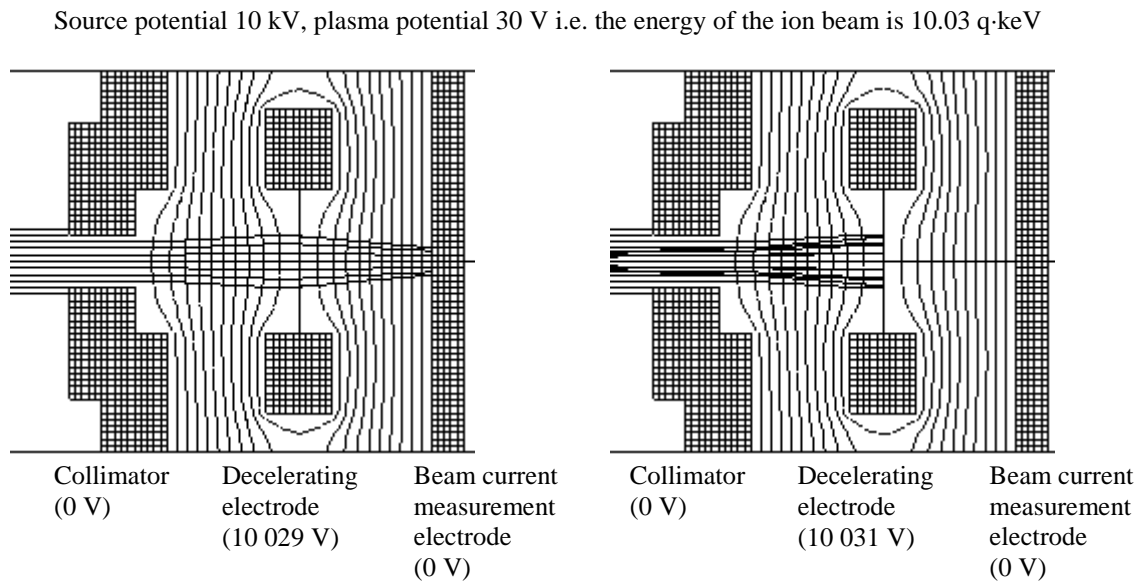


**Figure 4.3** Simulation for  $O^{6+}$  with a plasma potential of 30 V.

As the figure shows, ions cannot pass the mesh when the adjustable mesh voltage exceeds the plasma potential. It can be also seen that the electric field focuses the ion beam. The size of the ion flux mark at the back plate of the device has been experimentally found to correspond the simulation results very accurately. The voltage regulated power supply for the mesh floats on the high voltage of the ion source ( $V_{source}$ ), which eliminates possible measurement error of the source potential. The voltage of the mesh can be controlled with a computer through an optic cable. The current values are also stored by the computer. Figure 4.4 presents a schematic drawing of the plasma potential measurement setup.

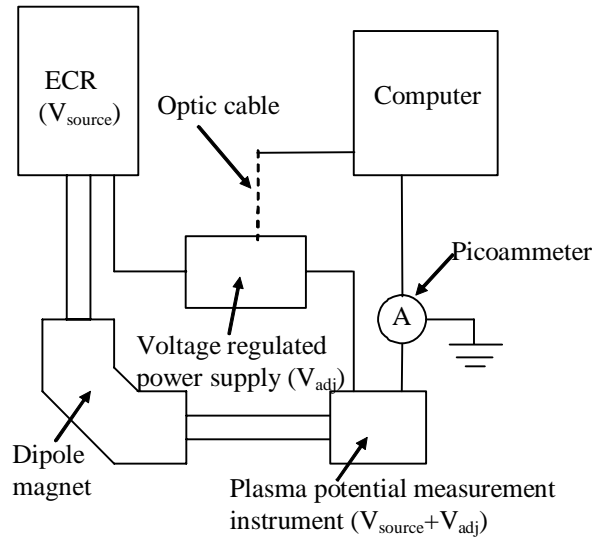


Figure 4.4 A schematic drawing of the plasma potential measurement setup.

### 4.3. Emittance scanner

The emittance scanner used in the experiments is an Allison-type scanner similar to the device used in LBNL [99]. The scanner consists of two slits with deflecting plates between them, and it can be used to measure the emittance either in  $x$ - or  $y$ -plane. Therefore, measuring the emittance in both planes requires two scanners. The position ( $x$ ) and divergence ( $x'$ ) coordinates of the phase space are defined for different particles by moving the scanner ( $x$ ) while applying an adjustable deflecting voltage to the plates ( $x'$ ) and measuring the beam current corresponding to each position – voltage combination. The emittance of the ion beam can be determined from the measured data (which is analyzed offline after the scan) with an elliptical fit. Figure 4.5 shows a schematic drawing of the emittance scanner.

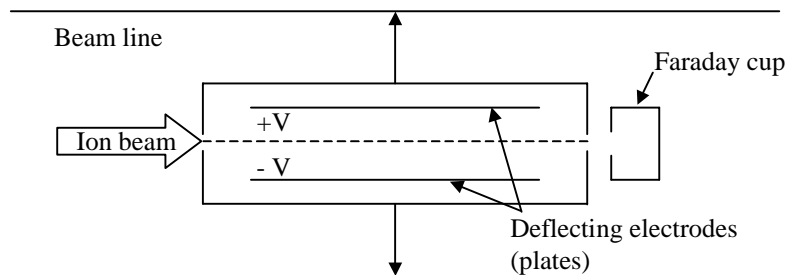


Figure 4.5 A schematic drawing of the Allison-type emittance scanner.

## 5. PRODUCTION EFFICIENCY AND REDUCTION OF CARBON CONTAMINATION OF AN ECRIS

The use of expensive isotopes such as  $^{48}\text{Ca}$  at the JYFL Accelerator Laboratory gave a strong impetus to study the production efficiency of different ion beams extracted from the ECR ion source. Of special interest was the effect of gas mixing when ion beams were produced either from gaseous compounds or metallocenes with the MIVOC method. Another motivation for the work was to understand the phenomena affecting carbon contamination related to the MIVOC method. The improved production efficiency minimizes the consumption rate of the material, which is a considerable issue in the case of expensive isotopes or compounds. It also reduces the disadvantageous contamination when metal ion beams are produced with the MIVOC method.

The most obvious way to improve the production efficiency of ECR ion sources (at least in the case of gaseous elements) is to minimize the pumping speed of the plasma chamber. However, lower pumping speeds require techniques used in ultra high vacuum technology. The reduced pumping speed would not be as beneficial in the case of solid elements that condense on the cold walls of the plasma chamber. All the production efficiency measurements presented here were performed with the JYFL 6.4 GHz ECRIS, which is mainly used for ion source research and development. The results obtained in the experiments (see references [66] and [100]) help users of the MIVOC-method to improve the production efficiency of metal ion beams and to reduce carbon contamination. Some production efficiency measurements have also been reported in reference [101].

### 5.1. The effect of gas mixing on the ion beam production efficiency from gaseous compounds

The production efficiency of an ion source can be defined as the ratio of extracted ions measured with a Faraday cup to the number of consumed atoms. As a consequence, this definition for the production efficiency includes the ionization efficiency of the ion source and the efficiency of the transport system. By applying the equation of state for an ideal gas ( $pV = NkT$ ), the equation for the production efficiency,  $\eta$ , can be written for gaseous materials as

$$\eta = \frac{kT}{p\dot{V}} \sum_q \frac{I_q}{qe}. \quad (32)$$

Here the sum runs over beam currents of all measurable charge states and  $\dot{V}$  denotes the consumption rate ( $\text{cm}^3/\text{unit time}$ ) of the material. The feed rate of the gas [ $\text{cm}^3/\text{h}$  at NTP] was measured with the aid of its partial pressure in the plasma chamber. The calibration was performed for different gases with several feed rates. During the calibration the plasma was not ignited to ensure that different source tunings used in the measurements can not affect the calibrated leak. According to Dalton's law, the total pressure is a sum of the partial pressures of the gas constituents and therefore the calibrated leaks could also be used for gas mixing measurements.

The beneficial effect of gas mixing on the production of highly charged ions has been studied experimentally by several groups, for example by Drentje [6] and Melin *et al.* [22]. However, no systematic measurements concerning the effect of gas mixing on the production efficiency of ECR ion sources have been carried out. In this work, the production efficiency of gaseous elements was studied with argon ion beams and different mixing gases (Ar mixed with He, N<sub>2</sub>, O<sub>2</sub>, Ne or Kr). An extraction voltage of 12 kV was chosen in order to ensure that the performance of the ion source limited the beam output rather than space charge in the extraction gap (see equation (27)). This was assured by measuring the dependence of the extracted ion beam current as a function of the source voltage. The extracted current was observed to saturate at about 10 kV as the source voltage was increased. Figure 5.1 [66] shows the highest achieved production efficiency of argon with different mixing gases.

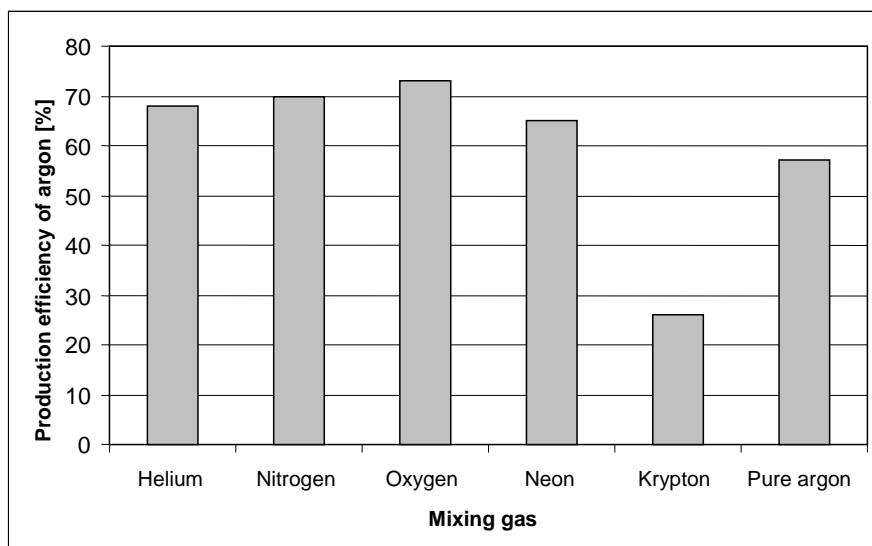


**Figure 5.1** Production efficiencies of argon ion beams with different mixing gases [66].

The microwave power was set to 250 W and the feed rate of argon to 0.11 cm<sup>3</sup>/h in all cases shown (except with the pure argon plasma). In the measurements with pure plasmas of different gases it was observed that the production efficiency increased as the microwave power was increased or as the gas feed rate was decreased. However, the growth of the overall production efficiency saturated at the microwave power of approximately 250 W. The production efficiency was higher for heavier gases, probably due to different pumping properties caused by their lower mobility or due to the fact that the (first) ionization potential decreases with atomic number  $Z$  (see table 2.1). From figure 5.1 it can be seen that the production efficiency of argon ion beams improves when a lighter element is added into the plasma whereas the efficiency decreases as a consequence of adding a heavier element (e.g. krypton). The production efficiencies of helium, nitrogen, oxygen and neon decreased significantly compared to their production efficiencies with pure plasmas i.e. from 40 – 55 % (pure plasmas) to 15- 25 % (mixed with argon).

These results imply that the confinement of heavier ions improves due to gas mixing while the confinement of lighter ions decreases. This effect can be explained by the ion cooling process. It can be expected that the confinement of carbon ions is rather low in MIVOC plasmas (carbon is the lighter element in the compound). Therefore a significant fraction of the consumed carbon will accumulate on the walls of the plasma chamber. However, the results imply that at least helium, being lighter than carbon, can be used to reduce the carbon contamination during a MIVOC-run by improving the confinement of carbon ions.

## 5.2. Reducing the carbon contamination by gas mixing

The reduction of carbon accumulation by gas mixing was studied with ferrocene, Fe(C<sub>5</sub>H<sub>5</sub>)<sub>2</sub>. The consumption of ferrocene was calibrated to correspond to a certain partial pressure in the plasma chamber. Then the JYFL 6.4 GHz ECRIS was tuned for maximum output of a Fe<sup>15+</sup> ion beam with a pure ferrocene plasma. The production efficiencies of iron and carbon ion beams were subsequently measured. The measurements were repeated after adding helium, nitrogen or oxygen to the plasma. The optimal ferrocene feed rate for the production of Fe<sup>15+</sup> ions was found to be 1.7 mg/h for a pure ferrocene plasma and 0.2-0.3 mg/h for gas mixing plasmas. Figure 5.2 shows the fraction of consumed carbon extracted from the plasma with different mixing gases and mixing gas feed rates. Figure 5.3 shows the corresponding amount of extracted iron (certain charge states) compared to the total iron consumption.

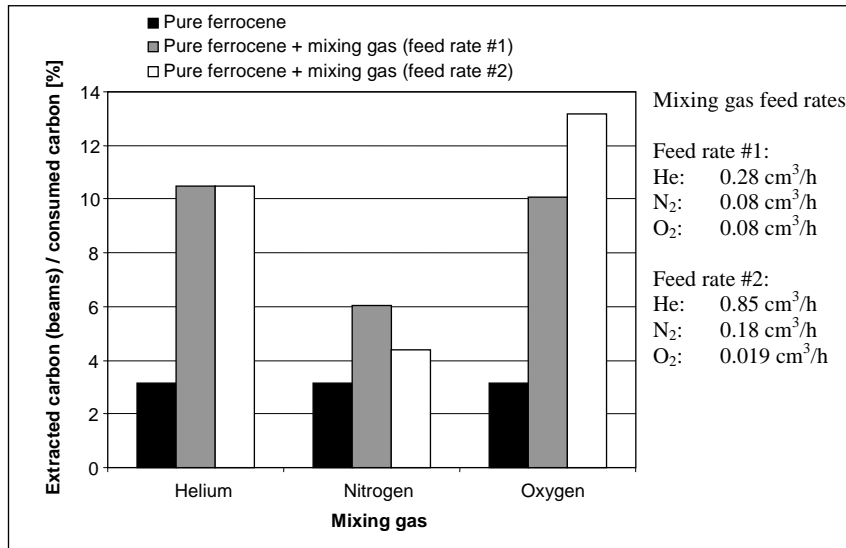


Figure 5.2 Fraction of the consumed carbon that was extracted with different mixing gases and mixing gas feed rates.

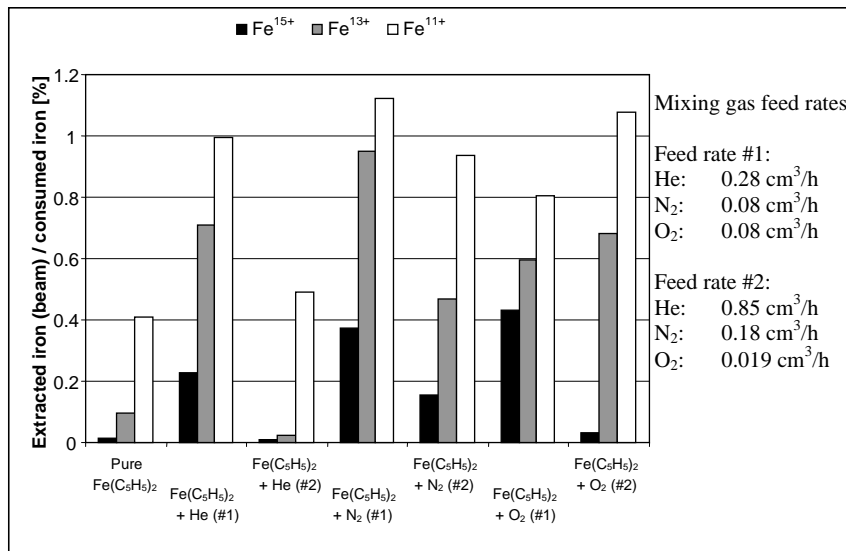


Figure 5.3 Percentage values of certain charge states of iron ion beams compared to consumed iron with different mixing gases and gas feed rates.

With the aid of helium the fraction of extracted carbon increased by factor of three. Adding helium made it possible to reduce the feed rate of ferrocene and still the intensities of highly charged iron ion beams increased compared to a pure ferrocene plasma. This significant result demonstrates that the amount of carbon contamination can be decreased with the aid of a mixing gas. Increasing the feed rate of helium did not affect the amount of extracted carbon but caused the intensities of iron ion beams to decrease, which can be explained by the higher probability of charge exchange reactions. In the case of helium, the increase of extracted carbon can be explained by ion cooling

since helium is lighter than carbon. Therefore, it can be expected that the confinement of carbon (and iron) ions improves as helium is added into a ferrocene plasma.

According to figure 5.2 the production efficiency of carbon ion beams increases when a small amount of nitrogen is added into the plasma. The feed rate of ferrocene was reduced also in this case. However, the effect of nitrogen was not found to be as beneficial as the effect of helium. The beneficial effect of nitrogen cannot be completely explained by the collisions between carbon and nitrogen because carbon is a lighter element than nitrogen. Therefore the confinement time of carbon should decrease due to the energy exchanging collisions with nitrogen. A possible explanation is that adding nitrogen to the ferrocene plasma decreases the average energy of all ions. Also the probability of collisions between iron and carbon ions can decrease due to the addition of nitrogen mainly because of the lowered feed rate of ferrocene and, therefore, reduced density of iron and carbon ions in the plasma. This is supported by the fact that the intensities of highly-charged iron ion beams increased as nitrogen was added into the plasma. Consequently, the confinement of carbon becomes better. The highest production efficiency for carbon (approximately 13 %) was obtained when oxygen was used as a mixing gas. The charge state distribution of iron ion beams obtained with oxygen corresponded to the distribution obtained with nitrogen, which can be explained by their masses being almost equal. Therefore, it can be expected that the ion cooling properties of nitrogen and oxygen are nearly the same in collisions with iron atoms. Increasing the feed rate of oxygen shifts the charge-state distribution (CSD) of iron ion beams towards lower charges. However, the cleaning effect i.e. the production efficiency of carbon improves as the feed rate of oxygen is increased.

Figure 5.4 [66] is a concluding figure, which shows the extracted current of  $\text{Fe}^{15+}$  ions compared to the carbon accumulated on the walls of the plasma chamber [ $\mu\text{A}/(\text{mg}/\text{h})$ ] with different mixing gases. The figure shows clearly that the most effective mixing gas for the production of highly charged iron ion beams (with the MIVOC-method) and for minimizing the carbon contamination is oxygen.

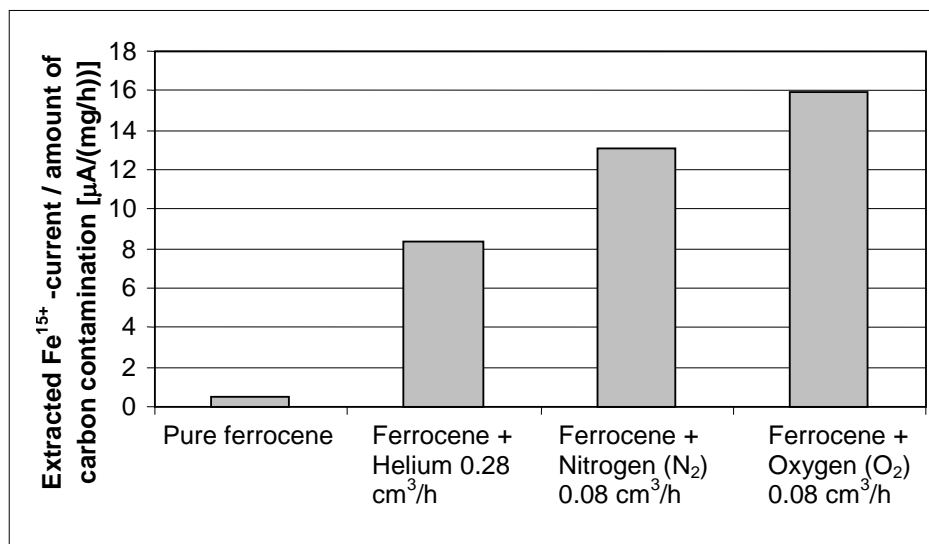


**Figure 5.4** The extracted  $Fe^{15+}$  current compared to the level of accumulated carbon contamination with different mixing gases.

According to the observations, low-charge state oxygen and carbon ions can carry the kinetic energy of ions away from the plasma more effectively than the carbon ions alone. This process eventually leads to enhanced confinement of highly charged iron ions. Another explanation for the reduction of carbon contamination with oxygen could be based on chemical reactions. As oxygen is a reactive element it can be expected to form compounds (CO and CO<sub>2</sub>) with the carbon accumulated on the plasma chamber walls. These compounds can drift back into the plasma and become ionized again. The probability of extracting carbon as an ion beam increases, which reduces the amount of the contamination. It was observed, for example, that the intensity of the (CO)<sup>+</sup> ion beam doubled as oxygen was fed into a ferrocene plasma, which supports this conclusion.

### 5.3. Removal of the carbon contamination

The study of the parameters affecting the reduction of carbon contamination carried out with the JYFL 6.4 GHz ECRIS includes three aspects. The reduction of contamination with gas mixing during a MIVOC-run [66], removal of contamination with the aid of a plasma after the MIVOC-run [100] and understanding the physical processes leading to the contamination.

The parameters affecting the cleaning process of the plasma chamber have been studied with nitrogen and oxygen plasmas after intentional production of contamination with carbon dioxide (CO<sub>2</sub>). According to the production efficiency measurements 70 – 80 % of the consumed carbon is accumulated on the cold walls of the plasma chamber with a carbon dioxide plasma. After

producing the contamination either a nitrogen or oxygen plasma was ignited in order to remove the carbon layer. The extraction rate ( $\dot{m}$ ) of carbon ions was determined by measuring the extracted currents of different carbon ion beams (charge states) and using the equation

$$\dot{m} = \sum_q \frac{I_q}{qe} \cdot 12u. \quad (33)$$

Here  $u$  is the atomic mass unit ( $\approx 1.661 \cdot 10^{-27}$  kg). After the measurements with a nitrogen plasma the plasma chamber was cleaned and a  $\text{CO}_2$  plasma was used to produce a similar contamination for the oxygen measurements. The level of contamination was controlled by measuring the feed rate and time for  $\text{CO}_2$ . Figures 5.5 and 5.6 [100] show carbon removal rates with nitrogen and oxygen, respectively, as a function of microwave power and gas feed rate.

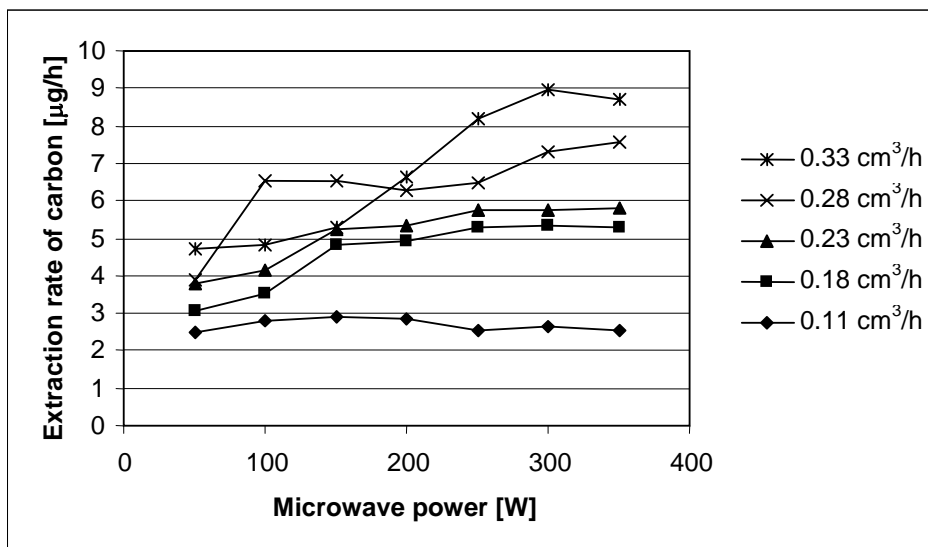


Figure 5.5 The extraction rate of carbon with a nitrogen plasma [100].

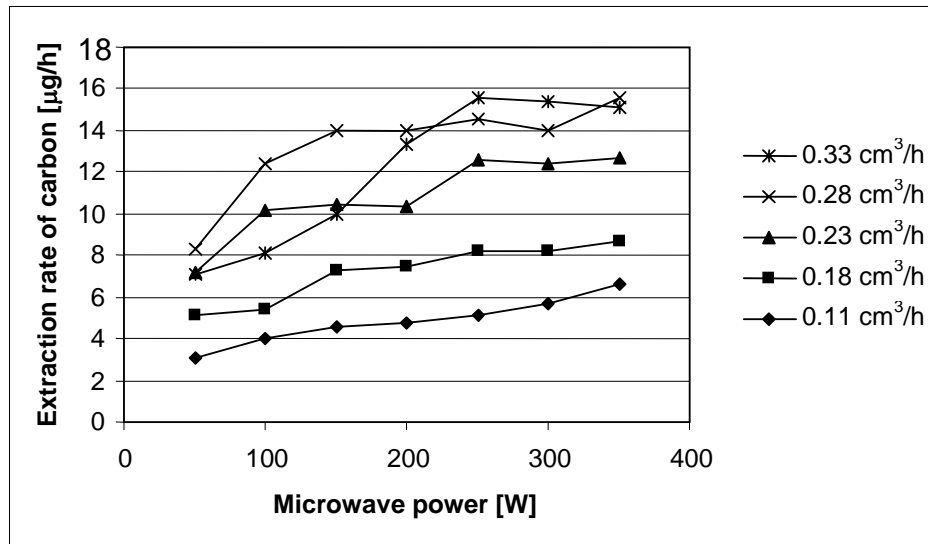
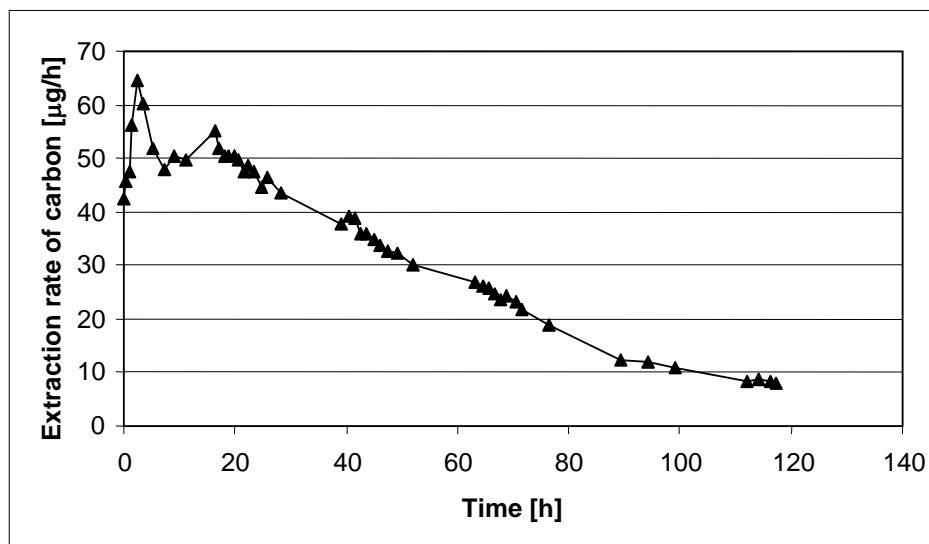


Figure 5.6 The extraction rate of carbon with an oxygen plasma [100].

The extraction rate of carbon tends to increase when either the microwave power or the gas feed rate is increased. The results obtained with different gases can be compared since the level of contamination and the gas feed rates were the same in both cases. Compared to the nitrogen plasma the extraction rate of carbon with the oxygen plasma was about twofold. A possible explanation for the difference could be that nitrogen is a chemically nonreactive element while oxygen forms compounds with carbon (in suitable plasma conditions). This encouraged us to measure the level of CO and CO<sub>2</sub> evacuated from the plasma chamber by pumps during the production of iron ion beams with the MIVOC-method with and without oxygen as a mixing gas. With a residual gas analyzer it was observed that the level of CO<sub>2</sub> increased by 42 % as oxygen was fed into the plasma (feed rate 0.6 cm<sup>3</sup>/h) compared to the situation without oxygen feeding. The corresponding increase for CO was 33%. Feeding nitrogen or argon into the plasma chamber did not affect the detected values of these compounds.

The extraction rate of the carbon contamination as a function of time was studied with nitrogen and oxygen after a MIVOC-run producing a significant contamination. In this case the extraction rate was again found to be about two times higher for the oxygen plasma. Figure 5.7 presents the extraction rate of carbon with an oxygen plasma as a function of time (0.28 cm<sup>3</sup>/h, 300 W) [100].



*Figure 5.7* The extraction rate of carbon as a function of time with an oxygen plasma after a MIVOC-run [100].

At the beginning, the extraction rate of carbon fluctuated significantly. This was due to the problems with the extraction of the JYFL 6.4 GHz ECRIS, which was not capable of handling a drain current exceeding 1.5 mA. Otherwise, the extraction rate of carbon decreased almost linearly as a function of time. Cleaning of the contamination is very time consuming. In this case it took about five days to reach the level of carbon observed before the MIVOC-run. Using a higher feed rate of oxygen and higher microwave power can be used to decrease the required time. However, this result emphasizes the importance of the carbon production efficiency and reduction of contamination during MIVOC-runs.

#### 5.4. Distribution of the carbon contamination

In order to gain information concerning the distribution of the carbon contamination a plasma electrode with a thickness of 0.5 mm was constructed. After producing the contamination with a ferrocene plasma the electrode was cut into small pieces for thermal analysis showing the level of carbon at different points on the surface of the electrode. Any error due to the measurement device (thermal analysis) was eliminated by calibration with reference samples. The thermal analysis was performed in the Department of Chemistry, University of Jyväskylä, by heating the samples and measuring their precise mass before and after the carbon formed compounds (due to increased reaction rate during the heating) and evaporated off from the sample. It was observed that the carbon contamination is heavily concentrated in the area covered by the electron flux escaping from

the plasma. Figure 5.8 [100] shows the locations of different samples taken from the plasma electrode.

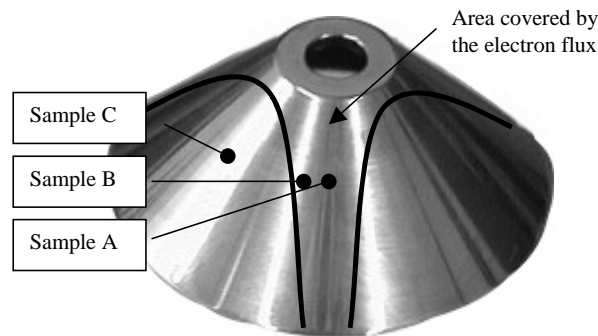


*Figure 5.8 Locations of the samples on the surface of the plasma electrode [100].*

The amount of carbon at the center of the flux (sample A) was about fourfold compared to the sample taken from the edge of the flux (sample B). Practically no carbon was detected in sample C taken from the area between the electron flux marks. This result means that practically all carbon atoms in the ECRIS are ionized (at least at the extraction end) and they follow the electrons very strictly out of the plasma despite the fact that the ions are not magnetically confined. Based on this measurement it can be assumed that also the radial ion losses (which are theoretically more significant than the axial ion losses [30]) are concentrated on the magnetic poles where the electron flux intersects with the plasma chamber surface. The result also shows that it could be possible to design localized shielding against the carbon contamination and to improve the recirculation of  $^{48}\text{Ca}$ , for example.

## 6. PLASMA POTENTIAL AND EMITTANCE MEASUREMENTS

The production efficiency measurements yielded a great deal of information about the effects of gas mixing and carbon contamination on the performance of ECR ion sources. In order to understand the different plasma processes causing these effects a series of plasma potential measurements was carried out. In these measurements the plasma potential measurement device was located in the beamline further downstream from the bending magnet, which made it possible to compare the plasma potential curves measured with different charge states. Some of the plasma potential measurements with the JYFL 14 GHz ECRIS were performed in conjunction with emittance measurements that will also be considered in this section. Figure 6.1 shows the beam lines of the JYFL 6.4 and JYFL 14 GHz ECR ion sources including the ion optical and diagnostic devices used in this work.

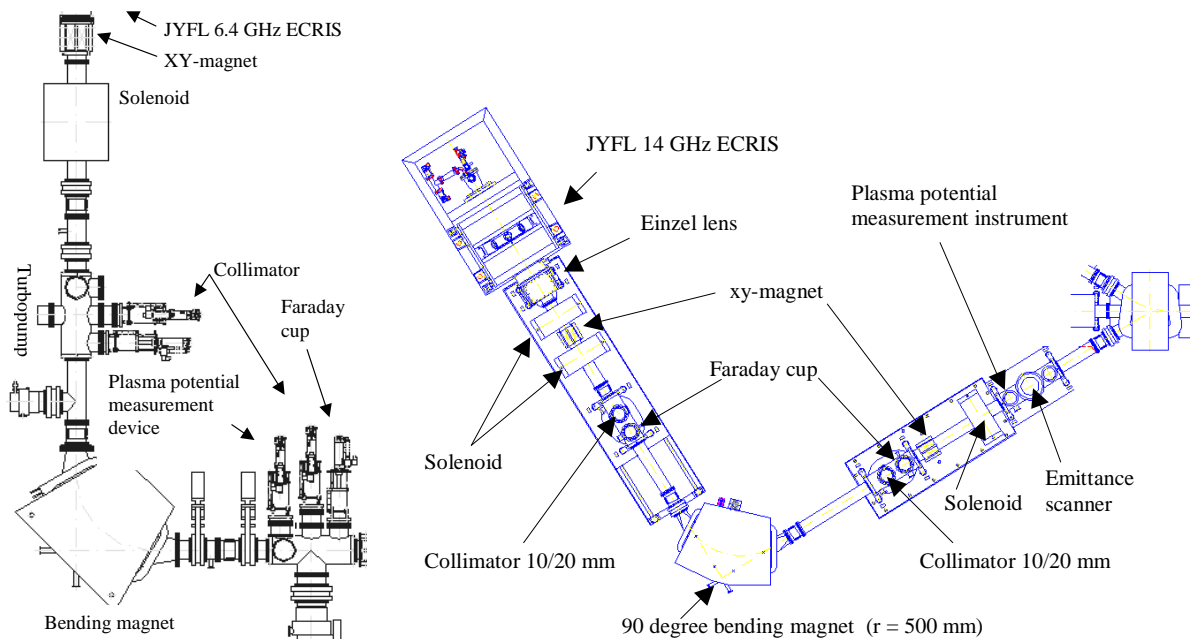


**Figure 6.1** Beam lines of the JYFL ECR ion sources. The locations of the plasma potential measurement instruments and the emittance scanner are shown.

### 6.1. Beam current decay curves

The energy of the ion beams extracted from ECR ion source is due to the source potential, plasma potential and ion temperature i.e.  $E = q \cdot (V_{source} + V_{plasma\ potential}) + kT_i$ . As a consequence, the plasma potential can be determined by measuring the beam current as a function of a decelerating voltage ( $V_{stopping} = V_{source} + V_{adj}$ ) applied into the central electrode (mesh) of the plasma potential

measurement instrument. The adjustable voltage supply for the mesh floats on the high voltage of the ion source ( $V_{source}$ ), which eliminates the possible measurement error of the source potential. The power supply has to be voltage regulated in order to avoid the charging effects due to the beam hitting the mesh.

### 6.1.1. Determination of the plasma potential

Figure 6.2 shows a typical beam current decay curve measured with the JYFL 6.4 GHz ECRIS. The method of determining the plasma potential is clarified in the figure.

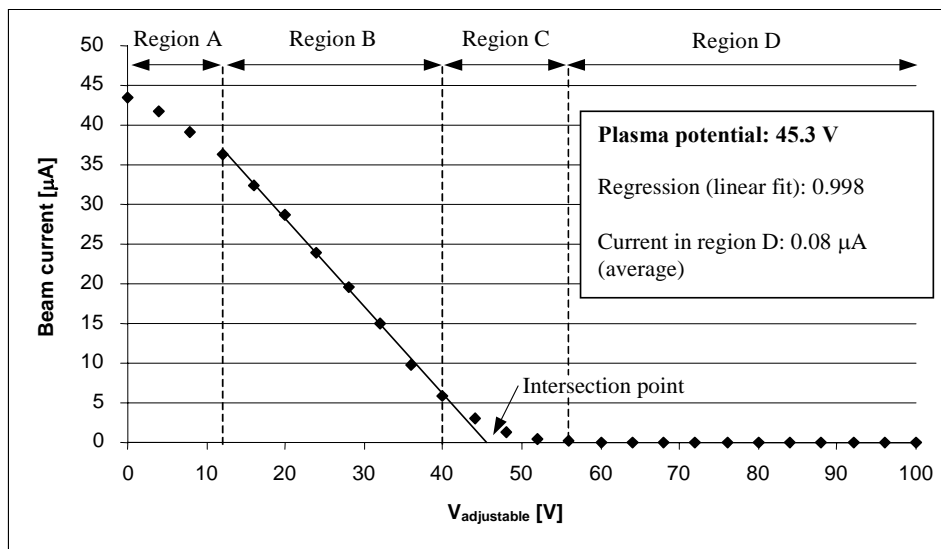


**Figure 6.2** A typical ion beam current decay curve measured with the plasma potential measurement instrument. The measurement was performed with the JYFL 6.4 GHz ECRIS.

In region A the measured current decreases slightly. In region B the decrease is nearly linear until saturation starts in region C. Eventually, in region D the measured current attains a certain value that has been observed to be dependent on the ion beam current passing the front plate of the instrument and on the level of residual gases (i.e. the pressure) inside the instrument. This “residual current” is probably due to ionization of the residual gas between the central electrode and the current measurement electrode. In measurements with the JYFL 14 GHz ECRIS and ECR2 at ANL the beam current starts to decrease linearly as the adjustable voltage exceeds zero volts. In practice this means the absence of region A observed in all the measurements with the JYFL 6.4 GHz ECRIS. This is probably due to the different plasma potential profiles (see the discussion later in this section). The voltage at the intersection of the linear fit (calculated from the data points in region B) and the horizontal line corresponding to the average value of the measured currents after

saturation (data points in region D) defines the plasma potential. These lines are presented in figure 6.2 In this case (nitrogen plasma) the value of the plasma potential was determined to be approximately 45 V. The slope regression factor of the linear fit is normally between 0.995 and 1. Defining the plasma potential to be the voltage at the afore-mentioned intersection is similar to the procedure applied in ECRIS plasma diagnostics with a Langmuir probe (see reference [39]).

The error related to the plasma potential values has been estimated to be 1 volt in the case of the JYFL 6.4 GHz ECRIS and less than one volt ( $\approx 0.5$  V) for the JYFL 14 GHz ECRIS and ECR2 at ANL. This is estimated by consecutively measuring the plasma potential several times and changing the focus of the ion beam during the series in order to confirm that different focusing does not affect the determined potential value. It was also observed with the JYFL 14 GHz ECRIS that the measured value of the plasma potential changed by less than 1 volt as the emittance ellipse was rotated in  $(x, x')$  phase space by changing the currents of the focusing solenoids. By rotating the ellipse in phase space the maximum angular distribution of the ion beam was varied between 25 and 5 mrad (for an emittance fit corresponding to 95 % of the beam). The area of the ellipse (i.e. the emittance) was observed to remain nearly unchanged despite the rotation. This implies that the determined value of the plasma potential is affected by the transverse acceptance of the measurement instrument only slightly. The effect of the instruments' transverse acceptance on the shape of the measured plasma potential curves was also studied by changing the collimator at the front plate of the instrument. No changes in the plasma potential values or in the shape of the measured curves were observed, although the maximum beam current measured at the back plate of the device changed due to different collimation. The transverse acceptance of the instrument must be high enough to ensure that the spatial distribution of the ions relative to the potential profile inside the plasma chamber does not affect the measured plasma potential value (i.e. one does not measure only ions originating from a certain volume element of the plasma). A collimator with a diameter of 4 mm was used in the measurements described in this section. Since the error margin has been observed to be independent of the plasma potential value, all the following plasma potentials are given without errors.

### ***6.1.2. Simulated beam current decay curves***

The shape of the measured plasma potential curve (current decay curve) depends on the plasma potential profile, the spatial distribution of the ions in the ECRIS plasma and ion temperature. The spatial distribution of electrons is implicitly included in the plasma potential profile. The shape of

the measured plasma potential curve seems to depend on the ion temperature especially in the saturation region (region C in figure 6.2). In order to study the effect of the ion temperature on the measured plasma potential curves, a simple computer simulation code has been developed [76]. The code was written with the Mathematica 4.1 program and the input parameters are the plasma potential profile on the axis of the plasma chamber, the temperature of the ions, the spatial distribution of the ions relative to the potential profile and the ion properties (mass and charge). The height and shape of the potential profile are adjustable and a negative potential dip [38] can be included. Some shapes of the axial potential profiles used during the calculations are presented in figure 6.3 (with arbitrary maximum potential 10 V).

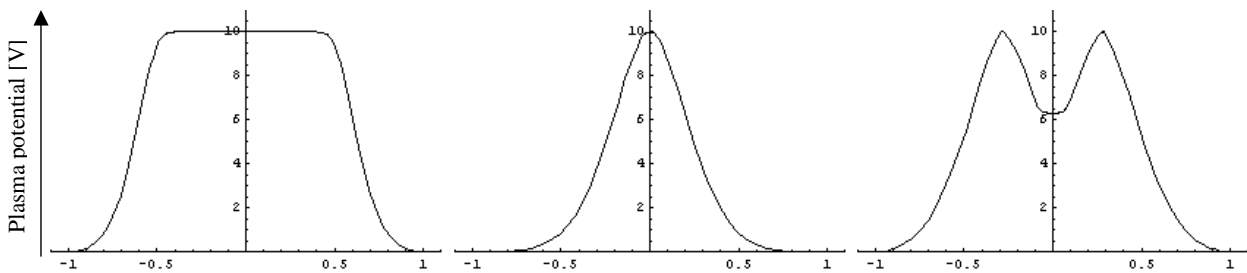


*Figure 6.3 Axial plasma potential profiles used in the simulations.*

In the simulation, the velocity distribution of the ions inside the ECRIS plasma was assumed to be Maxwellian due to the high collision frequency of the ions. The spatial distribution refers to the number of ions originating from a certain value of the plasma potential i.e. from a certain point of the potential profile. The simulation is not self-consistent, since the potential profile and the spatial distribution of the ions that are highly correlated have to be used as input parameters. Although there is no exact information concerning these profiles, with the aid of the simulation it has been demonstrated that the temperature of the ions affects the shape of the measured beam current decay curve in the saturation region, whereas the shape of the curve at low stopping voltages (region A) is strongly dependent on the potential profile and the spatial distribution of the ions. Figure 6.4 [67] shows the effect of the ion temperature (increasing from 3 eV to 6 eV) on the simulated beam current decay curves (normalized) in the case of  $O^{7+}$  (a) and  $O^{2+}$  (b) ions. The plasma potential profile (the maximum value being 15 volts) and the spatial distribution of the ions were the same in all cases.

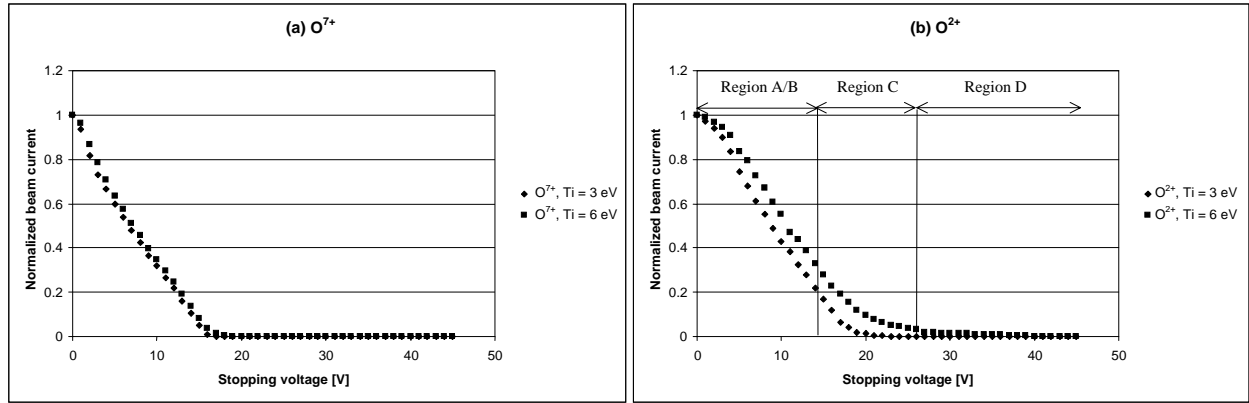


**Figure 6.4** Simulated beam current decay curves (normalized) for  $O^{7+}$  and  $O^{2+}$  ion beams with ion temperatures of 3 eV and 6 eV.

According to the results of the simulation, the effect of the ion temperature is considerable for low charge-state ion beams and can be seen most clearly with stopping voltages exceeding the value of the maximum plasma potential (15 volts) i.e. in the saturation region (region C). It can also be seen that the most reliable plasma potential values are measured with highly-charged ion beams, since the effect of the ion temperature on the curves measured with them is diminutive compared to those measured with low charge states. Also, the shape and the height of the central dip have an effect on the simulated voltage-current curves, although by changing the potential profile and/or the spatial distribution of the ions the effect of the dip can be eliminated. Since different combinations of the potential profile and the spatial distribution of the ions lead to similar simulation results, the simulation cannot be used to determine the ion distribution in the plasma.

## 6.2. Effect of different ion source parameters on the plasma potential and emittance

The plasma potentials of the JYFL 6.4 GHz ECRIS, the JYFL 14 GHz ECRIS and ECR2 at ANL were measured extensively as a function of several source parameters. In addition, the effects of gas mixing and multiple frequency heating on the emittance was studied (mainly with the JYFL 14 GHz ECRIS). The results discussed in the following have been reported in references [44, 76, 77]. The source potential was set to 10 kV in all the experiments with the JYFL ion sources and 12 kV with ECR2 at ANL. The ion beam current measured with a faraday cup was optimized by using a xy-magnets, solenoid (glaser at ANL) and a 90 degree bending magnet. The results of the measurements are presented in this section along with a discussion of the effect of the ion beam momentum spread on the beam quality.

**6.2.1. Plasma potential and beam current decay curves vs. charge state of the ion beam**

Measurements with the new device were begun by measuring the plasma potential of the JYFL 6.4 GHz ECRIS with different oxygen ion beams (charge states). Table 6.1 [44] shows the plasma potentials and extracted oxygen ion beam currents with an oxygen ( $O_2$ ) feed rate of  $0.19 \text{ cm}^3/\text{h}$  and microwave power of 150 W.

Ion beam	Plasma potential [V]	Extracted current [ $\mu\text{A}$ ]
$O^+$	49	44
$O^{2+}$	48	68
$O^{3+}$	48	102
$O^{4+}$	49	185 <sup>(*)</sup>
$O^{5+}$	47	133
$O^{6+}$	47	75
$O^{7+}$	49	5

**Table 6.1** Extracted currents and plasma potentials of the JYFL 6.4 GHz ECRIS measured with different charge states of oxygen ion beams [44] (\* = overlapping with  $C^{3+}$ ).

The table shows that the deviation of the plasma potential for different charge states is within the error margin ( $\pm 1 \text{ V}$ ) in the case of the JYFL 6.4 GHz ECRIS. Similar results were obtained with different gas feed rates and microwave power. Therefore, it can be concluded that in the case of the JYFL 6.4 GHz ECRIS any charge state can be used to determine the plasma potential. This is also indicated by the results shown in figure 6.5 [76] presenting normalized plasma potential curves of different oxygen charge states. The plasma potential values determined from the curves were 39.6 V ( $O^{6+}$ ), 40.2 V ( $O^{5+}$ ) and 39.4 V ( $O^{3+}$ ).

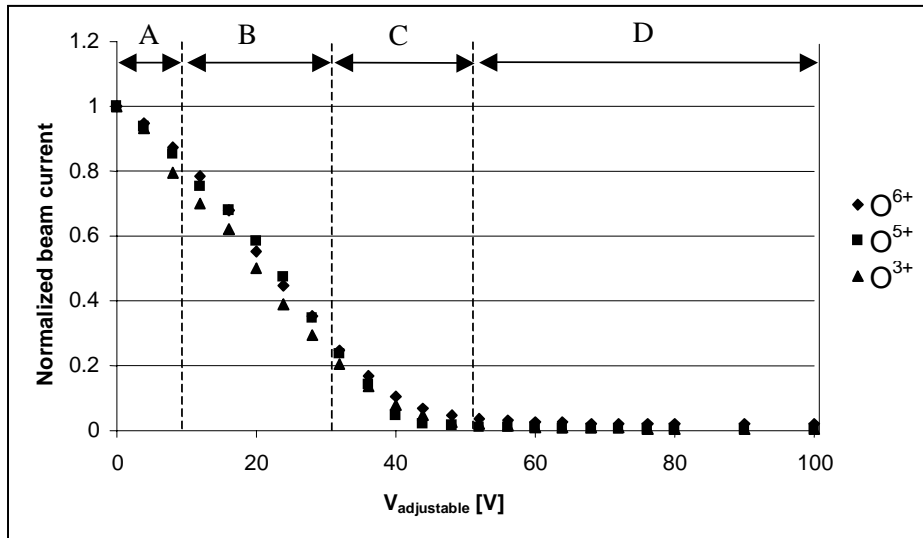


**Figure 6.5** Plasma potential curves measured with the JYFL 6.4 GHz ECRIS for different charge states of oxygen ion beams [76].

Table 6.2 [44] shows the results when the JYFL 6.4 GHz ECRIS was tuned for different charge states of oxygen ion beams by changing the microwave power, oxygen feed rate, biased disk voltage (negative compared to source potential) and the axial mirror ratio i.e. ( $B_{max}/B_{resonance}$ ). The charge state distributions and plasma potentials corresponding to certain source settings are given in the table. The axial mirror ratios were calculated with the FEMM computer code [102]. The average charge state of the ions was estimated from the extracted beam currents. However, the actual charge state distribution in the plasma is probably concentrated in higher charge states than the charge state distribution of the extracted ions.

Current [ $\mu\text{A}$ ] / ECRIS settings	JYFL 6.4 GHz ECRIS tuned for						
	$\text{O}^+$	$\text{O}^{2+}$	$\text{O}^{3+}$	$\text{O}^{4+}$	$\text{O}^{5+}$	$\text{O}^{6+}$	$\text{O}^{7+}$
$\text{O}^+$	128	76	63	52	45	36	36
$\text{O}^{2+}$	79	131	106	111	90	72	72
$\text{O}^{3+}$	22	89	138	186	186	118	118
$\text{O}^{4+}$ (*)	9	58	135	229	208	142	142
$\text{O}^{5+}$	0.6	22	81	138	162	128	128
$\text{O}^{6+}$	0.2	7	29	50	63	106	106
$\text{O}^{7+}$	0	0.5	2	3	5	9	9
<b>Drain current [mA]</b> (**)	1.02	1.13	1.03	1.59	1.36	1.23	1.23
<b>Power [W]</b>	60	120	210	230	270	340	340
<b>Gas feed rate [cm<sup>3</sup>/h]</b>	0.62	0.62	0.28	0.25	0.24	0.23	0.23
<b>Biased disk voltage [V]</b>	-36	-44	-40	-63	-85	-87	-87
<b>Axial mirror ratio</b>	4.61	4.71	4.95	5.03	5.05	5.09	5.09
<b>Plasma potential [V]</b>	$46.4 \pm 0.6$	$50.7 \pm 1.2$	$47.8 \pm 0.8$	$35.8 \pm 0.8$	$39.7 \pm 0.3$	$47.7 \pm 0.6$	$47.7 \pm 0.6$
<b>Average charge state</b>	1.35	2.00	2.55	2.92	3.07	3.19	3.19

**Table 6.2** Extracted currents and plasma potentials of the JYFL 6.4 GHz ECRIS measured when the ion source was tuned for different charge states [44].

(\*) Overlapping with another ion beam due to the same  $q/m$  ratio.

(\*\*) The drain current includes secondary electrons emitted from the puller electrode.

The plasma potential was measured with  $\text{O}^{3+}$ ,  $\text{O}^{5+}$  and  $\text{O}^{6+}$  ion beams. The error related to the plasma potential is the standard deviation calculated from the results obtained with different charge states. Low values of the plasma potential are usually related to well-performing ECR ion sources [32] with a substantial output of highly charged ions. However, the lowest plasma potential with the JYFL 6.4 GHz ECRIS was measured when the source was tuned for  $\text{O}^{4+}$  rather than for higher charge states ( $\text{O}^{5+}$ ,  $\text{O}^{6+}$  and  $\text{O}^{7+}$ ), which leads to higher density gradients and greater losses of cold electrons. During the measurements it was observed that low values of the plasma potential usually correspond to high drain currents, which supports the fact that the loss rate of ions greatly affects the plasma potential. However, the plasma tended to become unstable as the ion source tuning was changed in order to increase the drain current.

It has also been observed by Biri *et al.* with the ATOMKI 14.5 GHz ECRIS that the plasma potential is affected by the ion extraction (drain current) [41]. Using a Langmuir probe it was observed that the plasma potential is significantly higher when the extraction voltage of the ion source is off (zero drain current) compared to the situation when the extraction voltage is applied

(positive drain current). This result agrees with the observation made with the JYFL 6.4 GHz ECRIS that the plasma potential depends on the drain current of the ion source (higher drain current corresponds to lower plasma potential).

Plasma potential measurements with the JYFL 14 GHz ECRIS and with ECR2 (14 GHz) at ANL were also initiated by measuring the plasma potential for different charge states of oxygen. It was observed that unlike the JYFL 6.4 GHz ECRIS the determined potential value was dependent on the charge state. Some results are shown in table 6.3 [76].

Ion Source	ANL ECR2 (14 GHz)		JYFL 14 GHz		JYFL 6.4 GHz
Power	333 W	485 W	350 W	497 W	150 W
	Plasma Potential [V] / Beam Current [ $\mu$ A]				
O <sup>7+</sup>	<b>7.7</b> / 7	<b>6.5</b> / 21	<b>17.3</b> / 53	<b>20.1</b> / 69	49 / 5
O <sup>6+</sup>	8.7 / 58	8.2 / 100	16.5 / 186	20.4 / 213	47 / 75
O <sup>5+</sup>	9.5 / 79	8.0 / 90	19.2 / 109	24.4 / 117	47 / 133
O <sup>4+</sup>	11.8 / 92	10.2 / 75	18.3 / 76	27.7 / 81	49 / 185
O <sup>3+</sup>	18.9 / 69	12.3 / 49	20.6 / 40	28.2 / 30	48 / 102
O <sup>2+</sup>	23.7 / 53	19.3 / 40	20.2 / 6	27.6 / 5	48 / 68
O <sup>+</sup>	19.9 / 6	24.0 / 10	- / -	- / -	49 / 44

**Table 6.3** Plasma potentials and beam currents measured with different ECR ion sources [76]. The bold number corresponds to the most reliable plasma potential value.

The plasma potentials of 14 GHz ion sources are significantly lower than those of the 6.4 GHz source, being only about 10 V in the case of the ECR2 at ANL. The only significant difference between ECR2 at ANL and the JYFL 14 GHz ECRIS is the strength of the radial multipole field, being 0.95 T and 0.85 T, respectively (on the wall of the plasma chamber). In addition, the level of carbon contamination on the wall of the plasma chamber is probably higher for the JYFL 14 GHz ECRIS, which is often used for MIVOC-runs (the effect of the contamination on the plasma potential is discussed in section 6.2.7.). The wall properties also can explain the difference between the 6.4 GHz ECRIS equipped with a copper plasma chamber and 14 GHz ECRIS' equipped with aluminium chambers. The dependence of the determined plasma potential on the charge state can be understood with the aid of the measured beam current decay curves. Figure 6.6 [76] presents normalized curves measured with different charge states (O<sup>6+</sup>, O<sup>3+</sup> and O<sup>+</sup>) of oxygen with ECR2 at ANL (14 GHz / 485 W).

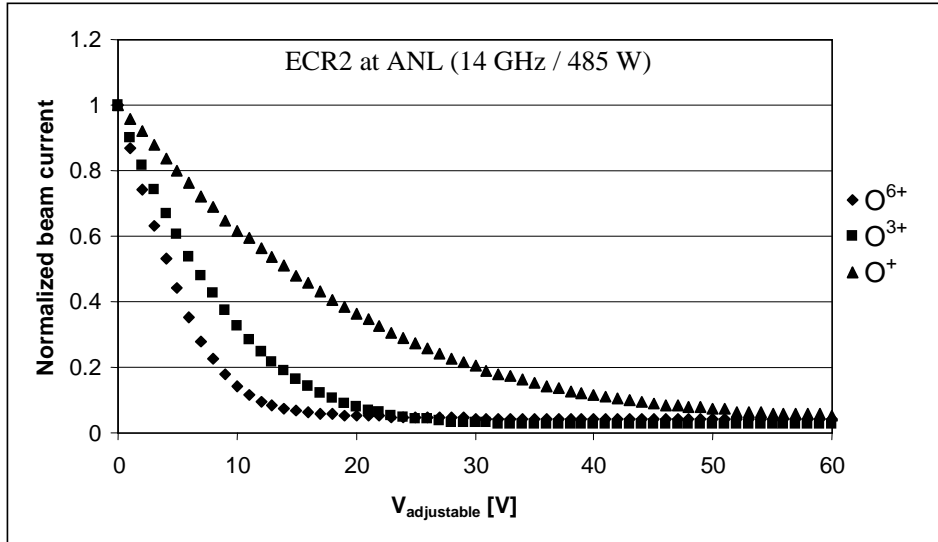


**Figure 6.6** Normalized plasma potential curves for different oxygen charge states [76].

The plasma potential values (determined as described earlier) were 8.2 V ( $O^{6+}$ ), 12.3 V ( $O^{3+}$ ) and 24.0 V ( $O^+$ ). The difference in transverse momentum between different charge states cannot explain the observed dependence of the beam current decay curves on the ion charge. The transverse momentum of low charge states can be assumed to be higher compared to high charge states (the effective extraction radius is larger for low charge states). This means that their longitudinal energy could be expected to be lower than the longitudinal energy of highly charged ions because the magnetic field induced beam rotation that converts longitudinal momentum to transverse momentum at the extraction depends on the effective ion extraction radius. Furthermore, this means that the voltage required to stop low charge states would be smaller than the voltage required to stop high charge states, which is contrary to the obtained result.

An explanation for the deviation between the shape of the beam current decay curves measured with different charges states is that the measurement always includes the thermal energy of the ions in addition to the plasma potential. The plasma potential has to be the same for all charge states because for each charge state there are ions originating near the source axis [36] where the potential is at maximum. The shape of the curve and thereby the value of the plasma potential is affected more by the ion temperature than in the case of the JYFL 6.4 GHz ECRIS. This is because the ratio of ion temperature and the plasma potential (about 10 V) is higher in the case of the 14 GHz ion source. The plasma potential curves measured with high charge states of oxygen ( $O^{7+}$ ,  $O^{6+}$  and  $O^{5+}$ ) were similar, as the plasma potential values given in table 6.3 indicate. According to reference [22], the ion temperature increases as the electron density of the plasma increases. With higher

frequencies one can achieve higher electron densities and consequently the ion temperature should also increase. If the ion temperature is high compared to plasma potential, the results which best represent the true plasma potential are obtained with high charge states. If we, for example, considered an ion originating from a plasma potential of 10 volts with a thermal energy of 7 eV, the decelerating voltage needed to stop  $O^{7+}$  ions is 11 volts, being 17 volts for  $O^+$  ions. In conclusion it can be stated that the most reliable plasma potential values are measured with high charge states (as indicated in table 6.3 with bold type). This observation is utilized in all the measurements presented in the following chapters.

In order to study the effect of ion temperature on the measured plasma potential curves (plasma potential +  $T_i$ ) the code described in section 6.1.2. was used. As was mentioned previously, with the aid of the simulation it was seen that the temperature of the ions indeed determines the shape of the measured voltage-current curve in the saturation region, whereas the shape of the curve at low stopping voltages depends mainly on the potential profile and the spatial distribution of the ions. The potential profile and the spatial distribution of the ions were chosen so that the simulated curves matched the measured curves with voltages lower than the plasma potential determined from the measured curve. The negative dip was not included in the potential profile. As an example, figure 6.7 shows a measured plasma potential curve (ANL ECR2, 12.28 GHz, 330 W) for an  $O^{7+}$  ion beam with the corresponding simulation result. The plasma potential value determined from the measured curve is 9.5 V, which was used as the maximum value of the potential (profile) in the simulation. An ion temperature of 20 eV was found to best match the measured curve in the saturation region (region C). This result was confirmed with the aid of an exponential fit into the data points in the saturation region resulting in the same value with extremely good correlation. The exponential fit reflects the exponential dependence of the Maxwellian velocity (and energy) distribution of the ions in the plasma.

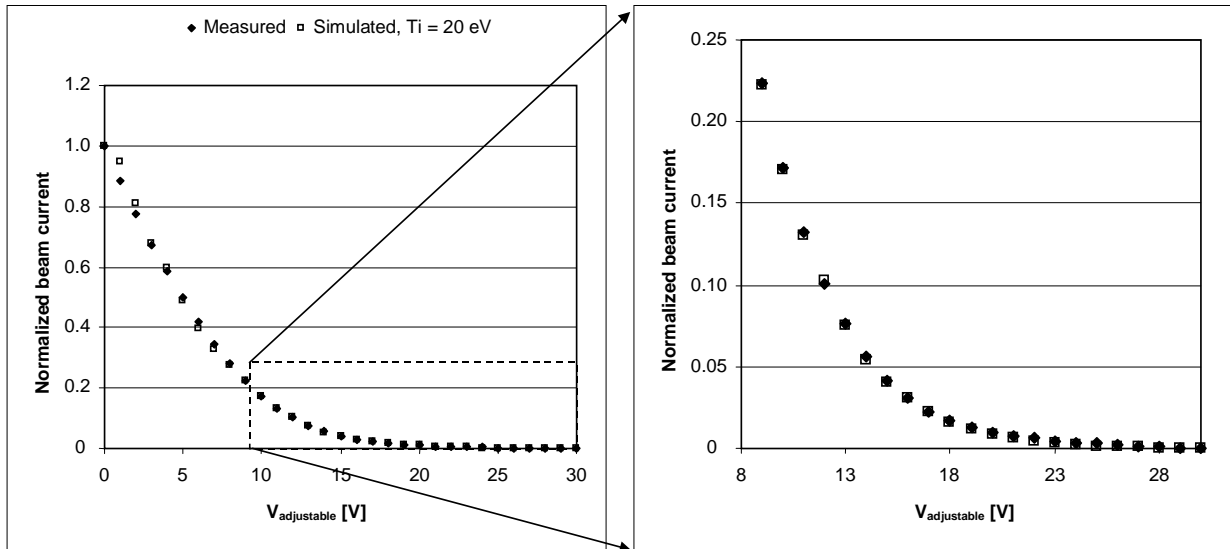


**Figure 6.7** Measured plasma potential curve (with  $O^{7+}$  ion beam / ANL ECR2 / 12.48 GHz / 330 W) and the corresponding simulation result. An ion temperature of 20 eV was found to best match the measured curve in the saturation region (region C).

Some ion temperatures for different charge states of oxygen ions, determined by comparing the simulated and measured plasma potential curves (ECR2 at ANL, 14 GHz / 626 W), are presented in figure 6.8. The value of the maximum plasma potential for each column was determined with the aid of the measured curve of  $O^{7+}$  and the same value was used for the other charge states. The error related to the ion temperature was estimated by comparing the correlation between simulation results and measured curves. It was observed that the error is about  $\pm 2$  eV for high charge states and about  $\pm 1$  eV for low charge states ( $O^+$  and  $O^{2+}$ ). The ion temperature value determined with the simulation was not observed to be very sensitive to variation of assumed plasma potential profile and ion spatial distribution although the method used to determine the ion temperature is model-dependent.

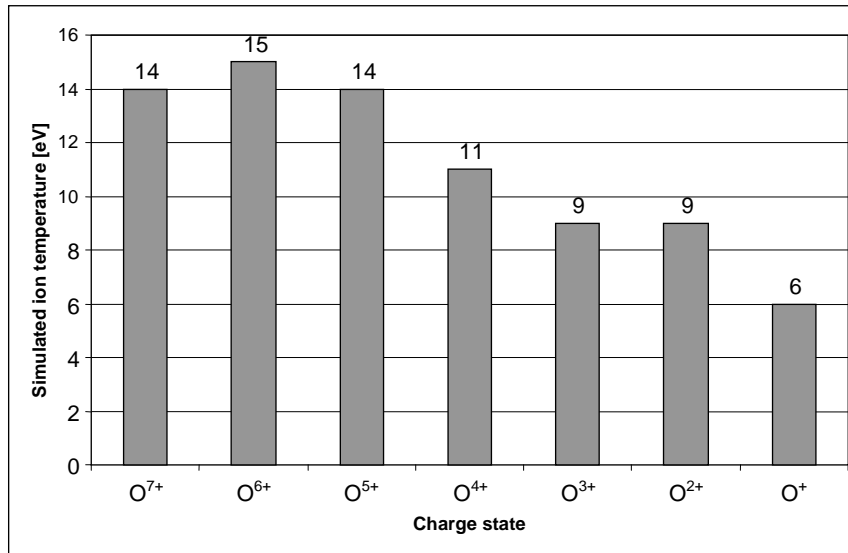


**Figure 6.8** Simulated ion temperatures for different oxygen charge states. The plasma potential curves were measured with ECR2 at ANL (14 GHz / 626 W).

The simulated ion temperatures increase with increasing charge state. However, the highest charge states seem to have the same temperature, around 15 eV. The simulation seems to overestimate the ion temperature in the ECRIS plasma even by an order of magnitude, compared to reference [22]. However, the ion temperatures presented in figure 6.8 are in the same order of magnitude with ion temperatures (6-13 eV) reported in reference [37]. Those results were obtained independently (and published later than the work presented in this thesis) with the aid of an energy analyzer located in the beam line before the dipole magnet. It was observed that the temperature-dependent part of the beam current decay curve including all charge states can be modeled with a single exponential function implying that “effective” ion temperatures are proportional to charge state [37], which is similar to our observation. It has to be taken into account that the simulated ion temperatures correspond to the thermal energy (temperature) of the extracted ions, which probably differs from the thermal energy of the ions that are well-confined in the plasma. It is possible that the extraction process favors those ions whose thermal energy is high enough, which would result in overestimation of the actual ion temperature inside the plasma. The calculated charge state dependence of the ion temperature speaks for the existence of the potential dip in the central plasma. In this confinement scheme the ion temperature of high charge states has to be higher than the ion temperature of low charges states to escape from the dip. It is also possible that the charge state dependence of the (measured) ion temperatures is partly generated in so-called Bohm-sheath region at the plasma boundary [37].

However, if the temperature of the cold electron population is assumed to be close to the plasma potential (see reference [17]), the temperature of this electron population would be 10-20 eV for 14 GHz ion sources. In this case, the equipartition time between oxygen ions and the cold electron population would be 20 – 60 ms as was shown in figure 2.8 (calculated for typical plasma parameters). In section 2.5.4. it was mentioned that the production times for different charge states vary from a few milliseconds to tens of milliseconds. It was also shown that the production time increases with increasing charge state (see references [45] and [46]). This means that highly charged ions would have enough time to thermalize with the cold electron population while low charge states escape before reaching equilibrium. Furthermore, it could be expected that highly charged ions are in thermal equilibrium with each other and cold electrons if the production time of high charge states exceeds the equipartition time with the cold electron population. This is exactly what the simulation results show. It is also of note that the ion sound wave heating is more effective for high charge states [49]. In the case of the JYFL 14 GHz ECRIS the simulated ion temperatures for oxygen ions are somewhat higher (~20 eV) than for ECR2 at ANL. Also, the plasma potential was observed to be higher for the former ion source. This could mean that the average energy of the cold electron population is higher since it can be assumed to be related to the value of the plasma potential. The plasma potential is related to the loss rate of electrons (and ions) and therefore reflects the cold electron energy. The simulated ion temperature values for the JYFL 6.4 GHz ECRIS were close to those simulated for the JYFL 14 GHz ECRIS.

In reference [33] ion temperatures of ~20 eV measured with a single cell quadrupole mirror (Constance B) for plasma parameters rather close to an actual ECRIS are reported. The temperatures (that were observed to increase with increasing charge state) were determined by measuring the Doppler broadening of the emission lines for oxygen ions. Constance B was built as a plasma confinement device for fusion plasma experiments. Thus it was optimized for particle confinement rather than for ion extraction. The large dimensions of the Constance B plasma (about 20 cm in diameter, and about 50 cm in axial length) together with the magnetic structure properties lead to slightly higher densities and confinement times than those of an ECRIS [31]. The higher electron density (with the same average electron energy as in ECRIS) and ion confinement time should result in higher ion temperatures than in the case of ECR ion sources, if the ions are assumed to have time not only to thermalize with the cold electron population but also to gain energy from the warm electrons [31].

### 6.2.2. Plasma potential vs. microwave power and gas feed rate

The plasma potentials of oxygen and argon plasmas were measured with the JYFL 6.4 GHz ECRIS as a function of the microwave power launched into the plasma chamber. Different gas feed rates were used and the main criteria for the chosen feed rate was the stability of the plasma. An example of the results obtained with an argon plasma are presented in figure 6.9 [44].

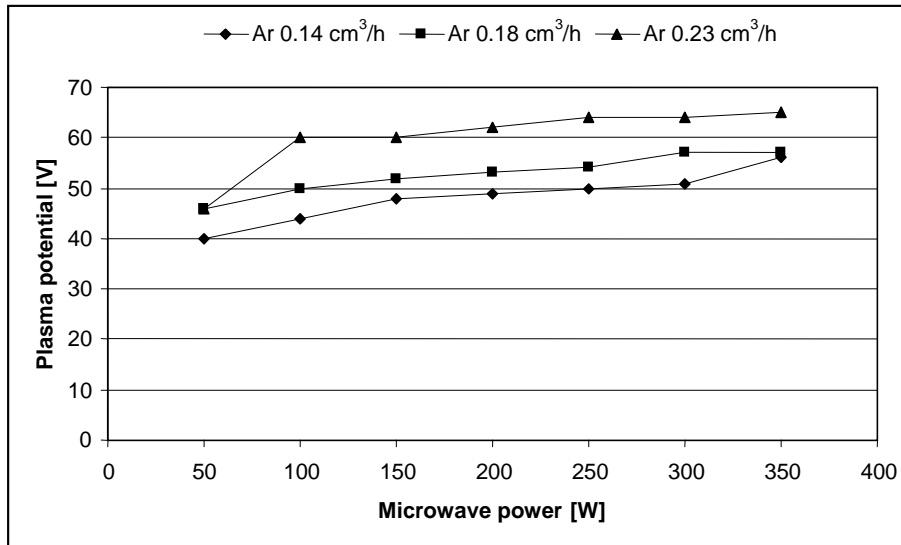


**Figure 6.9** Plasma potential of the JYFL 6.4 GHz ECRIS with different microwave power and argon feed rates. The charge state  $Ar^{9+}$  was used in the measurement [44].

The plasma potential tends to increase as the microwave power or the gas feed rate is increased. These tendencies are probably due to the increased plasma density and density gradients, which eventually lead to faster escape of electrons from the plasma [34]. A higher plasma potential is consequently needed to balance the loss rates of electrons and ions. The dependence of the plasma potential on microwave power and gas feed rate is similar to ambipolar diffusion. The results are consistent with those reported in reference [34].

In the case of the JYFL 14 GHz ECRIS, the plasma potential was observed to increase with increasing microwave power while it remained the same (or even decreased) for ECR2 at ANL. The effect of the microwave power on the plasma potential for an oxygen plasma is shown in figure 6.10. This behavior could mean that the secondary electron emission properties of these ion sources are different. In reference [34] it was reported that coating the copper plasma chamber with aluminum oxide, which has high secondary electron emission coefficient, made the plasma potential

nearly independent of the microwave power. The effect of secondary electrons emitted from the plasma chamber walls on the plasma potential is discussed further in chapter 6.2.7. It is also possible that increasing the microwave power above a certain threshold does not affect the electron energy distribution and the proportion of low energy electrons responsible for the plasma potential build up. It was shown in chapter 2.3.2. that the temperature of the high energy electron population saturates as the microwave power is increased. Therefore, it could also be expected that the temperature of low-energy electrons and the value of the plasma potential saturates when the microwave power is increased.

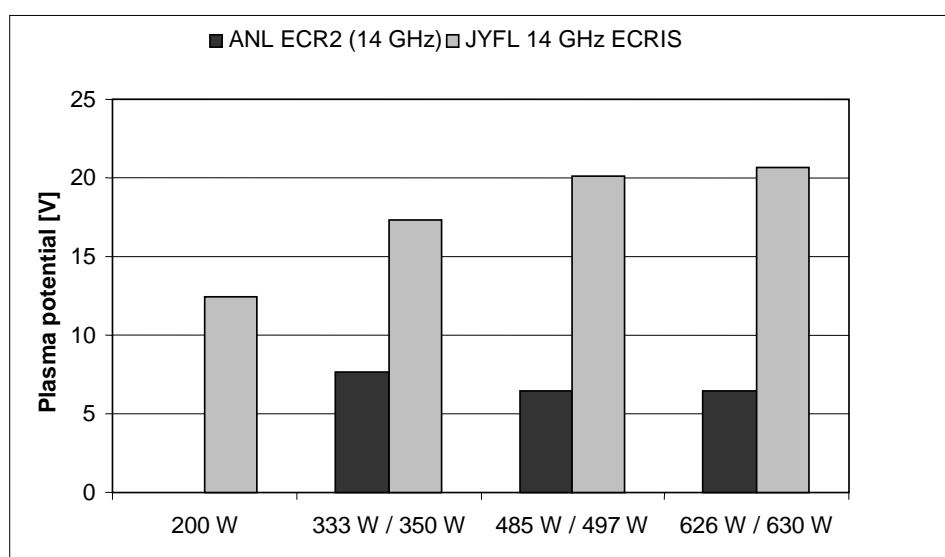


*Figure 6.10 Plasma potential of an oxygen plasma as a function of the microwave power for different ion sources.*

### 6.2.3. Plasma potential vs. mass of the ionized gas

The plasma potential of the JYFL 6.4 GHz ECRIS has been studied with different elements ranging from hydrogen (1 amu) to krypton (84 amu, the most abundant isotope). The measurements were performed with several microwave power settings (50 – 380 W) and gas feed rates, while the other source parameters were kept constant. It was again observed that the plasma potential tends to increase as the microwave power or the gas feed rate is increased. The range of plasma potential values for different gases is presented in table 6.4 [76].

Plasma	Plasma potential range [V]	Gas feed rate [cm <sup>3</sup> /h]
Hydrogen ( <sup>1</sup> H)	22 – 33	0.41 - 0.81
Deuterium ( <sup>2</sup> H)	19 – 39	0.40 - 0.82
Helium (He)	36 – 47	0.59 - 1.25
Nitrogen (N)	36 – 46	0.12 - 0.22
Oxygen (O)	32 – 60	0.09 – 0.22
Neon (Ne, natural)	43 – 60	0.08 – 0.17
Argon (Ar)	40 – 65	0.14 – 0.23
Krypton (Kr, natural)	47 - 62	0.16 – 0.20

**Table 6.4** Range of plasma potentials obtained for different elements with the JYFL 6.4 GHz ECRIS [76].

The measured plasma potentials were somewhat higher in the case of heavier ions. This is probably due to the fact that the mobility of heavier ions is lower than the mobility of lighter ions (see equation (20)). A higher plasma potential is therefore needed to balance the electron and ion losses (loss rates of negative and positive charge). Figure 6.11 clarifies the effect of the ion mass by showing the range of plasma potentials as a function of the average mass of the ions in the plasma of the JYFL 6.4 GHz ECRIS. The average mass was estimated from the spectrum of extracted ion beams taking into account residual gases. The error bars in average mass correspond to situations with different gas feed rates. A trend line fitted to the measured data is also shown. It is of note that the increase of the plasma potential with the ion mass is almost logarithmic, which supports the validity of equation (21) for ECRIS plasmas (also taking into account the increase of the average charge).

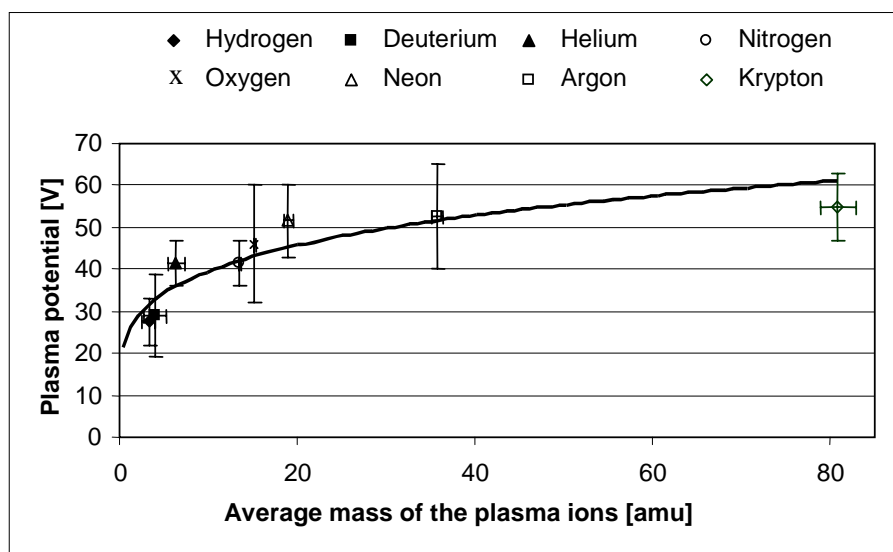


**Figure 6.11** Range of plasma potentials as a function of the average mass of the ions in plasma of the JYFL 6.4 GHz ECRIS.

#### 6.2.4. Plasma potential vs. negative voltage of the biased disk

The effect of the negative voltage of the biased disk on the plasma potential was studied with the JYFL 6.4 GHz ECRIS. Measurements with  $O^{6+}$  ion beam were performed for several microwave power settings. The tuning of the ion source was kept constant as the voltage of the disk was varied between  $-10$  and  $-100$  volts. The measurement was not performed with zero disk voltage because the power supply used for the bias is not capable of regulating negative voltages lower than  $-10$  V (or to provide positive voltages). The following oxygen ( $O_2$ ) feed rates and biased disk voltages were found to be optimal for different microwave powers:  $0.17$   $cm^3/h$  and  $-41$  V for  $100$  W,  $0.25$   $cm^3/h$  and  $-43$  V for  $200$  W and  $0.24$   $cm^3/h$  and  $-48$  V for  $300$  W. The highest  $O^{6+}$  beam currents were obtained with these source settings. Figure 6.12 shows the plasma potential as a function of biased disk voltage with different microwave power settings.

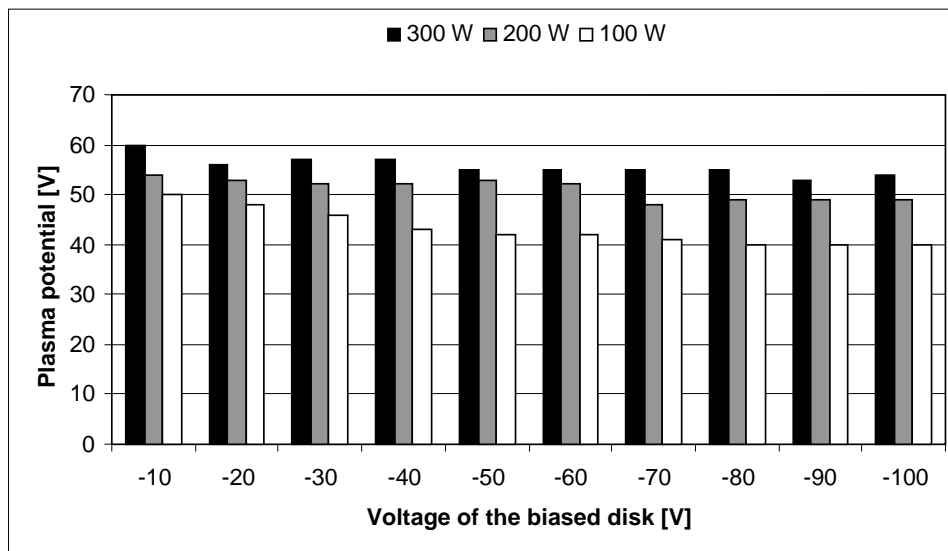


**Figure 6.12** Plasma potential of the JYFL 6.4 GHz ECRIS as a function of the biased disk voltage with different microwave power settings (measured with oxygen plasma).

The plasma potential tends to decrease when the voltage of the biased disk becomes more negative compared to the source potential ( $10$  kV). A possible explanation is that by changing the voltage of the biased disk one affects the loss rates of electrons and ions at the injection end of the plasma chamber, which affects the balance of Simon short circuit currents. Applying higher negative voltage to the disk pushes cold electrons towards the plasma and drags ions out of it more effectively near the biased disk. It has been shown that the electron flux hitting a biased electrode decreases as the negative voltage is increased [40], which supports the conclusion. Due to this process, the positive plasma potential that builds up in order to compensate for the loss rates of the

charge particles is reduced. In the work presented in reference [40] it was shown that the role of secondary electrons emitted from the biased disk is only minor.

Normally, a lower plasma potential leads to enhanced production of highly charged ions (HCI). However, in this case increasing the voltage of the biased disk over optimal values reduced the extracted current of the  $O^{6+}$  ion beam although the plasma potential was lowered. A possible explanation is that the voltage of the biased disk forms a loss channel for the ions to the injection end of the ion source reducing the number of ions available for extraction, which is also a loss process. The currents of highly charged ions can also decrease due to enhanced neutralization on the surface of the disk as the (negative) disk voltage is increased. This would reduce the average charge of the plasma.

#### ***6.2.5. Plasma potential vs. strength of the (axial) magnetic field***

The plasma potential of the JYFL 6.4 GHz ECRIS was measured as a function of the current in the coils producing the axial magnetic field. Initially the extracted beam current of highly charged ions was optimized by varying the gas feed rate with constant microwave power (200 W) and biased disk voltage (-60 V) when the coils (four coils, two of them located at the injection end and two at the extraction end of the source) were excited with maximum current i.e. 200A/250A/250A/250A. The stability of the plasma was also used as a criterion for the optimal feed rate of the gas. The corresponding plasma potential was measured, before decreasing the coil current to 99% of the maximum. The plasma potential was subsequently measured and the procedure was repeated until the current in the coils was only 85 % of the maximum. The change in the coil current corresponds to a change of 13 %, from 5.24 to 4.57, in the axial mirror ratio ( $B_{max}/B_{resonance}$ ). The magnetic field values on the axis of the plasma chamber corresponding to maximum current in the coils are the following: at the injection 1.20 T ( $B_{inj}$ ), at the extraction 0.64 T ( $B_{ext}$ ) and in the centre of the plasma chamber 0.16 T ( $B_{min}$ ). The strength of the magnetic field decreases linearly with the decreasing current in the coils. The measurement was performed with oxygen and argon plasmas. Figure 6.13 presents the results obtained with argon.

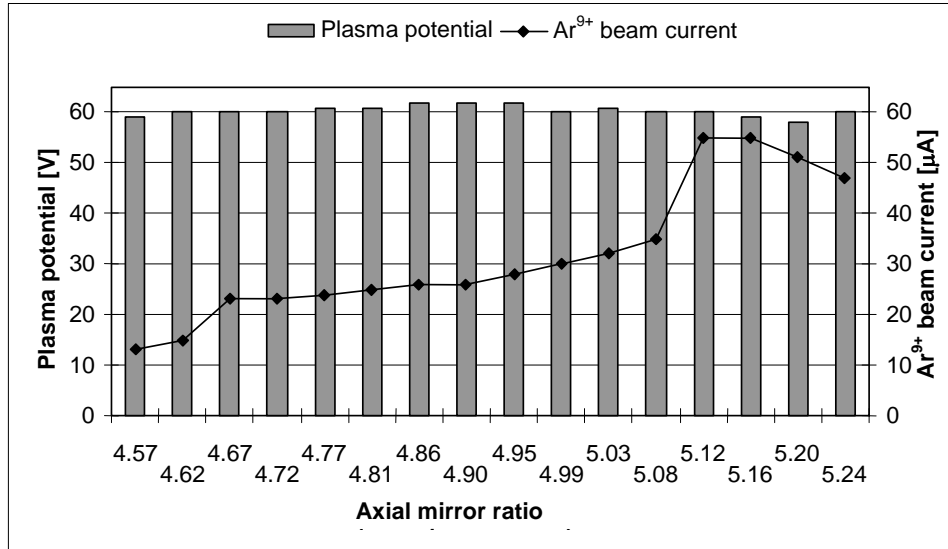


**Figure 6.13** Plasma potential of an argon plasma and  $\text{Ar}^{9+}$  beam current as a function of the (axial) magnetic field strength.

The plasma potential remains unchanged as the strength of the magnetic field (mirror ratio) increases. The highest  $\text{Ar}^{9+}$  ion beam current was obtained when the mirror ratio was nearly at the maximum. A possible explanation for the observed behavior is the increasing electron density of the plasma, which leads to enhanced production of highly charged ions. However, it was observed that the plasma potential is not strongly dependent on the field strength. It has been suggested that highly charged ions are trapped in a potential dip in the centre of the plasma [38]. The central dip would be caused by the strongly confined hot (and warm) electron population, which has gained energy in the ECR resonance zone. This electron population (mainly responsible for the production and confinement of highly charged ions) is affected more by the magnetic mirror effect than the thermal electron population. Thermal electrons having high collision frequency are easily scattered into the loss cone (confined weakly) and therefore they are mainly responsible for plasma potential build up, which explains the observation that the potential remains almost constant as the strength of the magnetic field is varied. Shortening the confinement time has been observed to decrease the extracted currents of highly charged ions such as  $\text{Ar}^{9+}$  and to increase the extracted currents of lower charge states [2].

#### 6.2.6. Plasma potential vs. axial / radial microwave power ratio

The effect of feeding microwaves into the plasma chamber axially vs. radially was studied with the JYFL 6.4 GHz ECRIS [103]. Here axial or radial means that the power is launched into the plasma chamber through the injection plug or through the radial port of the plasma chamber, respectively.

The ratio of axially or radially launched power was varied continuously with the aid of a power divider. It was observed that the extracted beam currents of highly charged ions could be increased 5 - 10 % when a fraction of the microwave power was launched radially. The best results were obtained with power ratios ( $P_{axial} / P_{total}$ ) between 60 and 80 % [103]. The effect of launching the microwaves through two separate waveguides (axial and radial) on the plasma potential was studied with oxygen plasma. The results are presented in figure 6.14 showing that the plasma potential was practically constant despite of the power ratio. This indicates that the loss rate of cold electrons that are responsible for the plasma potential does not depend on the location of the power absorption or the standing wave mode excited in the plasma chamber. In order to study the dependence of the plasma potential on the wave mode it would be beneficial to repeat the measurements also as a function of the azimuthal and radial position of the axial waveguide. Unfortunately, the construction of the JYFL 6.4 GHz ECRIS does not provide this possibility.

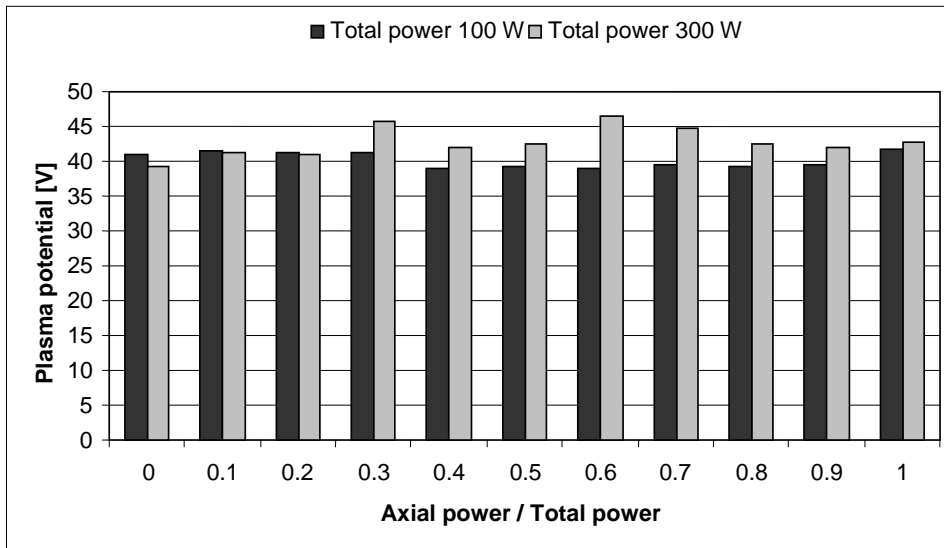


**Figure 6.14** Plasma potential of an oxygen plasma with different power ratios. The microwave power was launched into the plasma chamber through axial and radial waveguides.

### 6.2.7. The effect of carbon contamination on the plasma potential

The oxidized surface of the aluminium plasma chamber (JYFL 14 GHz ECRIS) acts as a source of secondary electrons. In table 3.1, it was shown that the coefficient for secondary electron emission is higher for alumina than for the carbon layer (soot). Consequently, secondary electron emission from the plasma chamber walls decreases significantly due to carbon contamination, which affects the performance of the ECRIS.

The effect of carbon contamination on the plasma potential curves was studied with the JYFL 14 GHz ECRIS. Before a MIVOC run ( $^{46}\text{Ti}$  with maximum intensity) the plasma potential was measured to be about 20 V depending slightly on the microwave power. After a MIVOC-run of almost three weeks the plasma potential was approximately 50 V. The corresponding maximum intensities of  $\text{O}^{7+}$  ion beam were  $160 \mu\text{A}$  (before the MIVOC-run) and  $48 \mu\text{A}$  (after the MIVOC-run). In section 5.3. it was shown that the carbon contamination can be removed with the aid of an oxygen plasma. However, in this case, the contamination was severe and removal with an oxygen plasma would have been too time consuming. Therefore the carbon was removed by cleaning the plasma chamber with alcohol, which caused the plasma potential to drop to 30 V and the intensity of the  $\text{O}^{7+}$  ion beam to increase to  $80 - 100 \mu\text{A}$ . Mechanical polishing of the plasma chamber would have restored the performance to the original level. In addition to higher plasma potentials it was observed that the shape of the measured plasma potential curve changed dramatically due to the contamination. The normalized plasma potential curves measured for different contamination levels are presented in figure 6.15.

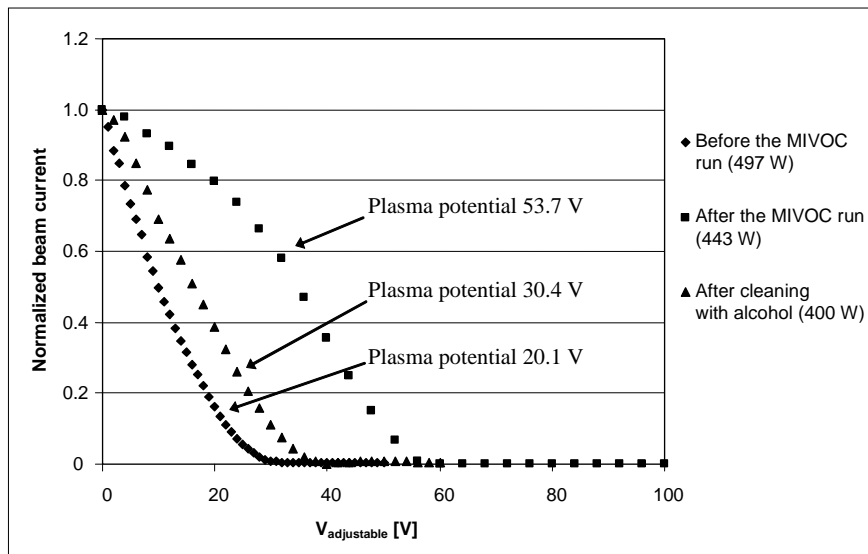


**Figure 6.15** Normalized plasma potential curves measured before and after a contaminating MIVOC-run. The curve measured after alcohol cleaning is also shown.

The measurement confirmed that feeding extra electrons into the ECRIS plasma reduces the plasma potential. According to figure 6.15, secondary electrons affect the profile of the plasma potential or the ion spatial distribution so that fewer ions (proportionally) originate from low potential in the case of severe contamination. In the case of severe contamination the plasma potential curves measured with the JYFL 14 GHz ECRIS were reminiscent of those measured with the JYFL 6.4

GHz ECRIS (copper chamber) i.e. region A appeared on the curve. The results presented in this chapter emphasize the importance of reducing carbon contamination during a MIVOC-run, which was discussed in chapter 5.2. Further evidence concerning the role of the secondary electrons was obtained with the JYFL 6.4 GHz ECRIS, which has been recently upgraded [104]. The effect of changing the copper plasma chamber to aluminum was dramatic. The plasma potentials for oxygen plasmas decreased from 40 – 50 volts to approximately 25 volts for copper and clean aluminum surfaces, respectively.

The plasma potential build up process is assumed to be related to ambipolar diffusion [34] and the diffusion rate of charged particles is proportional to density gradients. Secondary electrons emitted from the walls of the plasma chamber probably increase the overall electron density and decrease the density gradient as they flow towards the plasma from the exterior of it. This leads to a lower plasma potential. The electron flow towards the plasma also affects the Simon short circuit currents that describe the balance of particle losses from the plasma. The axial losses of electrons can increase when more electrons flow into the plasma radially, that would increase the extracted beam currents as the ions follow the electrons to the extraction.

#### ***6.2.8. Momentum spread of the ion beam and its influence on the emittance***

The growth of the emittance due to non-zero ion beam momentum spread and the dispersive matrix elements of the beam transport system was considered theoretically in section 3.3.3. The energy (momentum) distribution of the extracted ion beams can be studied experimentally with the aid of the plasma potential measurement instrument. By taking the derivative of the measured beam current decay curve with respect to the stopping voltage, the number of ions with a certain energy can be deduced since the energy of the ions can be expressed in electron volts as  $Q \cdot V_{stopping}$ . For ECR2 at ANL, for example, the energy spread was found to be 8-20  $q$  eV. This result is in good agreement with the results measured with the Oak Ridge ECRIS [105].

Precise energy distribution measurements would require stronger collimation of the ion beam, since the transverse acceptance of the retarding field analyzer restricts the longitudinal energy resolution. However, the transverse acceptance of the device must be high enough for a reliable plasma potential measurement. The longitudinal energy resolution  $\Delta E/E$  of the device with a 4 mm collimator was calculated with the aid of SIMION 7.0 program. The resolution was found to be approximately 0.035 % at 10 kV source potential for the maximum measured beam divergence

(maximum  $y'$  25 mrad for 95 % emittance fit). For lower divergence values the energy resolution is better. The calculation takes into account the electric field distribution inside the device. With a 10 kV acceleration voltage this corresponds to a change of 3.5 V in the stopping voltage. However, it was observed by simulation that the measured value of the plasma potential is affected less than 1 volt due to the energy resolution of the device, since the method of determining the plasma potential averages the divergence coordinates of all beam particles. It was also observed that the energy resolution can not explain the shape of the beam current decay curves in region C (see figures 6.2 and 6.4).

The observed energy distribution of the ion beams motivated us to study the effect of the energy spread and the plasma potential on the effective (measured) emittance of the ion beams for the JYFL ECR ion sources. This effect is mainly due to the dipole magnet, which is a dispersive ion optical component and ions with different momentum have a different radius of curvature. The growth of effective emittance was studied with the aid of a simulation developed with the Mathematica 4.1 program. The simulation is applicable to continuous beams since it utilizes 5x5 first-order transfer matrices of different ion optical components, taking into account the coupling of the emittance values in the bending plane of the dipole magnet ( $x$ -plane) and in the perpendicular plane ( $y$ -plane). The matrix elements for different ion optical components were taken from references [93] and [106]. The effects of the dipole magnet edges and fringe fields were also taken into account. The input parameters of the simulation are the plasma potential of the ion source (maximum momentum spread) and the phase space presentation of the emittance ellipse in both transverse planes at the first collimator located before the dipole magnet (see figure 6.1). The original phase space ellipses were given at this location since the ion beam is focused on the collimator corresponding to an upright ellipse (the shape of the ellipse is known best at this point). The effective emittance in both planes was calculated at the position of the emittance scanner (see figure 6.1.). The ion beam was assumed to be cylindrically symmetric, which restricts the coupling of  $x$  and  $y$  coordinates in the phase space. No coupling restrictions for the angular coordinates  $x'$  and  $y'$  were used. During the simulations it was observed that the Twiss parameters of the simulated emittance ellipses corresponded closely to those of the measured ellipses.

Table 6.5 shows the simulated emittance values for oxygen ion beams extracted from the JYFL 14 GHz ECRIS. The effect of momentum spread on the emittance in  $x$ - (bending plane of the dipole) and  $y$ -planes was simulated with three different plasma potential values, 0 V, 15 V and 25 V (maximum energy spread of the ion beam). The results are presented as area emittance values since

the output of the simulation is a phase space ellipse from which the emittance can be calculated with the aid of a fit. The source potential was set to 10 kV in the simulations. The area emittance was chosen to be  $60 \pi \cdot \text{mm} \cdot \text{mrad}$  for all charge states in the case of zero energy spread (zero plasma potential and ion temperature). The solenoid currents for different charge states were chosen to correspond the values used in the experiments described later. However, the focusing strength of the solenoids is insufficient for low charge states ( $\text{O}^{3+}$ ,  $\text{O}^{2+}$  and  $\text{O}^+$ ). The error related to the simulated emittance values for non-zero plasma potential can be estimated to be  $\pm 5 \pi \cdot \text{mm} \cdot \text{mrad}$ . This is due to the fact that the phase space area occupied by the beam is not an exact ellipse, as the momentum spread of the ion beam causes the ellipses corresponding to certain  $\Delta p/p$  value to drift differently in the phase space.

Plasma potential [V]	0		15		25	
Emittance [ $\pi \cdot \text{mm} \cdot \text{mrad}$ ]	$\epsilon^{xx'}$	$\epsilon^{yy'}$	$\epsilon^{xx'}$	$\epsilon^{yy'}$	$\epsilon^{xx'}$	$\epsilon^{yy'}$
$\text{O}^{7+}$	60	60	77	73	83	79
$\text{O}^{6+}$	60	60	78	73	83	78
$\text{O}^{5+}$	60	60	79	72	87	77
$\text{O}^{4+}$	60	60	81	71	88	77
$\text{O}^{3+}$	60	60	81	70	88	77
$\text{O}^{2+}$	60	60	77	68	86	77
$\text{O}^+$	60	60	75	66	83	76

**Table 6.5** Simulated emittance values, taking into account the effect of the energy spread of the ion beams due to the plasma potential [67].

The energy spread of the ion beam clearly affects the value of effective emittance in both planes. The simulated emittance values are higher in the bending plane of the dipole magnet ( $x$ -plane), the maximum effect of the energy spread being over 40 %. In the  $y$ -plane the maximum observed growth was a little over 30 %. The effect of the dipole magnet on the effective emittance is transferred to the  $y$ -plane due to the beam rotation caused by the solenoid. By changing the solenoid current one can affect the coupling of  $x$ - and  $y$ - emittance values. This was confirmed by setting the solenoid current to zero in the simulation: consequently no growth of the effective emittance due to the energy spread was observed in  $y$ -plane. The difference between the results obtained with different charge states can be explained partly as due to the error in the elliptic fit and partly due to the insufficient focusing strength of the solenoid for low charge states. Another issue that has to be taken into account is that the energy spread of low charge-state ions has been observed to be larger than the energy spread of highly charged ions (in units of  $\text{eV}/Q$ ). The growth of the emittance may

therefore be more significant for low charge states. The effect of the energy spread of the ion beams on their emittance can be reduced by increasing the source voltage (which increases the beam momentum). Another illustration of the emittance growth is presented in figure 6.16 showing the simulated emittance ellipses for  $O^{7+}$  in  $x$ - and  $z$ -planes for zero and non-zero ( $25q$  eV) energy spread. The emittance in the case of zero plasma potential is arbitrarily chosen to be  $52 \pi \cdot \text{mm} \cdot \text{mrad}$ .

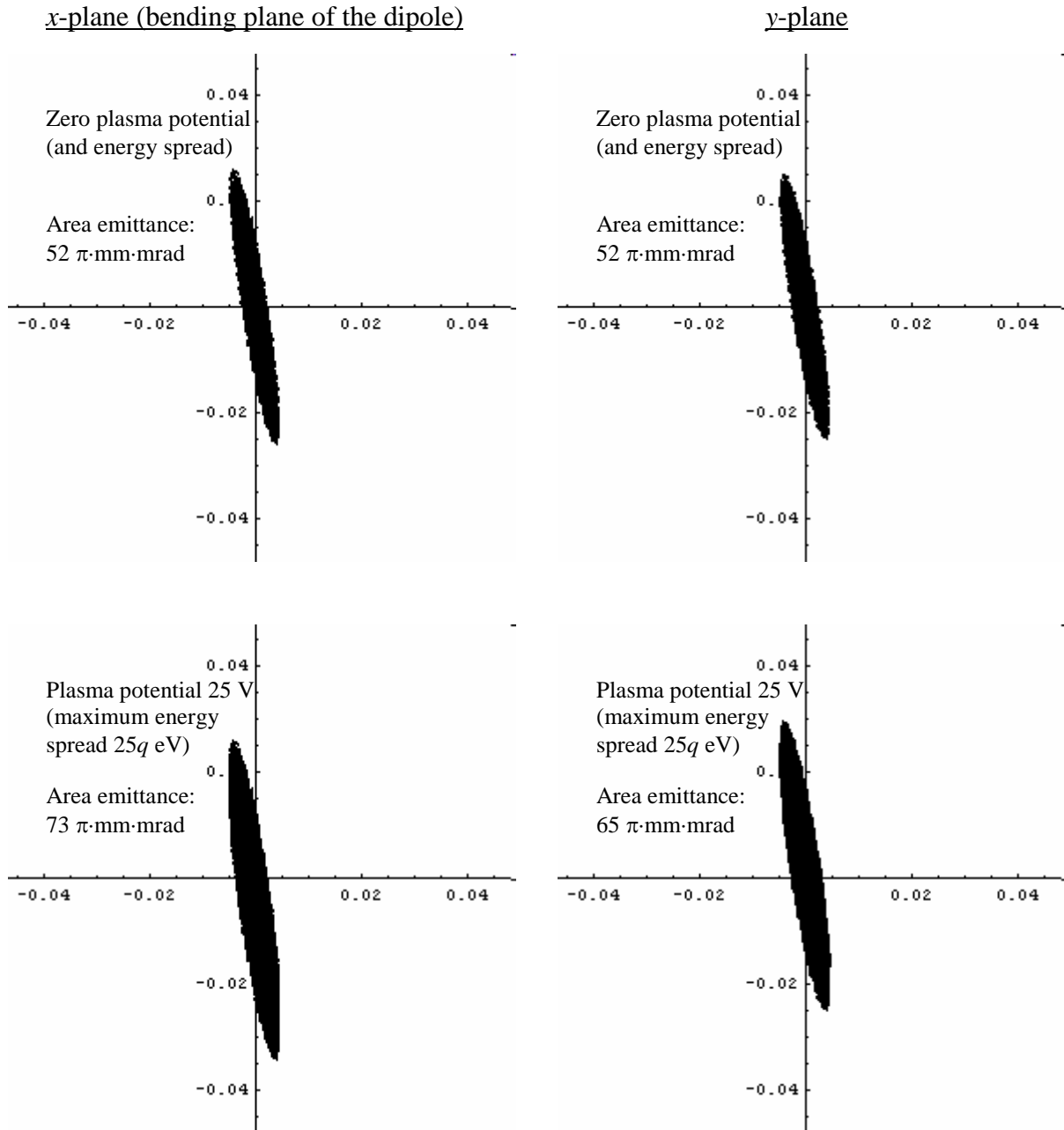


**Figure 6.16** Simulated emittance ellipses for  $O^{7+}$  ion beam in phase space for different energy spreads. The axis units are in meters (horizontal axis) and radians (vertical axis).

In the measurement set-up with the JYFL 14 GHz ECRIS (see figure 6.1), the measured emittance is dependent on the field strength of the solenoid and on the drift length between the solenoid and the emittance scanner. It would be beneficial to measure the emittance in both planes simultaneously if the emittance scanner is located after the dipole magnet and solenoid(s). This would also minimize the uncertainty due to aberrations, which are different in the  $x$ - and  $y$ -planes. Unfortunately, the present beam diagnostics in the beam lines of the JYFL ECR ion sources do not provide this possibility. No significant aberrations were, however, observed in the emittance measurements described in the following.

### 6.2.9. The effect of gas mixing on the emittance and plasma potential

The effect of the gas mixing technique on the emittance of extracted ion beams was first studied with the JYFL 6.4 GHz ECRIS. The results were reported in reference [107]. Figure 6.17 shows the normalized root mean square emittance of an analyzed  $O^{6+}$  ion beam as a function of the proportional partial pressure of mixing gas (helium). The emittance was measured in the bending plane of the dipole magnet. The emittance of the  $O^{6+}$  (high charge state) ion beam decreases slightly or remains constant when a small amount of helium is fed into the plasma chamber. When more helium is added the emittance starts to increase, which is probably due to the higher overall pressure that affects the plasma potential and ion temperature, and therefore the momentum spread of the ion beams. Similar results were obtained with nitrogen-helium ( $N^{5+}$ ) and argon-oxygen ( $Ar^{9+}$ ) plasmas.

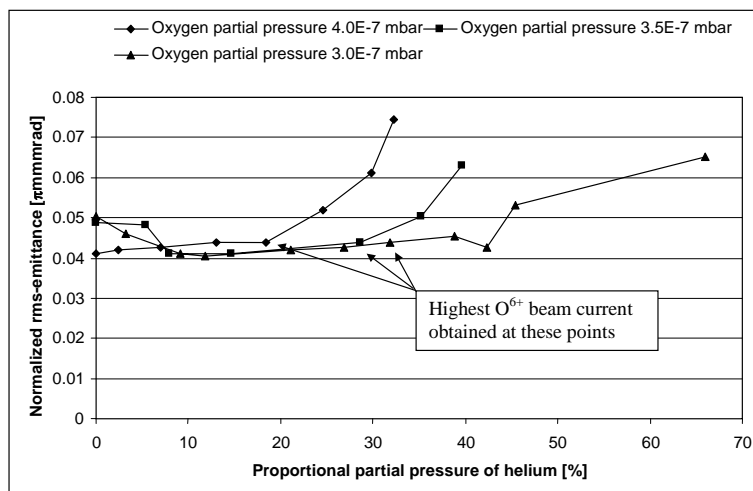


**Figure 6.17** Normalized root mean square emittance of an analyzed  $O^{6+}$  ion beam as a function of helium feed rate [107].

The emittance of the lighter mixing gas was studied by measuring the emittance of both high ( $O^{6+}$ ) and low ( $O^{3+}$ ) charge state oxygen ion beams with an oxygen-argon plasma. Figure 6.18 shows that the emittance of the lighter ions increases when even a small amount of the heavier mixing gas is fed into the plasma chamber. The observed behavior was confirmed with a helium-nitrogen plasma.

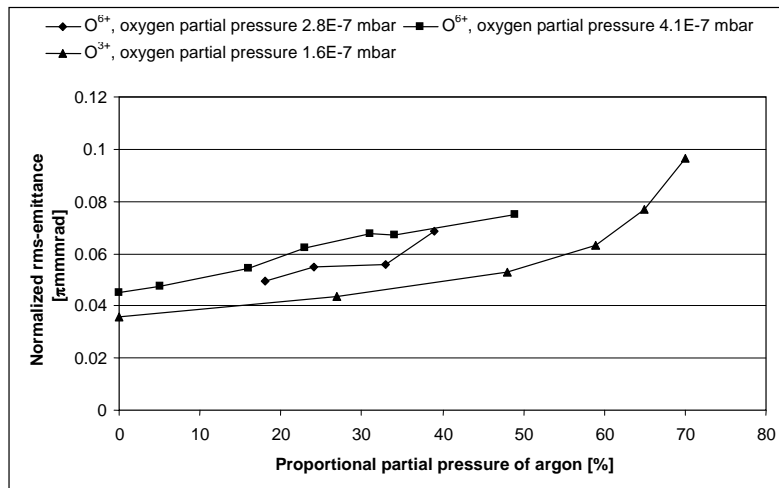


**Figure 6.18** Measured emittance of analyzed  $O^{3+}$  and  $O^{6+}$  ion beams with argon (heavier) used as a mixing gas [107].

Theoretically, the emittance of ion beams extracted from an ECRIS is a sum of two terms (excluding the effects of the hexapole fringe field, see section 3.3.2.). Because the magnetic field configuration of the ion source was kept constant as the mixing ratio oxygen and argon was changed, it is relevant to discuss the effects of gas mixing on the ion temperature. According to the production efficiency results presented in section 5.1., adding a lighter element decreases the energy of the heavier ions. This should affect the emittance of the ion beams of the heavier element due to their decreased temperature. However, it was observed that, for example, adding oxygen into an argon plasma did not decrease the emittance of the  $Ar^{9+}$  ion beam. It has been deduced that highly charged ions are created close to the centre of the plasma [36, 99]. According to the model of ion confinement in the ECRIS plasma, it is possible that the hot electron population creates a small negative potential dip trapping the cold ions in the middle of the plasma, though the overall plasma potential is positive (unfortunately there are no studies either confirming or disproving the existence of this dip). The typical ion energy in the ECRIS plasma can be lowered to a few electron volts by the application of gas mixing [22]. However, the energy of the ions created in the middle of the plasma has to be high enough to overcome the potential barrier generated by the electrostatic well if they are to be extracted from the ion source. This could explain the observation that the emittance of highly charged ion beams remained practically constant although the average energy (temperature) of the heavier ions inside the plasma was probably decreased by gas mixing. For example, if the

depth of the electrostatic dip is 1 volt (based on the discussion in reference [17]), a thermal energy of 9 eV is required for  $\text{Ar}^{9+}$  to escape from the central plasma. The increasing emittance of the ion beams produced from the lighter element can be explained by the ion cooling process. The energy of the heavier ions is transferred to the lighter ones, which causes a growth in the emittance as their thermal energy increases.

The effect of the gas mixing technique on the plasma potential curves was initially studied with ECR2 at ANL. Firstly, oxygen was fed into the plasma chamber and the plasma potential curves were measured with different charge states (series #1). After this, helium was added into the plasma without changing the tuning of the ion source and the plasma potential curves were measured again (series #2). Finally, the measurement was repeated after adjusting the level of helium for maximum output of  $\text{O}^{7+}$  (series #3). The corresponding plasma potentials determined from the beam current decay curves as described in section 6.1.1. are presented in table 6.6, along with the beam currents. Since the plasma potential values shown in the table include the effects of the ion temperature, the most reliable plasma potential value, measured with  $\text{O}^{7+}$ , is presented in bold type.

Series #	1	2	3
Plasma	Oxygen	Oxygen + Helium	Oxygen + Helium
	Plasma potential [V] / Beam current [ $\mu\text{A}$ ]		
$\text{O}^{7+}$	<b>7.1</b> / 24	<b>5.9</b> / 47	<b>6.2</b> / 50
$\text{O}^{6+}$	7.1 / 92	6.7 / 182	7.5 / 194
$\text{O}^{5+}$	8.5 / 70	7.7 / 103	7.4 / 91
$\text{O}^{4+}$ ( $\text{He}^+$ )	9.1 / 59	8.0 / 132	8.2 / 132
$\text{O}^{3+}$	11.3 / 38	7.8 / 30	7.5 / 19
$\text{O}^{2+}$	19.7 / 31	8.1 / 21	7.3 / 12
$\text{O}^+$	23.5 / 16	9.9 / 9	8.0 / 4

**Table 6.6** The effect of gas mixing on the plasma potential determined with different charge states [76]. The values were measured with ECR2 at ANL with a microwave power of 570 W.

Adding helium to the oxygen plasma affects the plasma potential. The plasma potential is slightly lower in the case of gas mixing (7.1 V  $\rightarrow$  5.9/6.2 V) because the ions of the lighter element carry charge out from the plasma more effectively due to their higher mobility. The effect of gas mixing on the shape of the measured plasma potential curves (energy spread of the ion beams) for low charge states was dramatic, while the shape of the curves measured with high charge states did not change. The charge state dependence of the measured curves was observed to almost vanish due to

gas mixing. Figure 6.19 [76] shows normalized plasma potential curves of  $O^{7+}$  and  $O^+$  ion beams for oxygen (series #1) and oxygen-helium (series #3) plasmas. The effect of gas mixing on the curves measured with  $O^{2+}$  and  $O^{3+}$  ion beams was almost as clear as in the case of  $O^+$ . The results indicate that gas mixing affects the temperature of the low charge-state ions of the heavier element more than the temperature of the highly charged ions of the heavier element.

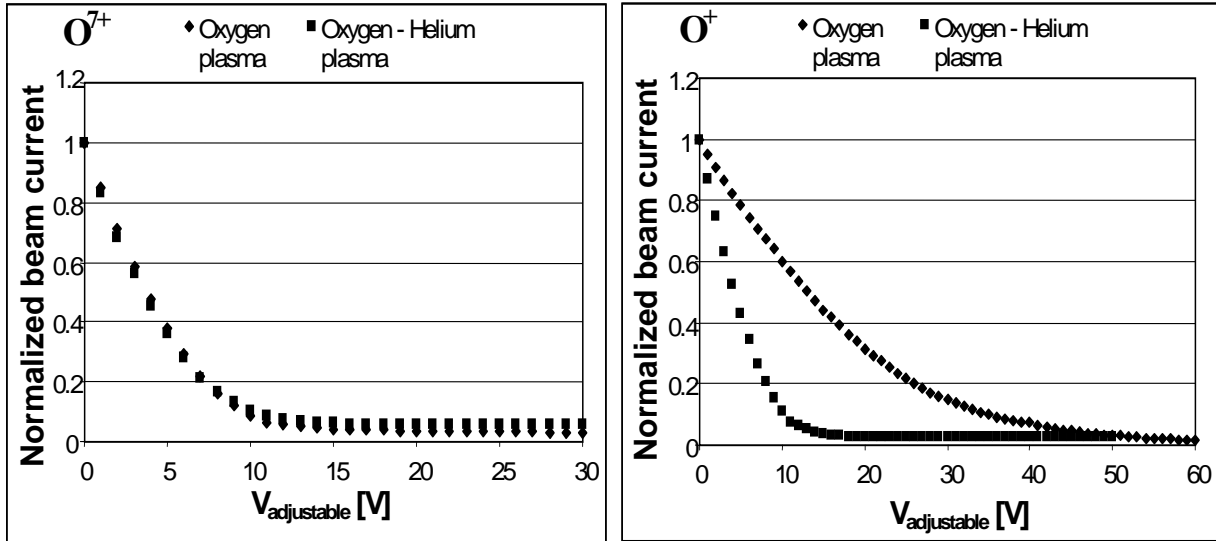


**Figure 6.19** The effect of gas mixing (helium) on the plasma potential curves measured with different charge states of oxygen.

The change in the plasma potential curves was studied also with the simulation described in section 6.1.2. The simulation results (ion temperatures) can be compared to those obtained with a pure oxygen plasma. Figure 6.20 shows the simulated ion temperatures for an oxygen plasma and an oxygen-helium plasma (with the same drain current and plasma potential). It can be seen that the simulated ion temperatures are nearly the same for high charge states, while the temperature of low charge-state ions of the heavier element seems to decrease due to gas mixing.

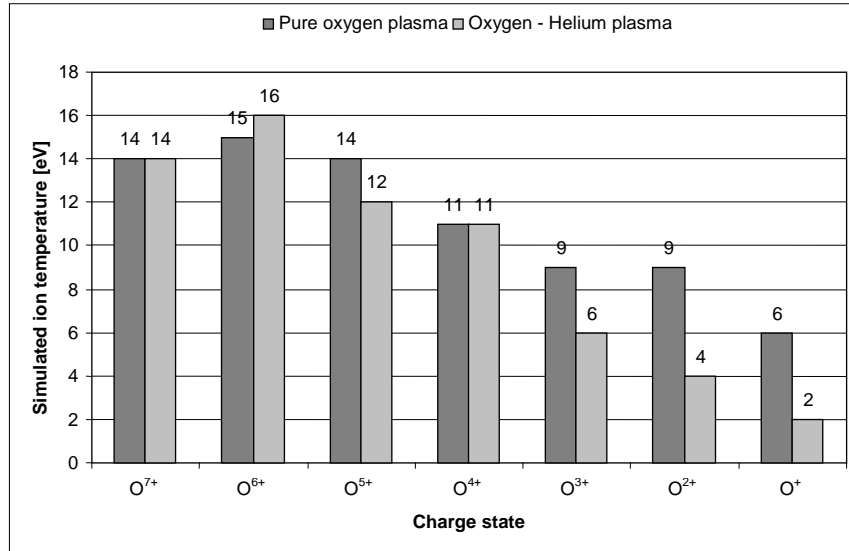


Figure 6.20 The effect of gas mixing (helium) on simulated ion temperatures for different charge states of oxygen.

The effect of gas mixing on the plasma potential and emittance was further studied with the JYFL 14 GHz ECRIS and different gas combinations (He, O, Ar and Kr). The plasma potential results are presented in table 6.7. It was observed that adding helium into the plasma of a heavier element is an effective means to reduce the plasma potential even up to several tens of percent. The higher mobility of helium ions compared to other ions can explain this effect (see equation (20)).

Mixing gas	Ion gas			
	He	O	Ar	Kr
	Plasma potential [V]			
He	16.4	16.7	16.4	20.2
O	-	18.4	19.0	26.0
Ar	-	-	21.0	-
Kr	-	-	-	25.9

Table 6.7 Plasma potential values of different mixed gas discharges (plasmas) measured with the JYFL 14 GHz ECRIS.

The results obtained with ECR2 at ANL implied that adding lighter mixing gas into the plasma lowers the temperature of low charged ions, which should affect their emittance. According to the simulation results presented in the previous chapter, the decreased energy spread should also result into lower effective emittance. Figures 6.21 and 6.22 present normalized root mean square emittance values of different ion beams extracted from the JYFL 14 GHz ECRIS for pure plasmas and mixed gas discharges. The emittance was measured in the y-plane perpendicular to the bending

plane of the dipole magnet in the beam line of the JYFL 14 GHz ECRIS. A more comprehensive set of measurement results is presented in reference [67].

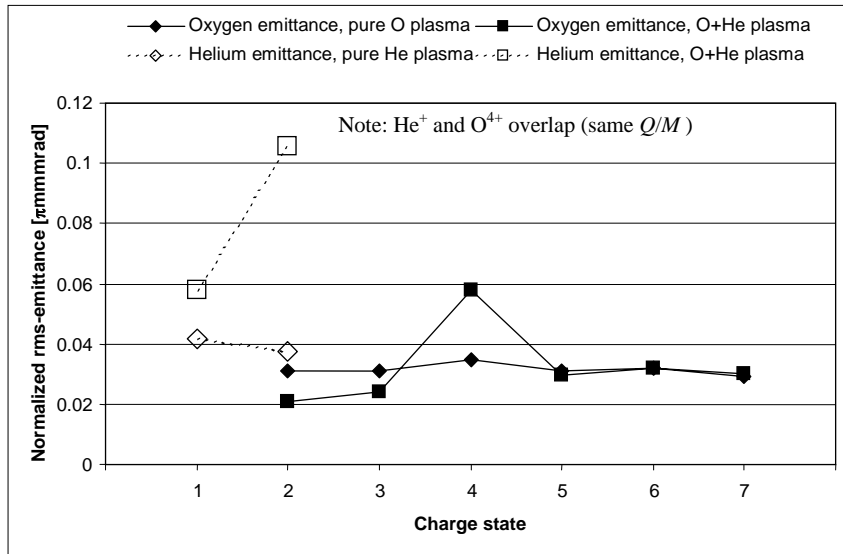


Figure 6.21 Normalized rms-emittance values obtained with pure oxygen, pure helium and oxygen-helium plasmas.

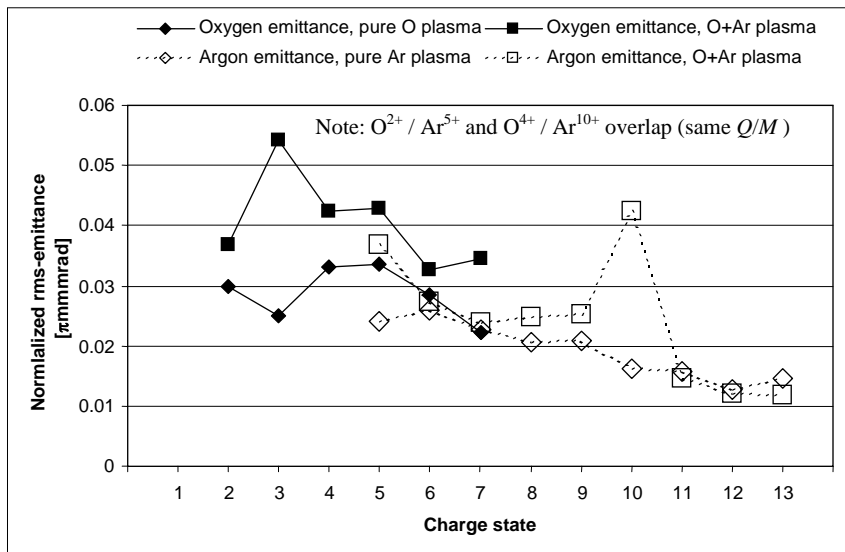
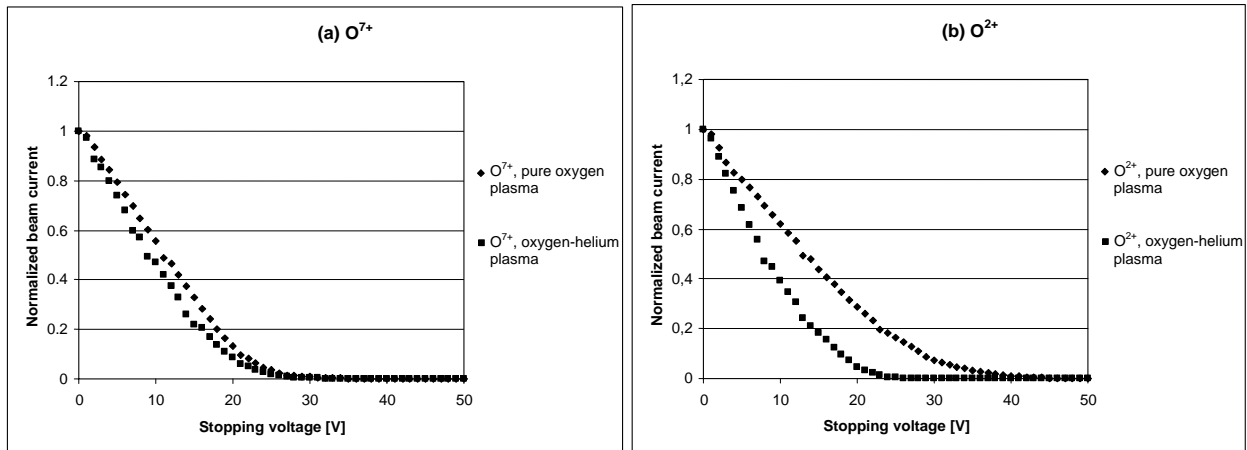


Figure 6.22 Normalized rms-emittance values obtained with pure oxygen, pure argon and oxygen-argon plasmas.

Figure 6.21 shows that the emittance of low charge-state oxygen ion beams decreased as helium was added into the oxygen plasma, while the emittance values measured with high charge states of oxygen remained nearly unchanged (note that  $O^{4+}$  and  $He^+$  cannot be separated with a dipole magnet due to the same  $Q/M$  ratio). The emittance values for helium ion beams were significantly lower for a pure helium plasma than in the case of gas mixing with oxygen. These results were reproducible. Since the magnetic field configuration of the ion source was kept unchanged, these results indicate that the temperature of low charge-state oxygen ions decreases as helium is added

into the plasma if all other parameters affecting the emittance remain constant. For example, the effective extraction radius of low charge-state ion beams may change due to gas mixing and. Figure 6.22 shows that for an oxygen-argon plasma the emittance values measured for the lighter element (oxygen) were also higher than in the case of a pure oxygen plasma. This indicates that the temperature of the oxygen ions increases as argon is added into the plasma chamber. The effect is especially clear for low charge-state oxygen ions, though the emittance values measured with highly charged ions were also higher. The emittance values measured with argon ion beams extracted from an oxygen-argon plasma did not differ much from the values measured without gas mixing (note that  $\text{Ar}^{5+}$  has the same  $Q/M$  ratio as  $\text{O}^{2+}$  and  $\text{Ar}^{10+}$  the same as  $\text{O}^{4+}$ ).

The effect of the momentum spread and ion temperature on the emittance can be estimated with the aid of the plasma potential curves measured in different cases. It seems that the drop in the emittance measured with low charge states of oxygen ion beams due to helium cannot be explained by the decrease of the plasma potential only, but is also due to the decrease of the ion temperature. This is demonstrated in figure 6.23, which shows normalized plasma potential curves measured with  $\text{O}^{7+}$  (a) and  $\text{O}^{2+}$  (b) ion beams with and without helium as a mixing gas. Figure 6.24 shows the effect of heavier mixing gas on the plasma potential curves measured with  $\text{O}^{7+}$  with argon as a mixing gas (a) and  $\text{He}^{2+}$  with krypton as a mixing gas (b), respectively.



**Figure 6.23.** Normalized plasma potential curves measured with  $\text{O}^{7+}$  (a) and  $\text{O}^{2+}$  (b) ion beams with and without helium as a mixing gas [67].

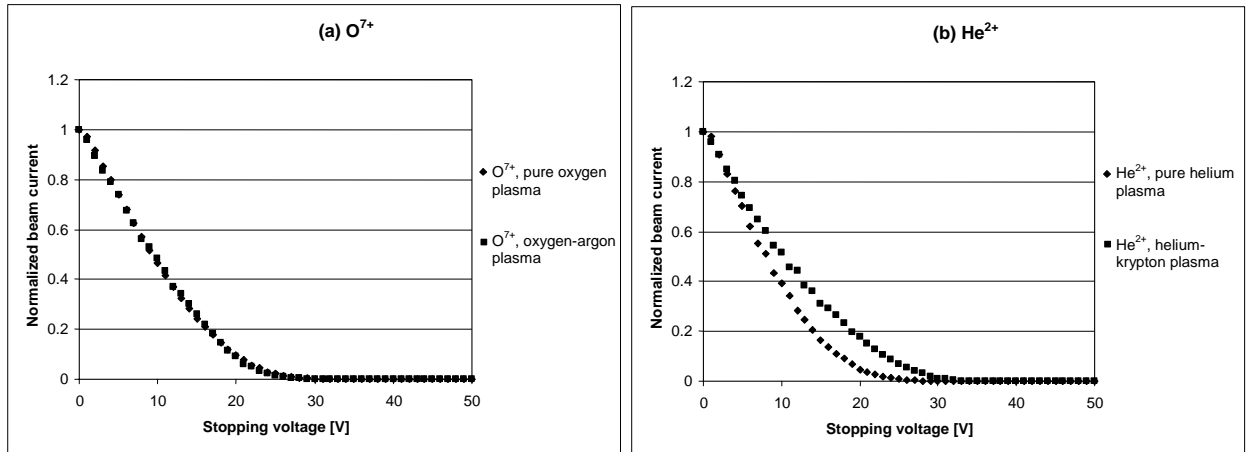


**Figure 6.24** Normalized plasma potential curves measured with  $O^{7+}$  (a) and  $He^{2+}$  (b) ion beams with and without heavier mixing gas (oxygen-argon and helium-krypton).

Figure 6.23 shows that the shape of the plasma potential curve measured with a highly charged ion beam ( $O^{7+}$ ) remains nearly unchanged as helium is added into the oxygen plasma. However, the change in the shape of the curve measured with the low charge-state ion beam ( $O^{2+}$ ) is dramatic, which confirms the result obtained with ECR2 at ANL. The width of the saturation region decreases significantly as helium is added i.e. the energy spread of the ion beam decreases. According to the simulation results (see section 6.1.2.) the temperature of the ions affects the shape of the curve in the saturation region. Our measurement therefore supports the conclusion that the temperature of low charge-state ions of the heavier element decreases when a lighter element is used as a mixing gas. The low charge-state ions of the lighter element gain energy in the collisions and due to their higher mobility carry kinetic energy out of the plasma more effectively. This gives the low charge-state ions of the heavier element a better chance to be further ionized and reach high charge states before escaping the plasma, which explains the increase in current of highly charged ion beams. According to figure 6.24a adding argon into the oxygen plasma does not affect the shape of the plasma potential curve measured with an  $O^{7+}$  ion beam. A similar result was also obtained with an oxygen-krypton plasma. The effect of adding heavier gas into a plasma of the lighter element can also be seen in figure 6.24b, which shows that the energy spread of the low charge-state ion beam ( $He^{2+}$ ) increased significantly as krypton was added into the plasma. The effect of the heavier gas on the beam current decay curves measured with low charge states of the lighter element was observed also with helium-argon, oxygen-argon and oxygen-krypton plasmas. This indicates that the temperature of low charge-state ions of the lighter element increases due to the gas mixing. These observations support (along with the emittance measurements) the conclusion that ion cooling explains the beneficial effect of gas mixing. However, the observed ion temperature

deviations between different charge states strongly suggest that in addition to ion cooling the Landau damping of the ion sound wave that heats highly-charged ions (and lighter ions) more effectively can have an effect on ion temperature in ECRIS plasmas [70].

It was confirmed with a simulation that the change in the energy spread due to plasma potential cannot totally explain the change of emittance when mixing gas is added. Also this indicates that the temperature of the ions changes due to mixing gas. Unfortunately, the effects of gas mixing on the ion temperature, plasma potential profile and the spatial distribution of the ions in the plasma cannot be separated directly from the measured data without computer simulations. Gas mixing probably affects not only these parameters, but also the confinement time for different charge states [22]. However, the change in the spatial distribution of the ions cannot explain why the plasma potential curves measured with low-charged ions become “wider” as heavier gas is added into the plasma. If this was caused only by a change in the spatial distribution, more low charge-state ions would originate from the central plasma where the plasma potential profile is at a maximum. This is contradictory to the assumption that losses of low charge-state ions increase due to gas mixing. Experimental results presented in this chapter emphasize the role of low charge-state ions in the ion cooling of ECRIS plasmas, which was studied earlier by Drentje *et. al.* The effect of gas mixing on the ion temperature from extracted beam currents was deduced with the aid of theoretically derived equations [61]. In addition, the results presented in this chapter imply that different ion species are not in thermal equilibrium, in agreement with recent theoretical calculations [48, 49].

#### ***6.2.10. The effect of microwave frequency on the plasma potential and emittance***

The effect of the microwave frequency on the plasma potential was studied with both ECR2 at ANL and the JYFL 14 GHz ECRIS. The measurements with the latter ion source were performed in conjunction with emittance measurements. Both of these ion sources can be operated in multiple frequency heating mode, in which the primary frequency is provided by a 14 GHz klystron and the secondary frequency by a traveling wave tube amplifier (TWTA) with a tunable frequency ranging from 10.75 GHz up to 12.75 GHz. Use of the TWTA made it possible to perform plasma potential and emittance measurements as a function of microwave frequency. The results obtained for ECR2 at ANL with oxygen plasma are presented in figure 6.25.

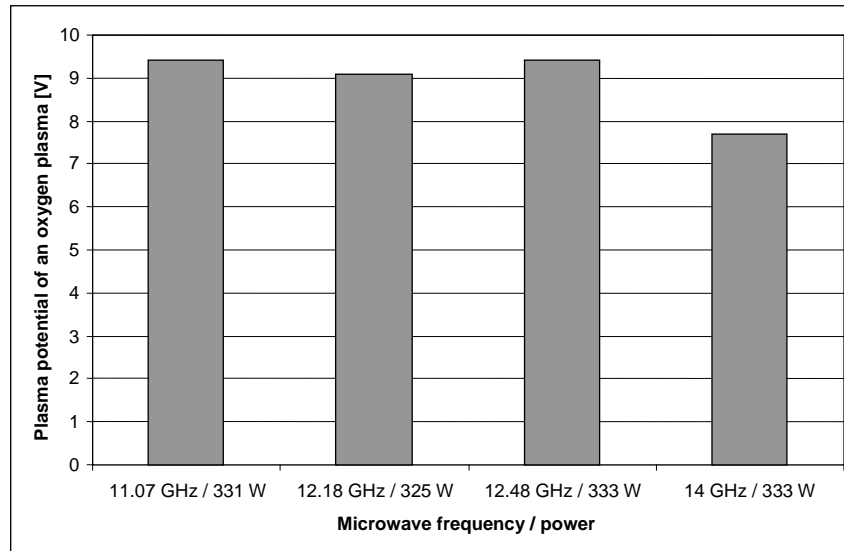


*Figure 6.25 Plasma potential of ECR2 at ANL as a function of microwave frequency.*

The plasma potential measured with 14 GHz microwave frequency is somewhat lower than the potential with frequencies between 11 and 12.5 GHz (with approximately same microwave power). However, there is practically no difference in plasma potential values obtained with different frequencies launched from the TWTA. A similar set of measurements was performed with the JYFL 14 GHz ECRIS [77]. The results (plasma potential and normalized rms-emittance of  $O^{7+}$ ) are presented in figure 6.26. The first series in the figure was measured as the source was tuned for maximum output of  $O^{7+}$  with 14 GHz and all other parameters were kept constant when changing the frequency. The second series corresponds to a measurement in which the source was tuned separately for an  $O^{7+}$  ion beam.

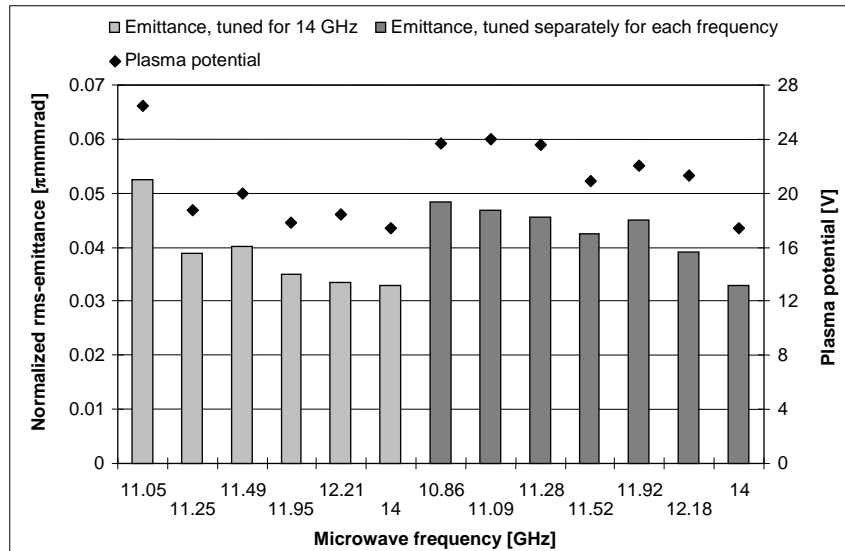


**Figure 6.26** The emittance of  $O^{7+}$  ion beam and the plasma potential as a function of microwave frequency (measured with the JYFL 14 GHz ECRIS).

According to the results, the emittance and the plasma potential decrease as the microwave frequency increases. This effect was found to be reproducible. No satisfactory explanation for the difference between the results obtained with the JYFL 14 GHz ECRIS and ECR2 at ANL was found. A similar tendency in emittance values was also observed with other charge states. According to our simulations, the main contribution to emittance growth with lower frequencies is dispersion in the dipole magnet caused by the momentum spread increase (plasma potential profile) due to higher plasma potential. However, changes of the plasma potential do not totally explain the frequency dependence of the emittance. No extensive explanation for the observed behavior was found, though the stability of the plasma, which has been observed to affect the emittance [108], was observed to be better with higher frequencies.

### 6.2.11. The effect of multiple frequency heating on the plasma potential and emittance

Plasma potential measurements were performed in double frequency electron heating mode with both ECR2 at ANL and the JYFL 14 GHz ECRIS. Because the results were consistent, only the measurements performed with the JYFL 14 GHz ECRIS are considered here. The effect of double frequency heating on the plasma potential and emittance of oxygen ion beams was studied with several combinations of microwave power and frequencies. The source was tuned for  $O^{7+}$  with each frequency, paying attention not only to the maximum current but also the stability of the plasma. The magnetic field configuration, biased disk voltage and gas feed rate were changed as the frequency was varied. The magnetic field strengths used with different frequencies were chosen to

closely correspond to those used in the series described in the previous section in order to compare the results. The emittance values for  $O^{7+}$  ion beams and the corresponding plasma potentials with different microwave frequencies and combinations of primary and secondary powers are shown in figure 6.27.

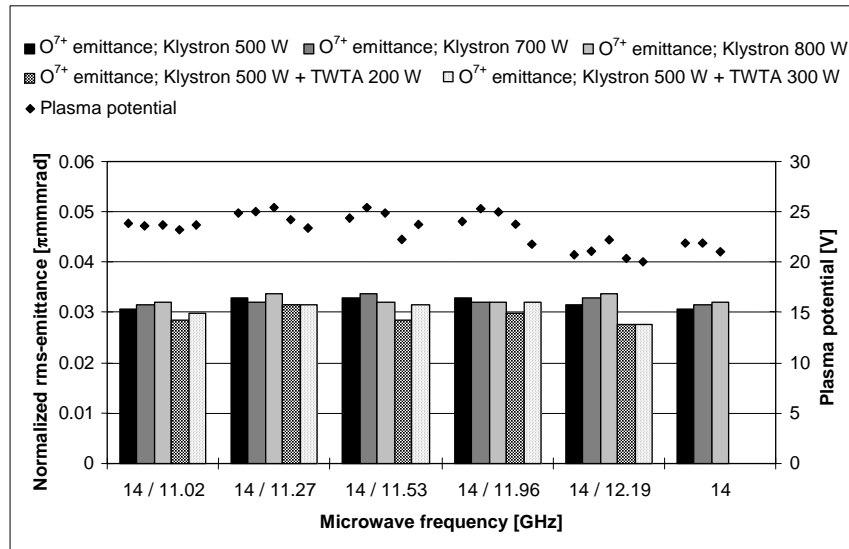


**Figure 6.27** Normalized rms-emittance values for  $O^{7+}$  ion beam and the plasma potentials with different frequencies and combinations of primary/secondary power [77].

The figure shows that there is no significant difference between  $O^{7+}$  emittance values in single and double frequency heating modes. The emittance and plasma potential were slightly lower for double frequency heating (with the same total power and source settings). It was also observed that the stability of the plasma was improved due to the secondary frequency, which may explain the difference in plasma potential and emittance. It has been observed also with the VENUS ion source at LBNL that improved plasma stability results in slightly lower emittances for double frequency tunes [109]. Therefore, based on the emittance results, it cannot be concluded whether the ion temperature changes due to the secondary resonance or not (see eq. 30). No difference between emittance values in single and double frequency operation modes was observed for low charge states ( $O^{3+}$  and  $O^{2+}$ ) with the JYFL 14 GHz ECRIS. The emittance values were found to be lower in double frequency heating mode than in single frequency operation with the TWTA (see figure 6.27). The plasma potentials obtained with higher secondary frequencies are somewhat lower than those obtained with lower secondary frequencies, which was found to be reproducible. In conclusion it can be said that double frequency heating improves the quality (brightness) of ion beams extracted from an ECRIS by increasing the currents of highly charged ions while their emittance remains nearly unchanged.

### 6.2.12. The effect of microwave radiation bandwidth on the plasma potential

The effect of increased resonance volume on the plasma potential was also studied with the JYFL 6.4 GHz ECRIS [79]. Plasma potential values for an argon plasma produced with broadband microwave radiation (200 MHz bandwidth, central frequency 6.4 GHz) were compared with the results obtained for an argon plasma produced by conventional bandwidth ( $\sim 1$  MHz) radiation. The measurements were performed with a wide range of pressures measured at the injection end of the plasma chamber. Figure 6.28 shows that there is practically no difference between the plasma potential values obtained with broadband and narrow bandwidth microwave radiation with the same input power (200 W). The lowest plasma potential values were measured at a pressure corresponding to the highest output of highly charged ions (also highest drain current). At this pressure the beam current of highly charged argon ion beams was enhanced by a factor greater than 2 with broadband microwave radiation compared to narrow bandwidth radiation [79].

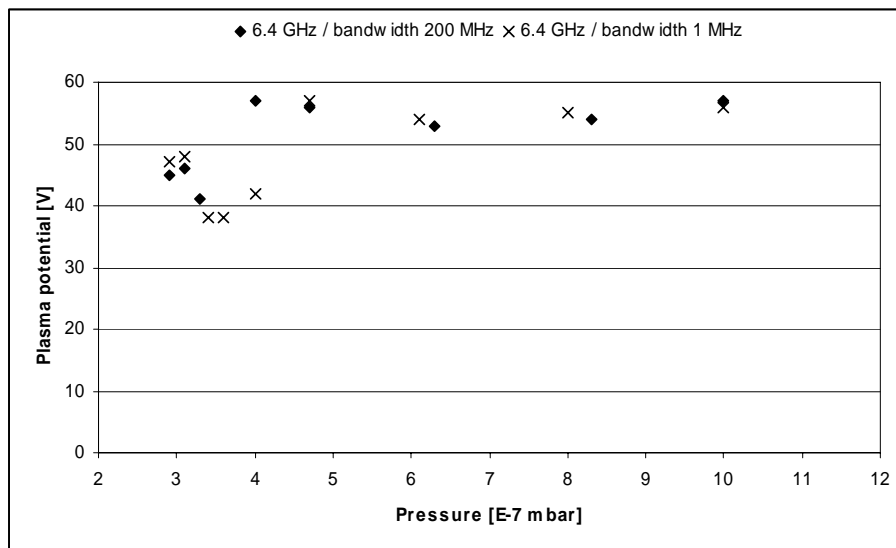


**Figure 6.28** Plasma potentials with different microwave radiation bandwidths as a function of the plasma chamber pressure measured from the injection end. A microwave power of 200 W was used in the measurement.

### 7. SUMMARY

Electron cyclotron resonance ion sources are widely used for the production of highly charged ion beams from various materials. Their performance can be improved with several techniques such as gas mixing and multiple frequency heating. However, the plasma processes leading to enhanced production of highly charged ions due to these methods are not completely understood. The goal of this work was to study the plasma properties of ECR ion sources. The information obtained can be used to improve their efficiency and quality of extracted ion beams.

The effect of the gas mixing technique on the production efficiency of different ion beams was studied with both gaseous and solid materials. It was deduced from the observations that gas mixing improves the confinement of the heavier element while the confinement of the lighter element is reduced. Especially important information was obtained when the effect of gas mixing on MIVOC-plasmas was studied with several mixing gases. The MIVOC-method can be used for the production of ion beams from solid elements. The drawback of the method is the inevitable carbon contamination, which has restricted the use of this method in different laboratories. It was observed that the level of contamination can be reduced significantly with the aid of gas mixing, which improves the production efficiency of carbon and makes it possible to reduce the consumption of the MIVOC-compound. Oxygen was found to be the best mixing gas for this purpose. It was shown that the beneficial effect of oxygen is partly due to chemical reactions i.e. the formation of compounds such as CO and CO<sub>2</sub>. Studying the distribution of the carbon contamination made it clear that although ions are not magnetically confined in ECRIS plasmas due to their high collision frequency, the ion losses are concentrated at places where the electron flux escapes the plasma.

In order to understand the different plasma processes causing, for example, the beneficial effect of gas mixing, a series of plasma potential and emittance measurements was carried out. An instrument which can be used to measure the plasma potential in a single measurement without disturbing the plasma was developed for this work. Studying the plasma potential of ECR ion sources is important not only in understanding different plasma processes but also because the information can be used as an input parameter for beam transport simulations. Knowledge of the plasma potential is also essential for the design of efficient extraction systems for ECR ion sources. The plasma potential measurements performed in this work also help to understand the effects of different parameters affecting the efficiency of charge breeder ion sources [110]. The charge breeder ECR ion source is a variation on a standard ECR ion source. It is based on the realization

that the plasma potential can be used to capture low charge-state injected ions and subsequently ionize them up to high charge states by electron bombardment in the ECRIS plasma. Knowledge of the effects of different source parameters on the plasma potential can be used to optimize the capture process and improve the efficiency of ECR charge breeders, which is important for the production of radioactive ion beams for future nuclear physics experiments.

The experiments performed have revealed clear dependencies of the plasma potential on certain source parameters such as the microwave power and frequency, pressure, biased disk voltage and drain current. It was observed that the plasma potential depends strongly on the level of carbon contamination accumulated on the walls of the plasma chamber during a MIVOC-run. This is an illustrative example of the fact that the plasma potential reflects the performance of an ECR ion source. It was also observed that gas mixing affects not only on the production efficiency of the ion beams but also their energy distribution, which strongly supports the conclusion that ion cooling explains the beneficial effect of this technique. The effect was observed to be more prominent for low charge-state ions, which emphasizes the importance of their efficient confinement. The emittance results implying that the temperature of low charge-state ions changes due to gas mixing are also consistent with this conclusion. It has also been demonstrated with simulations that the momentum spread of the ion beam, which is partly due to the the plasma potential, affects the emittance of the ion beams extracted from ECR ion sources through dispersive ion optical components. An important observation was also that double frequency heating does not affect the plasma potential and more importantly emittance of ion beams. The result confirms that this method can be used to improve the extracted beam currents of highly charged ions without a detrimental effect on the beam quality.

**REFERENCES**

- [1] E.Liukkonen, 13th. Intern. Conf. on Cyclotrons, Vancouver, (1992), p. 22.
- [2] R. Geller, Electron Cyclotron Resonance Ion Sources and ECR Plasmas, Institute of Physics Publishing, London, (1996), ISBN 0740301074.
- [3] J. Ärje, V. Nieminen, J. Choinski and T. A. Antaya, Proceedings of the 10<sup>th</sup> International Workshop on ECR Ion Sources, ORNL, (1990), p. 343.
- [4] H. Koivisto, P. Heikkinen, V. Hänninen, A. Lassila, H. Leinonen, V. Nieminen, J. Pakarinen, K. Ranttila, J. Ärje and E. Liukkonen, Nucl. Instr. and Meth. in Phys. Res., B174 (2001), p. 379.
- [5] A. Virtanen, J. Hyvönen, K. Ranttila, I. Rekikoski and J. Tuppurainen, Nucl. Instr. And Meth. in Phys. Res., A426 (1999), p. 68.
- [6] A.G. Drentje, Nuclear Instruments and Methods in Physics Research, B9, (1985), p. 526.
- [7] H. Koivisto, J.Ärje and M.Nurmia, Nucl. Instr. and Meth. in Phys. Res., B94, (1994), p. 291.
- [8] A. Girard, D. Hitz and G. Melin, Review of Scientific Instruments, Vol. 75, No. 5, (2004), p. 1381.
- [9] S. Bliman, R. Geller, W. Hess and B. Jacquot, IEEE Trans. Nucl. Sci. NS-19, (1972), p. 200.
- [10] R. Geller, Proceedings of the 15<sup>th</sup> International workshop on ECR ion sources, Jyväskylä, (2002), p. 1.
- [11] J. Arianer and R. Geller, Annu. Rev. Nucl. Part. Sci. Vol. 31, (1981), p. 19.
- [12] R. J. Goldston and P. H. Rutherford, Introduction to Plasma Physics, Institute of Physics Publishing, London, (1995), ISBN 075030183X.
- [13] M. C. Williamson, A. J. Lichtenberg, M. A. Lieberman, J. Appl. Phys., 72, 9, (1992), p. 3924.
- [14] T. H. Stix, Waves in Plasmas, Springer-Verlag, New York / Berlin / Heidelberg, (1992), ISBN 0883188597.
- [15] K. G. Budden, Radio Waves in the Ionosphere, Cambridge University Press, Cambridge, (1966), pp. 474-479.
- [16] C. Barué, M. Lamoreux, P. Briand, A. Girard and G. Melin, J. Appl. Phys., 76, 5, (1994), p. 2662.

- [17] G. Douysset, H. Khodja, A. Girard and J. P. Briand, *Phys. Rev. E*, 61, 3, (2000), p. 3015.
- [18] C. M. Lyneis, D. Leitner, S. R. Abbott, R. D. Dwinell, M. Leitner, C. S. Silver and C. Taylor, *Rev. Sci. Instrum.*, 75, No. 5, (2004), p. 1389.
- [19] C. M. Lyneis, D. Leitner, D. Todd, S. Virostek, T. Loew, A. Heinen and O. Tarvainen, to be published in *Rev. Sci. Instrum.* (Proceedings of the 11<sup>th</sup> International Conference on Ion Sources).
- [20] Y. Jongen, Proceedings of the 6<sup>th</sup> Int. Workshop on ECR Ion Sources, Berkeley (1985), p. 238
- [21] H. Koivisto, *Rev. Sci. Instrum.*, 70, (1999), p. 2979.
- [22] G. Melin, A. G. Drentje, A. Girard and D. Hitz, *J. Appl. Phys.*, 86, 9, (1999), p. 4772.
- [23] W. Lotz, *Z. Phys.* 216, (1968), p. 241.
- [24] Handbook of Chemistry and Physics, 55th Edition, Edited by R. C. Weast, CRC Press, Inc. (1974).
- [25] H. Tawara and T. Kato, *Atomic Data and Nuclear Data Tables*, Vol. 36, No. 2, (1987).
- [26] H. Knudsen, H. K. Haugen and P. Hvelplund, *Phys. Rev. A.*, 23, 2, (1981), p. 597.
- [27] F. F. Chen, *Introduction to Plasma Physics*, Plenum Press, (1974), ISBN 0306307553.
- [28] S. Gammino *et al.*, *Rev. Sci. Instrum.*, 67 (12), (1996), p. 4109.
- [29] S. Gammino *et al.*, Proceedings of the 14<sup>th</sup> International Workshop on ECR Ion Sources, (1999), p. 5.
- [30] A. G. Drentje, A. Kitagawa, M. Muramatsu, H. Ogawa and Y. Sakamoto, *Rev. Sci. Instrum.*, 75, 5, (2004), p. 1399.
- [31] G. Melin, Private communication.
- [32] A. G. Drentje, *Review of Scientific Instruments*, Vol. 74, No. 5, (2003), p. 2631.
- [33] C. C. Petty, D. L. Goodman, D. K. Smith and D. L. Smatlak, *Journal de Physique (Paris)* Vol. 50, C1, (1989), p. 783.
- [34] Z. Q. Xie and C. M. Lyneis, *Review of Scientific Instruments*, Vol. 65, No. 9, (1994), p. 2947.
- [35] D. Meyer, D. O. Bolshukhin, I. P. Vinogradov and K. Wiesemann, Proceedings of the 12<sup>th</sup> International Workshop on ECR Ion Sources, Riken, (1995), INS Rep. No. INS-J-182, p. 34.
- [36] D.J. Clark Proceedings of International Conference on ECR Ion Sources, East Lansing, (1987).

- [37] N. K. Bibinov, V. F. Bratsev, T. P. Kokh, P. I. Ochkur and K. Wiesemann, *Plasma Sources Sci. Technol.*, 14, (2005), p. 109.
- [38] V. P. Pastoukhov, *Review of Plasma Physics*, Vol. 13 (1987), p. 203.
- [39] Y. Kato and S. Ishii, *Review of Scientific Instruments*, Vol. 69, No. 2, (1998), p. 1176.
- [40] V. Mironov, K. E. Stiebing, O. Hohn, L. Schmidt, H. Schmidt-Böcking, S. Runkel, A. Schempp, G. Shirkov, S. Biri and L. Kenéz, *Review of Scientific Instruments*, Vol. 73, No. 2, (2002), p. 623.
- [41] S. Biri *et al.*, *Proceedings of the 16<sup>th</sup> International Workshop on ECR Ion Sources*, Berkeley, (2004), p. 67.
- [42] Y. Kawai, Y. Liu, G. D. Alton, H. Z. Bilheux and J. M. Cole, *Proceedings of the 16<sup>th</sup> International Workshop on ECR Ion Sources*, Berkeley, (2004), p. 223.
- [43] A. Nadzeyka, D. Meyer and K. Wiesemann, *Proceedings of the 13<sup>th</sup> International Workshop on ECR Ion Sources*, (1997), p. 185.
- [44] O. Tarvainen, P. Suominen and H. Koivisto, *Review of Scientific Instruments*, 75, (2004), p. 3138.
- [45] R. C. Vondrasek, R. H. Scott, R. C. Pardo and D. Edgell, *Review of Scientific Instruments*, Vol. 73, No. 2, (2002), p. 548.
- [46] R.C.Vondrasek, R.H. Scott, R.C. Pardo, H. Koivisto, O. Tarvainen and P. Suominen, *Proceedings of the 16<sup>th</sup> International Workshop on ECRIS*, Berkeley, (2004), p. 31.
- [47] T. Rognlien and T. Cutler, *Nucl. Fusion* 20, (1980), p. 1003.
- [48] K. Wiesemann, Oral presentation in the 11<sup>th</sup> International Conference on Ion Sources, Caen, France, 13.9.2005 / to be published in December 2005 in a special issue of *IEEE Transactions on Plasma Science*.
- [49] E. A. Vostrikova, L. I. Elizarov, A.A. Ivanov, K. S. Serebrennikov, will be published in *Rev. Sci. Instrum.* (*Proceedings of the 11<sup>th</sup> International Conference on Ion Sources*).
- [50] C. M. Lyneis, *Proceedings of International Conference on ECR ion sources and their Applications*, East Lansing, (1987), p. 42.
- [51] T. Nakagawa *et al.* *Jpn. J. Appl. Phys.*, Part 2, 30, (1991), L930.
- [52] D. Hitz *et al.*, *Proceedings of the 12<sup>th</sup> International workshop on ECR ion sources*, Wako, (1995), p. 126.
- [53] L. Schächter, S. Dobrescu, G. Rodrigues and A. G. Drentje, *Review of Scientific Instruments*, Vol. 73 , (2002), p. 570.

- [54] C. M. Lyneis *et al.*, Proceedings of the 10<sup>th</sup> International workshop on ECR ion sources, Knoxville, (1990), p. 47.
- [55] G. Melin *et al.*, Proceedings of the 10<sup>th</sup> International Workshop on ECR Ion Sources, Knoxville, (1990), INS Rep. No. Conf.-9011136, p. 1.
- [56] S. Gammino, J. Sibring and A. G. Drentje, Review of Scientific Instruments, Vol. 63, (1992), p. 2872.
- [57] S. Biri *et al.*, Proceedings of the 14<sup>th</sup> International Workshop on ECR Ion Sources, Geneva, (1999), p. 81.
- [58] S. Runkel *et al.*, Review of Scientific Instruments, Vol. 71, (2000), p. 912.
- [59] A. G. Drentje, U. Wolters, A. Nadzeyka, D. Meyer and K. Wiesemann, Review of Scientific Instruments, Vol. 73, (2002), p. 516.
- [60] D. Bolshukhin, D. Meyer, U. Wolters and K. Wiesemann, Review of Scientific Instruments, 69, (1998), p. 1197.
- [61] A.G. Drentje, A. Girard, D. Hitz and G. Melin, Review of Scientific Instruments, 71, (2000), p. 623.
- [62] R. Geller *et al.*, Proceedings of the 8<sup>th</sup> International Workshop on ECR Ion Sources, East Lansing, (1987), p. 1.
- [63] T. A. Antaya, Proceedings of the 9<sup>th</sup> International Workshop on ECR Ion Sources, Grenoble, J. Phys. Colloq., 50, (1989), p. 707.
- [64] G. D. Shirkov, Plasma Sources Sci. Technol., 2, (1993), p. 250.
- [65] M. Delaunay, Review of Scientific Instruments, 63, (1992), p. 2861.
- [66] O. Tarvainen, P. Suominen and H. Koivisto, Nucl. Instrum. and Meth. in Phys. Res. (section B), Vol. 217, No. 1, (2004), p. 136.
- [67] O. Tarvainen, P. Suominen, T. Ropponen, T. Kalvas, P. Heikkinen and H. Koivisto, Rev. Sci. Instrum., 76, (9), (2005).
- [68] A.G. Drentje, Review of Scientific Instruments, 63, (1992), p. 2875.
- [69] H. Koivisto, The MIVOC Method for the Production of Metal Ion Beams (thesis), Department of Physics, University of Jyväskylä Research Report No. 1/1998.
- [70] Y. Kawai, D. Meyer, A. Nadzeyka, U. Wolters and K. Wiesemann, Plasma Sources Sci. Technol. 10, (2001), p. 451.
- [71] Z.Q. Xie and C.M. Lyneis, Proceedings of the 12<sup>th</sup> International Workshop on ECR Ion Sources, Riken, (1995), p. 24.
- [72] G. D. Alton *et al.* Rev. Sci. Instrum., 69, (1998), p. 2305.

- [73] R.C. Vondrasek, R.H. Scott and R.C. Pardo, Proceedings of the 15<sup>th</sup> International Workshop on ECR Ion Sources, Jyväskylä, (2002), p. 63.
- [74] R. Vondrasek, R. Scott and R. Pardo, will be published in Rev. Sci. Instrum. (Proceedings of the 11<sup>th</sup> International Conference on Ion Sources).
- [75] H. Koivisto, P. Suominen, O. Tarvainen and A. Virtanen, to be published in Rev. Sci. Instrum. (Proceedings of the 11<sup>th</sup> International Conference on Ion Sources).
- [76] O. Tarvainen, P. Suominen, T. Ropponen, H. Koivisto, R.C. Vondrasek and R.H. Scott, Proceedings of the 16<sup>th</sup> International Workshop on ECRIS, Berkeley, (2004), p. 61.
- [77] O. Tarvainen, P. Suominen, T. Ropponen and H. Koivisto, to be published in Rev. Sci. Instrum (Proceedings of the 11<sup>th</sup> International Conference on Ion Sources).
- [78] R. C. Vondrasek, Private communication.
- [79] Y. Kawai, G. D. Alton, Y. Liu, O. Tarvainen, P. Suominen and H. Koivisto, will be published in Rev. Sci. Instrum. (Proceedings of the 11<sup>th</sup> International Conference on Ion Sources).
- [80] L. Celona, S. Gammino, G. Ciavola, F. Consoli and A. Galatà, Proceedings of the 16<sup>th</sup> International Workshop on ECR Ion Sources, (2004), p. 99.
- [81] S. Gammino, G. Ciavola, Rev. Sci. Instrum., 71 (2), (2000), p. 631.
- [82] F. Bourg, R. Geller, B. Jacquot and M. Pontonnier, Proceedings of the 4<sup>th</sup> International Workshop on ECR Ion Sources, Grenoble, (1982), p. 5.1.
- [83] R. Geller and B. Jacquot, Contributed Papers of the 7<sup>th</sup> Workshop on ECR Ion Sources, ISSN 0344-5798, (1986), p. 31.
- [84] R. Harkewicz, J. Stacy, J. Greene and R. C. Pardo, Rev. Sci. Instrum., 65, (1994), p. 1104.
- [85] D. J. Clark and C. M. Lyneis, Proceedings of the 9<sup>th</sup> International Workshop on ECR Ion Sources, Grenoble, J. Phys. Colloq., 50, (1989), p. C1-759.
- [86] R. Lang, J. Bossler, R. Ianucci and K. Tinschert, Proceedings of the 15<sup>th</sup> International Workshop on ECR Ion Sources, Jyväskylä, (2002), p. 180.
- [87] V. B. Kutner *et al.* Review of Scientific Instruments, 71, (2000), p. 860.
- [88] R. Harkewicz, P. J. Billquist, J. P. Greene, J. A. Nolen and R. C. Pardo, Review of Scientific Instruments, 66, (1995), p. 2883.
- [89] I.G. Brown, The Physics And Technology Of Ion Sources, John Wiley & Sons, (1989), ISBN 0-471-85708-4.
- [90] Z.Q. Xie, Thesis, Michigan State University, MSU CP-60, (1989), p. 58.

- [91] M.A. Leitner, D.C. Wutte and C.M. Lyneis, Proceedings of the Particle Accelerator Conference (PAC'01), Chicago, (2001).
- [92] P. Spädtke, Rev. Sci. Instrum., 75, (2004), p. 1643.
- [93] Karl L. Brown, A First-and Second-Order Matrix Theory for the Design of Beam Transport Systems and Charged Particle Spectrometers, SLAC 75, Revision 3, SLAC, (1972).
- [94] H. Koivisto, M. Moisio, V. Nieminen, P. Suominen and E. Liukkonen, Nukleonika, vol. 48, supplement 2, (2003), S81.
- [95] M. Schlapp *et al.*, Proceedings of the 13<sup>th</sup> International Workshop on ECR Ion Sources, College Station, (1997), p. 22.
- [96] T. A. Antaya and Z. Q. Xie, Proceedings of the 7<sup>th</sup> International Workshop on ECR Ion Sources, Jülich, (1986), p. 72.
- [97] Z. Q. Xie and C. M. Lyneis, Proceedings of the 13<sup>th</sup> International Workshop on ECR Ion Sources, College Station, (1997), p. 16.
- [98] J. A. Simpson, Rev. Sci. Instrum., 32, (1961), p. 1283.
- [99] D. Wutte, M.A. Leitner and C.M. Lyneis, Physica Scripta, T92, (2001), p. 247.
- [100] O. Tarvainen, P. Suominen, I. Pitkänen and H. Koivisto, Review of Scientific Instruments, 75 (5), May, (2004), p.1523.
- [101] R. Leroy, M. Bisch, P. Leherissier, J. Y. Pacquet, J. P. Rataud and P. Sortais, Proceedings of the 11<sup>th</sup> International Workshop on ECR Ion Sources, Groningen, (1993), p. 133.
- [102] D. Meeker, "Finite Element Method Magnetics," Version 3.2, Build 3Dec02, <http://femm.foster-miller.net/index.html>
- [103] H. Koivisto, P. Suominen, O. Tarvainen, J. Ärje, E. Lammentausta, P. Lappalainen, T. Kalvas, T. Ropponen and P. Frondelius, Proceedings of the 16<sup>th</sup> International Workshop on ECR Ion Sources, Berkeley, (2004), p. 27.
- [104] P. Suominen, O. Tarvainen and H. Koivisto, will be published in Rev. Sci. Instrum. (Proceedings of the 11<sup>th</sup> International Conference on Ion Sources).
- [105] F. Meyer, Proceedings of the 7<sup>th</sup> International Workshop on ECR Ion Sources, Jülich, (1986), p. 11.
- [106] PBO Lab<sup>TM</sup> (Particle Beam Optics Laboratory) User Manual, G. H. Gillespie Associates, Inc. (1997), ISBN 1-892267-00-4.
- [107] P. Suominen, O. Tarvainen and H. Koivisto, Review of Scientific Instruments, 75 (5), May, (2004), p.1517.

## REFERENCES

---

- [108] D. Leitner, Private communication.
- [109] D. Leitner, C. M. Lyneis, T. Loew, D. S. Todd, S. Virostek and O. Tarvainen, will be published in *Rev. Sci. Instrum.* (Proceedings of the 11<sup>th</sup> International Conference on Ion Sources).
- [110] R. Geller, C. Tamburella and J. L. Belmont, *Rev. Sci. Instrum.*, 67 (3), (1996), p. 1281.